EVOLUTIONARY AND DEVELOPMENTAL NOVELTY IN CETACEAN LIMBS AND TAIL FLUKES

A dissertation submitted

to Kent State University in cooperation with Northeast Ohio Medical University in partial

fulfillment of the requirements for the

degree of Doctor of Philosophy

by

Lia Michelle Gavazzi

August 2023

Dissertation written by

Lia Gavazzi

B.S., The Pennsylvania State University, 2017
M.A., The Pennsylvania State University, 2017
Ph.D., Kent State University, 2023

Approved by

_____, Co-chair, Doctoral Dissertation Committee
Lisa Noelle Cooper, Ph.D.

_____, Co-chair, Doctoral Dissertation Committee
J.G.M. Thewissen, Ph.D.

_____, Member, Doctoral Dissertation Committee
Mohammad 'Yunus' Ansari, Ph.D.

_____, Member, Doctoral Dissertation Committee
Henry C. Astley, Ph.D.

_____, Member, Doctoral Dissertation Committee
Eric Mintz, Ph.D.

Accepted by

_____, Director, School of Biomedical Sciences
John Johnson, Ph.D.

_____, Dean, College of Arts and Sciences
Mandy Munro-Stasiuk. Ph.D.

TABLE OF CONTENTS

LIST OF FIGURES

LIST OF TABLES

x

PREFACE

Chapters 1, 4, 5, and 7 of this document are original material written exclusively for the purposes of this dissertation. Chapter 2 was originally published in the Journal of Morphology as:

Gavazzi L, Cooper LN, Usip S, Suydam R, Stimmelmayr R, George JC, O'Corry-Crowe G, Hsu CW, Thewissen J. Comparative embryology of *Delphinapterus leucas* (beluga whale), *Balaena mysticetus* (bowhead whale), and *Stenella attenuata* (pan-tropical spotted dolphin) (Cetacea: Mammalia). J Morphology. 2023 Feb;284(2):e21543. doi: 10.1002/jmor.21543.

Chapter 3 was originally published in the Journal of Vertebrate Paleontology as:

L. M. Gavazzi, L. N. Cooper, F. E. Fish, S. T. Hussain & J. G. M. Thewissen (2020): Carpal morphology and function in the earliest cetaceans, Journal of Vertebrate Paleontology, DOI: 10.1080/02724634.2020.1833019 © copyright #2020, reprinted by permission of Informa UK Limited, trading as Taylor & Taylor & Francis Group

Chapter 6 has been submitted as a research article to the journal Developmental Dynamics and is currently in the peer-review process.

For all previously published material, research design was conceived by J. G. M. Thewissen, L. N. Cooper, and myself. Data collection and processing was performed by me. The manuscripts were written by me with contributions from J. G. M. Thewissen and L. N. Cooper during the review process. Co-authors on these studies provided intellectual and material support through specimen collection, protocol optimization, assistance with data interpretation, and feedback during the manuscript writing process.

ACKNOWLEDGMENTS

Thank you to the Thewissen Lab members past and present, including all of the high schoolers who patiently listened to me rant about whale flukes. I especially want to thank Sharon and David for all of your help. Your expertise and humor helped me immensely in the lab. Thank you to Jen and Ian for your friendship over the years.

A big thank you to my family for everything. My parents, Gina, and Levi supported and encouraged me every step of the way. Thank you to all of my dear friends: Nicole, Angela, Erin, Kelsey, Eleanor, Ryan, Brook, Cookie, Sindr, Ed, Sam, Adj, Nora, and Michael. I'm so blessed to know such kind and loving people. I especially want to acknowledge Rose, who started this grad school journey with me and has been a friend since day 1. There's nobody else I'd rather survive HDS/HAC with.

Lastly, I want to thank Cecil (and our little cat family) for all of the love throughout this whole process. I could never truly express how much your support has meant to me over the last five years. There was no way I could have finished my degree without you. You have made this journey both wonderful and meaningful.

CHAPTER 1   CETACEAN APPENDAGE EVOLUTION AND DEVELOPMENT

My research interests focus on the evolution and development of the postcranial vertebrate body with an eye towards the unusual mammals living in non-terrestrial environments. Cetaceans (whales, dolphins, porpoises) have often been referred to as the poster child of mammalian evolution. With an exceptional fossil record, the stepwise transition from land-to-water is documented at nearly every step. Additionally, the evolutionary changes necessary to facilitate an aquatic lifestyle are tractable within the embryos of cetaceans, which clearly show developmental and morphological shifts from a terrestrial mammalian bauplan to an exceptional body optimized for life in the seas. As such, this combination of fossils, embryos, and modern molecular research techniques creates an optimal environment for comprehensive evolutionary developmental biology research.

The cetacean transition from life on land to an exclusively aquatic niche is accompanied by a suite of morphological and skeletal changes that are well-documented in the fossil record and during embryonic development. The forelimb of early cetaceans transitioned from a weight-bearing pentadactyl limb to a flipper used for steering and control during locomotion. The formation of the cetacean flipper includes the maintenance of interdigital webbing between the digits and an increase in the number of phalanges on some fingers and reduction of phalanges on other digits. The hindlimbs, initially robust appendages that powered amphibious fossil cetacean taxa, are greatly reduced to internalized vestiges in modern animals.

Reduction of the hindlimbs occurred concurrently with morphological homogenization of the post-thoracic spine and the *de-novo* evolution of the soft-tissue flukes. The flukes insert onto the spine at the terminal caudal vertebrae and are used to propagate forces during tail driven locomotion. These three major transitions in skeletal morphology, the formation of the flippers, reduction of hindlimbs, and evolution of the flukes, all occurred within the span of approximately 8 million years during the Eocene and have been retained in modern taxa (Figure 1).

The goal of this dissertation is to investigate key aspects of cetacean appendage evolution and development, specifically those related to this shift from limb-powered to tail-powered locomotion. Moving cranially to caudally, each chapter investigate changes to the forelimb (**chapter 3**), hindlimb (**chapter 4**), and distal tail (**chapter 5, 6**) to better understand the embryology, morphology, and molecular regulators of the soft-tissue flipper, reduction of the hindlimb and pelvic skeleton, and the emergence of the novel soft-tissue flukes in cetaceans.
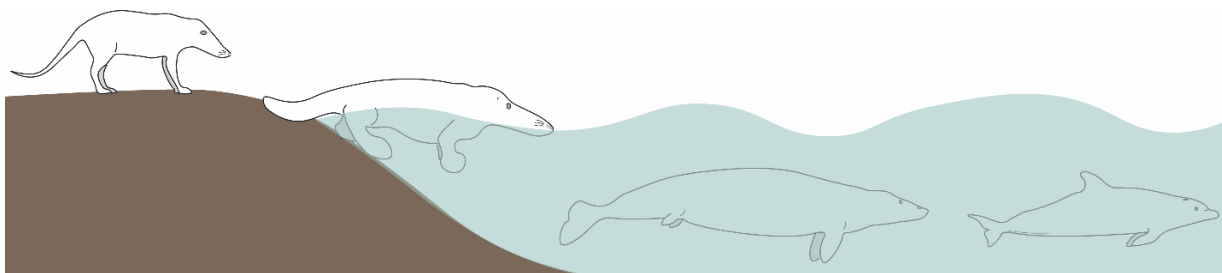
Figure 1: Evolution of the cetacean body starting from the earliest whales like *Pakicetus* (far left), the amphibious taxa, here represented by *Ambulocetus* (left), the first fully aquatic cetaceans, the basilosaurids (right), and the modern taxa like the common dolphin (far right)

Limb development and embryology

The embryology of the tetrapod limbs is a paradox as it is highly stereotypical, showing little variation from amphibian and reptilian limb development, and exceptionally plastic to allow for an incredible diversity of forms. Cow hooves, bat wings, mouse paws, and cetacean flippers all share the same underlying genetic and morphological and developmental blueprint (Bejder and Hall, 2002; Richardson and Oelschläger, 2002; Weatherbee et al., 2006; Hockman et al., 2008; Cooper et al., 2012a, 2014a, 2017; Varga and Varga, 2022). The limb initially develops *via* three major axes of gene signaling: the proximodistal axis (PD), anteroposterior (AP) axis, and dorsoventral axis (DV).

The PD axis of limb development (shoulder to digits) is primarily driven by expression of fibroblast growth factors (FGFs), notably FGF-4, FGF-8, and FGF-10. The distal epithelial tip of the developing limb bud expresses both FGF-8 and FGF-4 into the interior mesenchymal tissue (Mahmood et al., 1995; Vogel et al., 1996; Lewandoski et al., 2000; Moon and Capecchi, 2000; Moon et al., 2000; Boulet et al., 2004). These factors promote the expression of FGF-10 in this underlying mesenchyme, which re-stimulates FGF-8 expression (Ohuchi et al., 1997; Sekine et al., 1999). The region of tissue producing FGF-8 is referred to as the apical ectodermal ridge (AER). The AER is often visible as thickened region of columnar/cuboidal cells, though the presence of this cellular anatomy is variable across tetrapods (Cooper et al. 2011). Previous research has shown that the variation in AER shape and size is less critical for limb embryogenesis than the continual expression of FGF-8 in the epithelium (Lewandoski et al., 2000; Moon and Capecchi, 2000; Cooper et al., 2011).

Determination of the AP axis (thumb to pinky) is driven by the gene Sonic hedgehog (SHH) as it is expressed in a region of the developing mesenchyme called the zone of polarizing activity (ZPA).

SHH acts as a morphogen in the developing limb, forming a concentration gradient that dictates the formation and identify of the digits (McGlinn and Tabin, 2006; Scherz et al., 2007; Bastida et al., 2009; Lopez-Rios, 2016; Royle et al., 2021). Modifications to SHH often lead to significant changes in limb morphology both experimentally and evolutionarily (Harfe et al., 2004; Thewissen et al., 2006, 2012; Hockman et al., 2008; Newton and Smith, 2021).

Proper development of the DV axis (back of the hand versus the palm) occurs via opposing signals from the dorsal and ventral tissues. Dorsalization of the limb is facilitated by expression of the genes WNT7A in the epithelium and LMX1 in the mesenchyme (Parr and McMahon 1995). These signals are counteracted in the ventral region of the limb by signaling from the transcription factor EN1 (Loomis et al., 1996; Logan et al., 1997; Chen and Johnson, 2002).

Cetacean limb development

As marine mammals, cetaceans are both constrained by and highly divergent from the stereotypical terrestrial mammalian bauplan. Fore- and hindlimb organogenesis in cetaceans initiates using the same developmental pathways found in other mammals with the three axes of patterning and outgrowth. However, it is through major modifications to this choreography that create the hyperphalangeous flipper and reduced hindlimbs.

Protein signaling research in the pan-tropical spotted dolphin (*Stenella attenuata*) shows that these animals prolong the duration of FGF-8 signaling within their AER, which may contribute to the development of hyperphalangy. Also, where other mammals secrete bone morphogenetic proteins

between their digits to form independently movable fingers, the spotted dolphin shows additional expression of the protein Gremlin (GREM) (Cooper et al. 2017). BMP and GREM are antagonistic, and thus the additional signaling of GREM is hypothesized to promote maintenance of this interdigital webbing for formation of the flipper (Figure 2). Some baleen whales are tetradactylous (Cooper et al., 2007a) and these signaling factors may play a role in that digit loss.

Research again involving the pan-tropical spotted dolphin indicates that the cetacean hindlimb has extremely truncated SHH expression. The cessation of SHH activity in the hindlimb contributes to an absence of limb development, prohibiting formation of any major skeletal elements (Thewissen et al. 2006, Liang et al. 2022, Sun et al. 2022) (Figure 2). Development of the hindlimb is further investigated in **chapter 4**.

Figure 2: Pan-tropical spotted dolphin (*Stenella attenuata*) embryo stained with alizarin red for bone and alcian blue for cartilage. Specimen is on loan from the Natural History Museum of Los Angeles County (LACM) and is a Carnegie stage (CS) 20, the early fetal period of development. Major modifications to the common limb development pathways are indicated by their respective organ.

Vertebral development and osteology in cetaceans

The modularity of the vertebrate spine is a well-documented and highly stereotyped pattern found in all mammals. The plasticity of each region exists along a spectrum – almost all extant and fossil mammals have seven cervical vertebrae, save for the two-toed sloth and manatee (Böhmer et al., 2018). There is considerably more variability at the tail-end of the animal, cetaceans have taken their vertebral columns to the extreme and shown several unique adaptations for aquatic living. In many odontocetes (toothed whales), but not beluga whales (*Delphinapterus leucas*), and the bowhead (*Balaena mysticetus*), the cervical vertebrae are fused into one bony element (Moran et al., 2015). The chest cavity of many cetaceans is collapsible; this serves as a mechanism to resist and distribute water pressure during foraging or swimming dives (Brown and Butler, 2000; Lillie et al., 2017). The lumbar region is nearly homogenous in appearance to the sacral and caudal portions of the spine in all extant taxa, making individual identification of any single isolated skeletal element a challenge. Finally, the distal tail vertebrae of all cetaceans have been modified to support the insertion of collagenous fibers from the soft-tissue flukes. Tail flukes are a novel appendage that has only evolved in cetaceans and dugongs.

In this dissertation, **Chapter 2** compares morphology of developing appendages between embryos of three cetaceans: *Stenella attenuata* (pan-tropical spotted dolphin), *Delphinapterus leucas* (beluga whale), and *Balaena mysticetus* (bowhead whale). Ontogeny is best known in the spotted dolphin, which serves as a baseline for understanding development in beluga and bowhead. Through photography and inspection of the cetacean embryo collections on loan from the Los Angeles County Museums of Natural History (LACM) and the North Slope Borough Department of Wildlife

Management (NSB-DWM), I found that tracking fluke, flipper, and hindlimb development in these taxa allowed for direct cross-species comparisons (Figure 3). This chapter forms the framework for further investigation of cetacean embryology (**chapter 4**, **chapter 6**). This work has been published in the Journal of Morphology (Gavazzi et al. 2023).
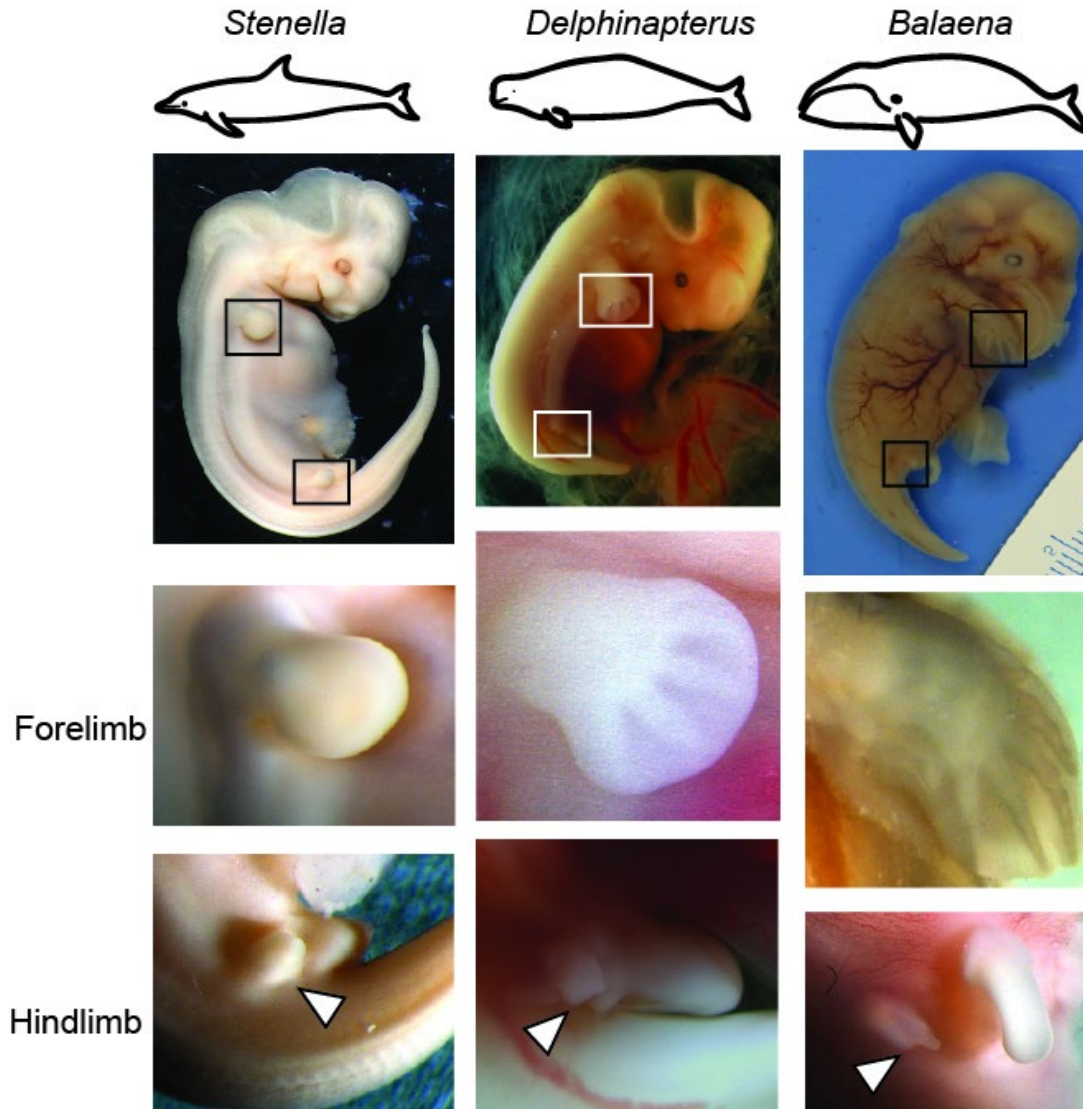
Figure 3: Photographs of a pan-tropical spotted dolphin (*Stenella attenuata*) (left), beluga (*Delphinapterus leucas*) (center), and bowhead (*Balaena mysticetus*) (right) embryo showing forelimb and hindlimb development in each taxa. All three specimens are approximately the same ontogenetic age, as defined in **chapter 3**.

During the land-to-water transition in the Eocene epoch (~48-40 mya), the cetacean forelimb transformed from a weight-bearing limb with mobile joints to a flipper with an immobile carpus. In **chapter 3,** I used micro-CT imaging to assess evolutionary changes in carpal size, orientation, and articulation within Eocene cetacean taxa associated with the transition from a terrestrial to amphibious niche. We compared *Ambulocetus natans*, a well-preserved amphibious fossil whale with other archaeocetes (ancient whales), and with Eocene terrestrial artiodactyls, the sister group to Cetacea. A cylindrical carpus in terrestrial taxa evolved into a mediolaterally flattened, cambered carpus in the semi-aquatic and fully aquatic cetaceans. Flattening of the carpus, including lateral rotation of the pisiform and medial rotation of digit I and the trapezium, likely relates to functional shifts from weight-bearing terrestrial locomotion to aquatic locomotion. This laterally projecting pisiform morphology is retained in all extant cetaceans. Our results suggest this shift, along with other modifications to the carpus, predominantly occurred during the middle Eocene epoch and facilitated an obligatorily aquatic lifestyle in late Eocene cetaceans. In modern cetaceans, the wrist is completely immobile within the flipper and many carpals are reduced, fuse, and and/or remain cartilaginous throughout the lifespan.

Cetaceans are one of two major mammalian groups that have drastically reduced the size and shape of their hindlimb – this change in body shape and proportions is documented in embryos (Kükenthal, 1889; Guldberg and Nansen, 1894; Ogawa, 1953; Sedmera et al., 1997a; Štěrba et al., 2000) and in the fossil record. Among cetaceans that maintain some remnants of the hindlimb, the bowhead whale (*Balaena mysticetus*) stands out as having comparatively elaborate hindlimbs. Cartilaginous and skeletal elements for the pelvis, femur, and occasionally a tibia and metatarsal have

been recovered from this taxon (Eschricht et al., 1866; Struthers, 1881; Thewissen et al., 2021b; Cooper et al., 2023). **Chapter 4** uses histology to document hindlimb embryology within the bowhead whale and speculates on the developmental mechanisms that this taxon may be modifying for the formation of these limb remnants.

The flukes are used to propagate forces generated by the tail and are supported by uniquely shaped vertebrae. Two distinct hypotheses are currently used to identify the presence of fluke vertebrae in extant and extinct cetaceans. First, flukes are expected to contain vertebrae that are wider than they are tall. The second hypothesis often used is related to the insertion point of the fluke tissue onto the vertebral column. Some researchers suggest that the hinge point of the flukes on the tail, called the peduncle, is associated with an overtly circular vertebra. This peduncular vertebra, also referred to as the ball vertebra, is referenced in both paleontological and biomechanical studies on cetaceans. These hypotheses were generated via skeletal collections and have not been empirically tested with respect to the overlying soft-tissue they claim to represent. As such, it is difficult to ascertain how specific these hypothetical metrics are when looking at a cetacean tail in-situ. In **chapter 5** I dissect one bowhead (*B. mysticetus*) and one beluga (*D. leucas*) tail to test these two hypotheses in fully articulated specimens.

Research on the flukes has primarily focused on the size, shape, and composition of this unusual organ to better understand cetacean locomotion (Ryder, 1885; Felts, 1966; Fish, 1998; Fish et al., 2006; Sun et al., 2010, 2011; Ayancik et al., 2020). Despite understanding the anatomy and morphological development of flukes, molecular signals driving outgrowth of this novel appendage are unknown. Using the beluga whale (*Delphinapterus leucas*) as the model taxon, in **chapter 6** I

demonstrate protein signaling in the developing flukes via immunohistochemistry (IHC). IHC was used to determine the spatial distribution of protein signaling in paraffin-sectioned tissue. Data from common proteins associated with morphogenesis (SHH, GREM, WNT, FGFs) show that flukes exapted signaling cascades common to fin/limb development. These common developmental proteins are found in similar spatial patterns and tissue types to both the tetrapodal limb and the cetacean flipper. These data suggest the morphological novelty of the flukes potentially evolved via recapitulation of appendage signaling within the tail, providing insight into the evolution of novel soft-tissue appendages. Given that the fossil record suggests flukes evolved only once within Cetacea, it is likely that these same proteins contributed to the development of the flukes in deep time.

CHAPTER 2 COMPARATIVE EMBRYOLOGY OF *DELPHINAPTERUS LEUCAS* (BELUGA

WHALE), *BALAENA MYSTICETUS* (BOWHEAD WHALE), AND *STENELLA ATTENUATA*

(PAN-TROPICAL SPOTTED DOLPHIN) (CETACEA: MAMMALIA)

This chapter was originally published in The Journal of Morphology by Wiley Periodicals LLC as an

open access article under the terms of the Creative Commons CC BY license.

Introduction

Nearly every aspect of cetacean (whales, dolphins and porpoises) biology is modified to

accommodate their exclusively aquatic lifestyle. This transition from land to water is a remarkable

feat, considering that these taxa are ultimately constrained by the mammalian bauplan and still

demonstrate classic mammalian features, such as live birth, nursing, homeothermy, and oxygen intake

via nares to lungs. Early during the embryonic period, cetaceans appear like other mammals with

processes like somite formation, forelimb bud development, and patterning of organ primordia

(Štěrba et al., 2000; Thewissen and Heyning, 2007). As development progresses, these embryos begin

to diverge from this mammotypical plan and take on cetacean-specific traits including loss of external

hindlimbs (Guldberg and Nansen, 1894; Ogawa, 1953; Sedmera et al., 1997a; Thewissen et al., 2006),

the formation of a soft-tissue fluke for tail-based propulsion (Ryder, 1885; Fish, 1998; Buchholtz, 2007; Thewissen, 2018), blowhole formation on the dorsum of the skull (Oelschläger, 2000; Haddad et al., 2012; Roston and Roth, 2019, 2021; Farnkopf et al., 2021), and hyperphalangy (Sedmera et al., 1997b; Richardson and Oelschläger, 2002; Richardson and Chipman, 2003; Cooper et al., 2007a, 2011, 2017; Richardson et al., 2009). Although other aquatic mammals such as Sirenia (manatees and dugongs) also lack external hindlimbs and display adaptations for tail-powered swimming (Buchholtz et al., 2007; Domning, 2018), only cetaceans evolved a blowhole on the top of their heads and hyperphalangy. Hyperphalangy is defined as an increase in the number of phalanges from the standard mammalian phalangeal formula, from anterior to posterior, of 2/3/3/3/3 (Richardson and Oelschläger, 2002; Richardson and Chipman, 2003; Fedak and Hall, 2004; Cooper et al., 2007a; Richardson et al., 2009). Variation in phalangeal count in cetacean taxa is often both intra- and inter-specific (Sedmera et al., 1997b; Cooper et al., 2007a).

Furthermore, most odontocetes (dolphins and porpoises) have more teeth than is typical for mammals and have developed homodonty (Armfield et al., 2013), whereas beaked whales have fewer, specialized teeth, and baleen whales (mysticetes) have replaced their dentition with keratin-based baleen plates, a novel adaptation for filter feeding (Pivorunas, 1979; Marx et al., 2017; Thewissen et al., 2017; Lanzetti et al., 2020).

The cetacean taxon for which ontogeny is best described is *Stenella attenuata*, the pan-tropical spotted dolphin. A collection of prenatal specimens curated and housed at the Natural History Museums of Los Angeles County illuminates almost the entirety of organogenesis and has been utilized in numerous studies of cetacean embryonic morphology (Sedmera et al., 1997b, 1997a, 2003; Oelschläger, 2000; Štěrba et al., 2000; Richardson and Oelschläger, 2002; Thewissen et al., 2006;

12

Thewissen and Heyning, 2007; Armfield et al., 2011; Moran et al., 2011; Roston et al., 2013; Roston and Roth, 2021). Furthermore, protein signaling studies have been conducted using this *Stenella* collection (Thewissen et al., 2006, 2017; Armfield et al., 2013; Cooper et al., 2017). The nearly complete range of developmental ages makes this collection unique, and thus forms the basis for our understanding of cetacean embryology and evolutionary developmental biology.

Other knowledge about prenatal cetaceans is based on material from commercial whaling operations (Ryder, 1885; Kükenthal, 1889; Guldberg and Nansen, 1894; Ogawa, 1953; Stump et al., 1960; Roston et al., 2013; Roston and Roth, 2021), collaboration with indigenous communities that harvest cetaceans for subsistence (Armfield et al., 2011; Heide-Jørgensen and Garde, 2011; Thewissen et al., 2017; Farnkopf et al., 2021), strandings (Berta et al., 2015b; Roston and Roth, 2021), and from cetacean bycatch during commercial fishing (Sedmera et al., 1997b, 1997a, 2003; Štěrba et al., 2000; Thewissen et al., 2006; Thewissen and Heyning, 2007; Armfield et al., 2011; Moran et al., 2011; Cooper et al., 2017; Roston and Roth, 2021). Many of these reports focus on morphological descriptions of fetal specimens. These fetal specimens answer important questions of allometry and scaling during gestation, particularly as there is access to multiple specimens of the same taxon that span an ontogenetic range (Heide-Jørgensen and Garde, 2011; Haddad et al., 2012; Roston et al., 2013; Hampe et al., 2015; Lanzetti et al., 2020; Roston and Roth, 2021). However, most features that define Cetacea, such as loss of external hindlimbs, fluke outgrowth, and hyperphalangy, are established earlier during the embryonic period, where samples or detailed studies are limited. Additionally, prenatal specimens from stranded pregnant females are usually too poorly preserved for use in developmental research as the RNA and proteins have degraded. Given the dramatic morphologies found in cetaceans, there is need for a better understanding of the molecular mechanisms that underpin these traits.

This study describes major features of critical stages of embryonic development in the beluga whale (*Delphinapterus leucas*) and the bowhead whale (*Balaena mysticetus*) taken during legal subsistence harvests in Alaska. Additionally, we describe a pre-somitic *Delphinapterus* specimen and compare our findings to other reports on early-stage cetacean embryos (Stump et al., 1960; Asada et al., 2001). We place these two taxa within the pre-existing cetacean Carnegie staging system developed by Thewissen and Heyning (2007). We highlight specific ontogenetic comparisons between multiple taxa during the embryonic period, notably phalangeal count, the timing of hindlimb loss, and fluke outgrowth from the tail. We discuss major transitions during embryonic development, divergences between mysticetes and odontocetes, and consider heterochronic shifts between the three taxa. We hypothesize a high level of similarity in relative developmental timing of the characters described here between the odontocetes. Thus, we anticipate that *Balaena* will show the greatest degree of heterochronic variation when compared to *Stenella*. Our data demonstrate the importance of utilizing externally visible characters, not just total length or weight, as metrics of developmental staging.

Methods

We examined the external morphology of embryonic and fetal specimens of three cetaceans: *Delphinapterus leucas*, *Balaena mysticetus*, and *Stenella attenuata*. Morphological features used here to define different Carnegie stages have been previously identified and categorized for *Stenella attenuata* (Štěrba et al., 2000; Thewissen and Heyning, 2007). Štěrba et al. (2000) utilized a few embryonic specimens of *Delphinus delphis*, the common dolphin, and *Phocoena phocoena*, the harbor

porpoise, in their staging system as well. All embryos and fetuses referenced herein are currently housed at the Northeast Ohio Medical University in Rootstown, OH, U.S.A.

The referenced collection of *Stenella* embryos was drawn from the Natural History Museums of Los Angeles County (LACM), and, before that, was housed at the National Oceanic and Atmospheric Administration in La Jolla, CA. These *Stenella* embryos were collected as incidental bycatch of the tuna fishing industry in the north Pacific in the 1970s. Both Štěrba et al. (2000) and Thewissen and Heyning (2007) used a portion of this collection to generate their respective staging systems. This collection provides the most complete ontogenetic series of the three taxa referenced here, covering early somitogenesis to fetal development.

In northern Alaska, Iñupiat and Siberian Yupik communities from 11 whaling communities legally harvest *Balaena* on their seasonal migration between the Bering and Beaufort Sea during the spring and fall (Suydam and George, 2021). Pregnant females are occasionally harvested unintentionally, carrying an embryo or fetus. Given that mating appears to be restricted to a short period in March or early April and the gestation of *Balaena* is 13-14 months (Reese et al., 2001; Tarpley et al., 2021), prenatal *Balaena* specimens obtained during these two seasonal harvesting periods include the embryo-fetus transition, mid-gestation, and perinatal fetuses. Collection of samples was led by the North Slope Borough Department of Wildlife Management (NSB-DWM) in collaboration with the Alaska Eskimo Whaling Commission. All specimens were collected under NOAA-NMFS permit 17350.

Iñupiat residents from Point Lay, Alaska also legally harvest *Delphinapterus* for subsistence purposes. The subsistence harvest typically occurs between late-June and mid-July with the migration of *Delphinapterus* within the Kasegaluk Lagoon. Like *Balaena*, only specific age ranges of embryos and

fetuses can be collected due to the timing of mating and harvest: around the embryo-fetal transition

and perinatal, given that *Delphinapterus* gestation lasts approximately 13 months (Suydam, 2009).

The *Delphinapterus* embryos and fetuses described were collected under NOAA NMFS permit 17350

under the lead of the NSB-DWM in collaboration with Point Lay. The collection of embryonic material

for both taxa is made possible through the continued support, generosity, and hospitality of the

communities of Point Lay and Utqiaġvik, Alaska during annual harvests. This work would not be

possible without the cooperation of the subsistence hunters.

The NSB-DWM ID system uses abbreviations to refer to the village in which the embryo was

recovered. Within *Delphinapterus leucas*, the addition of DL indicates the taxon to distinguish

from *Balaena*. The addition of an F at the end differentiates between the mother and the fetus (F).

All *Stenella* specimens references herein were preserved in 70% ethanol at ambient

temperature over several decades before being transferred to NEOMED. These specimens are

currently stored in fresh 70% ethanol at 4°C. The Alaskan cetacean specimens, *Delphinapterus* and

Balaena, were initially fixed in fresh-made 4% PFA mixed with seawater before being transferred to

70% ethanol for long-term storage at 4°C.

To document and describe a presomitic *Delphinapterus* specimen, (NSB-DWM 2017LDL21F),

we used a modified dice-CT protocol specific for embryonic tissue (Hsu et al., 2016, 2019). The

specimen was immersed in iodine overnight before being mounted and embedded in low melt

agarose. This agarose block was scanned on a Bruker SkyScan 1272 micro-CT Scanner at 2 microns at

the Baylor College of Medicine Optical Imaging and Vital Microscopy Core in Houston, Texas. Iodine

staining before micro-CT scanning allows for visible contrast and differentiation between soft tissue

structures. Additionally, iodine is removable from the tissue without causing permanent damage,

allowing for additional analysis via other methods. Using this micro-CT data, NSB-DWM 2017LDL21F

was virtually segmented for analysis of the internal structure using Avizo 2019.4 (ThermoFisher).

After scans were completed, the specimen was extracted from the agarose gel and immersed in

sodium thiosulfate to remove iodine. The specimen was then further prepared for paraffin-sectioned

histology and cut in 6-micron thick sections, mounted on glass slides, and stained using hematoxylin

and eosin.

All specimens described herein were referred to Carnegie stages based on the criteria of the

Stenella staging system (Thewissen and Heyning 2007). With one exception (the presomitic

Delphinapterus embryo), the specimens pertain to Carnegie stage 16-21. All specimen numbers,

lengths, and weights are recorded in Table 1.

Delphinapterus ID (NSB-DWM):	Stage:	CRL/TL (mm):	Weight (g):	Balaena ID (NSB-DWM):	Stage:	CRL/TL (mm):	Weight (g):
2017LDL21F	PS	2	U	1999B7F	17	87	U
2019LDL15F	16	33*	1.2	2018G3F	19	90	4.6
2013LDL6F	17	67*	2.1	2016B9F	20	128	25
2009LDL17F	19	90*	4.1	1999B6F	20	166	U
2011LDL11F	19	93	6.1	2013B1F	21	274	U
2009LDL9F	19	93	U	2000B3F	21	403	U
2019LDL25F	20	134	12.3	2007B16F	23	1,590	U
2013LDL4F	20	136	19.5	2009KK1F	23	1,630	U
2013LDL21F	20	139	20.1	2015B9F	23	4,220	U
2009LDL12F	20	139	19.3				
2017LDL3F	20	153	U	Stenella ID (LACM):	Stage:	CRL/TL (mm):	
2014LDL4F	20	156	39.7	94756	16	11*	
2014LDL5F	20	180	46	94601	16	15*	
2012LDL3F	F	184	64.3	94745	17	17*	
2014LDL7F	F	187	70.1	94820	17	19*	
2012LDL10F	F	197	U	94673	17	20*	
2019LDL11F	F	198	60.5	94717	18	21*	
2012LDL9F	F	200	61.4	94696	19	30*	
2016BDL3F	F	231	131.2	94743	19	34*	
2012BDL1F	F	255	157.6	95051	19	36*	
				90310	20	U	
				94646	20	103	
				95014	20	116	
				94676	20	117	
				94419	21/22	160	
				94413	21/22	151	
				94421	23	252	

Table 1: Summary of the *Delphinapterus*, Balaena, and Stenella embryo collection. Samples are either on loan from the North Slope Borough Department of Wildlife Management (NSB-DWM) or from the Natural History Museums of Los Angeles County (LACM). Village abbreviations: L: Point Lay, B: Barrow (Utqiaġvik), G: Gambell, KK: Kaktovik, Alaska. Within *Delphinapterus* leucas, the addition of DL indicates the taxon to distinguish from Balaena. All measurements rounded to nearest millimeter or nearest tenth of a gram. Measurement of crown-rump length (CRL) indicated with an asterisk*, total length (TL) indicated otherwise. Weight is wet weight after fixation. Unknown data points indicated with U. F = Fetus

Results

    Delphinapterus specimen NSB-DWM 2017LDL21F was collected from a sexually mature

female. One ovary had a corpus luteum, indicating pregnancy. The embryo has an oval shape,

approximately 2 mm in length and 1 mm in width, with a short, curved process and extensive fetal

membranes. These membranes were not embedded within the endometrium of the mother's uterus.

Fetal membranes: The membranes surrounding NSB-DWM 2017LDL21F (Figure 4A) are attached to one of the narrow ends of the specimen, at the same end as the curved process (red arrow). A narrow sac surrounds the embryo (Figure 4A, green arrow), and extraembryonic membranes surround both structures. A long, thin curled strip of tissue projects from this smaller sac (Figure 4A, orange arrow). Attached to the large extraembryonic membranes are two smaller pouches. Their attachment is by a narrow strip of opaque tissue (Figure 4A, blue arrow). All the external supporting membranes are similar in consistency.

External Morphology: The most prominent feature found on this specimen is the small, curved process (Figure 4C, red arrow) on one end of the embryo. In addition, there are two paired processes (Figure 4B) on the flat surface opposite of the curve process. These encircle a small pit (Figure 4D). Near these processes are two dense patches, one of which is visible in Figure 4C (arrow). On the surface opposite the paired projections, a thickened ridge of tissue occurs that may represent the presumptive midline of the specimen (Figure 4E, arrow).

Internal Morphology: Virtual segmentation of the micro-CT data reveals that the specimen has an internal cavity that is divided into regions. Towards the end of the specimen with the curled projection, two smaller chambers are separated by a thin septum. These chambers are a bilaterally symmetrical space with a small tissue projection into the center (Figure 4F). These chambers are not connected to a second space that constitutes the majority of the internal structure of the specimen (Figure 4G).
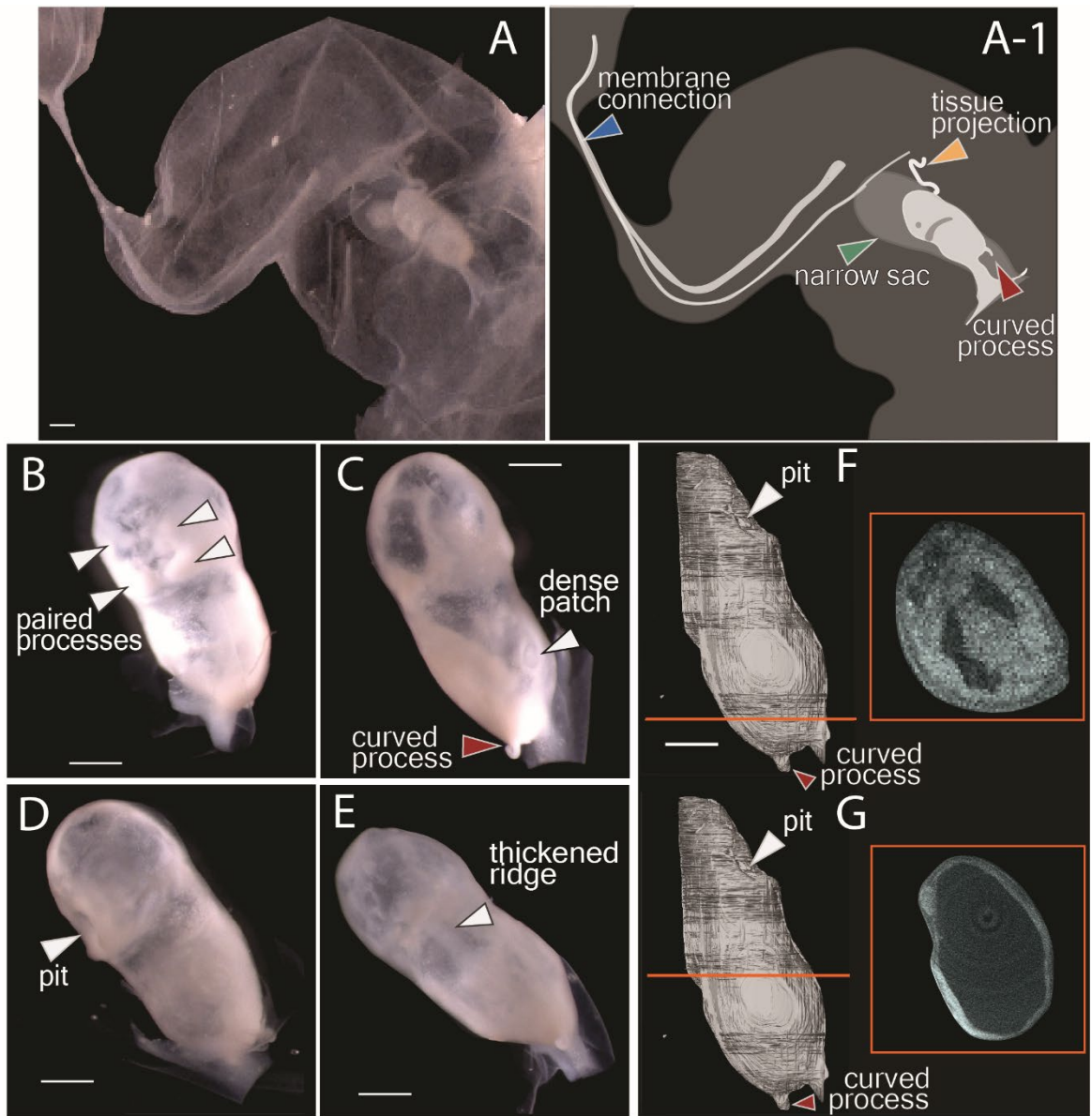
Figure 4: Photographs (**A-E**) and micro-CT images (**F-G**) of the presomitic Delphinapterus embryo (NSB-DWM 2017LDL21F). **A**: Specimen with supporting membrane with descriptive diagram of notable structures indicated to the right (**A-1**). **B-E**: Photographs of embryo with membranes removed. **F-G**: Micro-CT reconstructions with cross-sectional morphology. Orange line indicates plane of section. Scale bar equals 1 millimeter.

Histology: We describe four representative slides from this *Delphinapterus* specimen.

      Figure 5A – This section shows the curved process attached to the narrow end of the embryo (1, red arrow). This hypercellular region has little extracellular matrix. A large lumen is present in the main body of the specimen in this section (2, green arrow). This lumen is lined by a simple epithelium that is cuboidal or columnar in appearance. Nearly all of the cells in this outer layer are vacuolated. A connective tissue surrounds the lumen of the cavity; there is no endothelium. Two patches of circumferentially arranged mesenchymal tissue occur on the sides, with nuclei that are more dispersed compared to surrounding tissue and there are larger swaths of extracellular matrix (3, orange arrows).

      Figure 5B – The large cavity described in Figure 5A is also visible in this slide. The section is predominantly comprised of large regions of undifferentiated connective tissue. There is a small region of connective tissue that projects back into the lumen (4, blue arrow). As in Figure 5A, there is no epithelium lining the internal cavity. The internal connective tissue is hypercellular and shows no obvious architecture or differentiation. Patches of erythrocytes are scattered throughout the internal region (5, yellow arrow).

      Figure 5C – Unlike previous sections, some anatomical structures are apparent in this section. The most obvious is a large crescent-shaped region dense with erythrocytes that lacks an endothelial layer (6, purple arrow). This area may represent a cardiogenic region. The undifferentiated, patchy connective tissue in Figures 2A and 2B is replaced by a connective tissue internal to the blood-filled region. The connective tissue in this section has a patchy organization compared to the connective tissue seen in previous sections. External to the blood region are several layers of circumferentially arranged mesenchymal cells that appear morphologically similar to the two small lateral patches

found in Figure 5B. In the area surrounding the lumen, the morphology of the cells is different from previous sections. The connective tissue surrounding the lumen in Figure 5C is more diffuse, with more extracellular matrix between cells. In Figure 5B, this area was filled with cells that were homogenous and undifferentiated; in this section, there are differences between the mesenchyme and a small, densely cellular connective tissue layer that lines the cavity (7, pink arrow). Neither connective tissue layer has an endothelial layer. The appearance of this densely cellular connective tissue is similar to the hypercellular regions found in Figures 5A and 5B. In this section, a simple columnar epithelium encircles the different connective tissues, with some areas demonstrating a simple squamous morphology. No basement membrane is apparent between the epithelial and connective tissue layers. Some of the extraembryonic membranes (8, black arrow) are visible, although they do not attach directly to the specimen in this section.

Figure 5D – There is a centrally located patch within this section that is distinct from any other tissue observed thus far and is glandular in appearance (9, gray arrow). In previous sections there is a large lumen. In this section, this space is reduced in size, and it is surrounded by a hypercellular connective tissue with little extracellular matrix and no corresponding endothelium (7, pink arrow). This region appears to be more densely populated with cells than the corresponding layer in Figure 5C. The epithelium is predominantly squamous in this section, and most of the cells have vacuolated nuclei similar to Figure 5A. Most of the connective tissue is mesenchymal in appearance, although more densely packed than Figure 5C. The large blood-filled crescent is now reduced to a few small patches surrounding this glandular circle. The connection between the specimen and extraembryonic membranes is visible here (8, black arrow). At this connecting point, nuclei from the specimen appear to be circumferentially oriented around the attachment to the membranes. The

membranes themselves are largely comprised of extracellular matrix with a few nuclei that do not appear to be arranged. There is no epithelial tissue in this region.
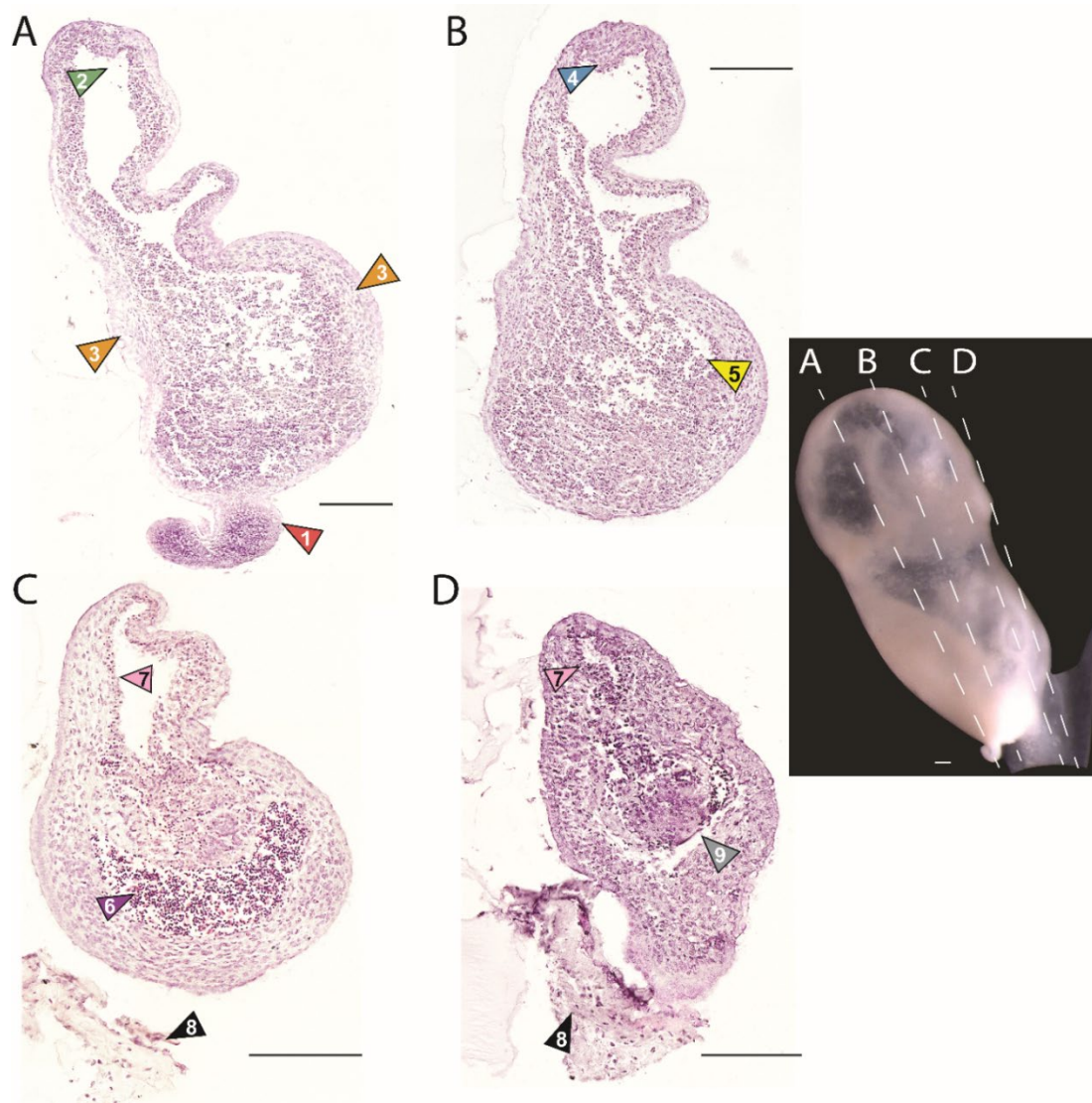
Figure 5: Histological sections for presomitic Delphinapterus embryo (NSB-DWM 2017LDL21F). Sections 6-microns thick and stained with hematoxylin and eosin. Scalebars equal 200 micrometers. **A**: 1, red– curved projection, 2, green – lumen, 3, orange– mesenchymal tissue. **B**: 4, blue– tissue projecting into lumen, 5, yellow– erythrocytes. **C**: 6, purple– erythrocyte region, 7, pink – connective tissue lining lumen, 8, black– extraembryonic membranes. **D**: 9, gray arrow – glandular cells. **Right**: A photograph of the embryo with dashed lines indicating the approximate plane of section for each histological image.

Comparative embryogenesis of *Delphinapterus*, *Balaena*, and *Stenella attenuata*

Stage 16: Carnegie stage (CS) 16 is characterized in *Stenella attenuata* by the absence of branchial clefts, and presence of a handplate, and eye pigmentation (Thewissen and Heyning, 2007).

Delphinapterus—In *Delphinapterus* specimen NSB-DWM 2019LDL15F (Figure 6A), there is a low eminence located just lateral to the genitals that we hypothesize is the hindlimb bud. This hindlimb bud has a pointed protrusion on the outermost edge of the structure. The gut is herniated into the umbilical cord. Just beneath the hernia, a small genital tubercle is present. The tail is elongated with no lateral outgrowths or indication of fluke formation. There is clear eye pigmentation and no formation of eyelids (Figure 6B). The nasal placodes are relatively large and divided within the fused medial and lateral frontonasal prominences. The left and right nasal prominences are located far from the midline and are located rostrally on the head, which is typical for mammalian development at this stage. The external acoustic meatus is marked by a small posterior prominence.

Comparisons with *Stenella*— Like the stage 16 *Stenella* embryo (Figure 6C), the *Delphinapterus* specimen (NSB-DWM 2019LDL15F) has eye pigmentation, no branchial clefts, and a handplate. The *Delphinapterus* handplate is mediolaterally expanded, dorsoventrally flat with digital rays with no individual phalangeal segments. This morphology is reached at a later stage in *Stenella*, which does not form digital rays until CS 17. The digital rays of *Delphinapterus* are present as anlagen. Both *Delphinapterus* and *Stenella* embryos at CS 16 have hindlimb buds. In *Stenella*, this is the stage where hindlimb buds begin to regress.

Stage 17: Carnegie stage 17 in *Stenella* is defined by digital ray formation, a digit III that is longer than digit II, and initiation of fluke outgrowth (Thewissen and Heyning 2007).

Delphinapterus— In this *Delphinapterus* specimen (NSB-DWM 2013LDL6F, Figure 6D), individual digit rays are visible within the flipper and the forelimb shows slight differential outgrowth of digits, with digit III being nearly equal in length to digit II. Hyperphalangy is present in this specimen and readily visible with five individual phalanges visible in digits III and IV. The presence of hindlimb buds cannot be determined due to damage to the abdomen. Loops of small intestine protrude into the umbilical cord, as they do in later embryos. This is the first stage that shows initiation of lateral fluke outgrowths, appearing as a small diamond. The eye is pigmented with no eyelid (Figure 6E). A small hillock is located posterior to the external acoustic meatus. Left and right nasal pits are separated in the midline from each other, though greatly reduced in size in comparison to the Carnegie stage 16 *Delphinapterus* specimen, NSB-DWM 2019LDL15F.

Balaena— This *Balaena* specimen (NSB-DWM 1999B7F, Figure 6F) has a pointed flipper with segmentation of the individual phalanges. Digits II and IV have four phalanges while digit III has five. Digit III is also longer than digit II. The intestines are herniated into the umbilical cord. The hindlimb bud is small and round. There are small fluke outgrowths budding off the tail, creating a slight diamond shape (Figure 11). The eye has no visible pigmentation, and the eyelids are fused. There is a large auricular hillock present, with a smaller hillock just superior to it. The external acoustic meatus is located just posterior to these hillocks. Along the curved rostrum, there is a distinct notch for the nasal pits, which are unfused along the midline.

Comparisons with *Stenella*—The flipper in this *Delphinapterus* specimen (Figure 6A) is more developed than the *Stenella* flipper (Figure 3G). The *Delphinapterus* digits are segmented, and digits II and IV are hyperphalangeous, while the *Stenella* digital rays have not yet segmented. All other features mentioned for *Delphinapterus* are similar to *Stenella* embryos of this stage, including most notably fluke outgrowth (Figure 10).

Like the *Delphinapterus* embryo, the *Balaena* flipper has a more developed morphology, with hyperphalangy already clearly present. Hyperphalangy is present in digits II, III, and IV in *Balaena*. At this stage, digits II and IV have equal numbers of phalanges in *Delphinapterus*. Digit III of *Balaena* has the greatest number of phalanges for that taxon at five while the other hyperphalangeous digits, digits II and IV, have four phalanges. While both the *Balaena* and *Stenella* have a visible beak at this stage, the *Balaena* rostrum is already highly elongated and ventrally curved compared to the smaller *Stenella* beak.
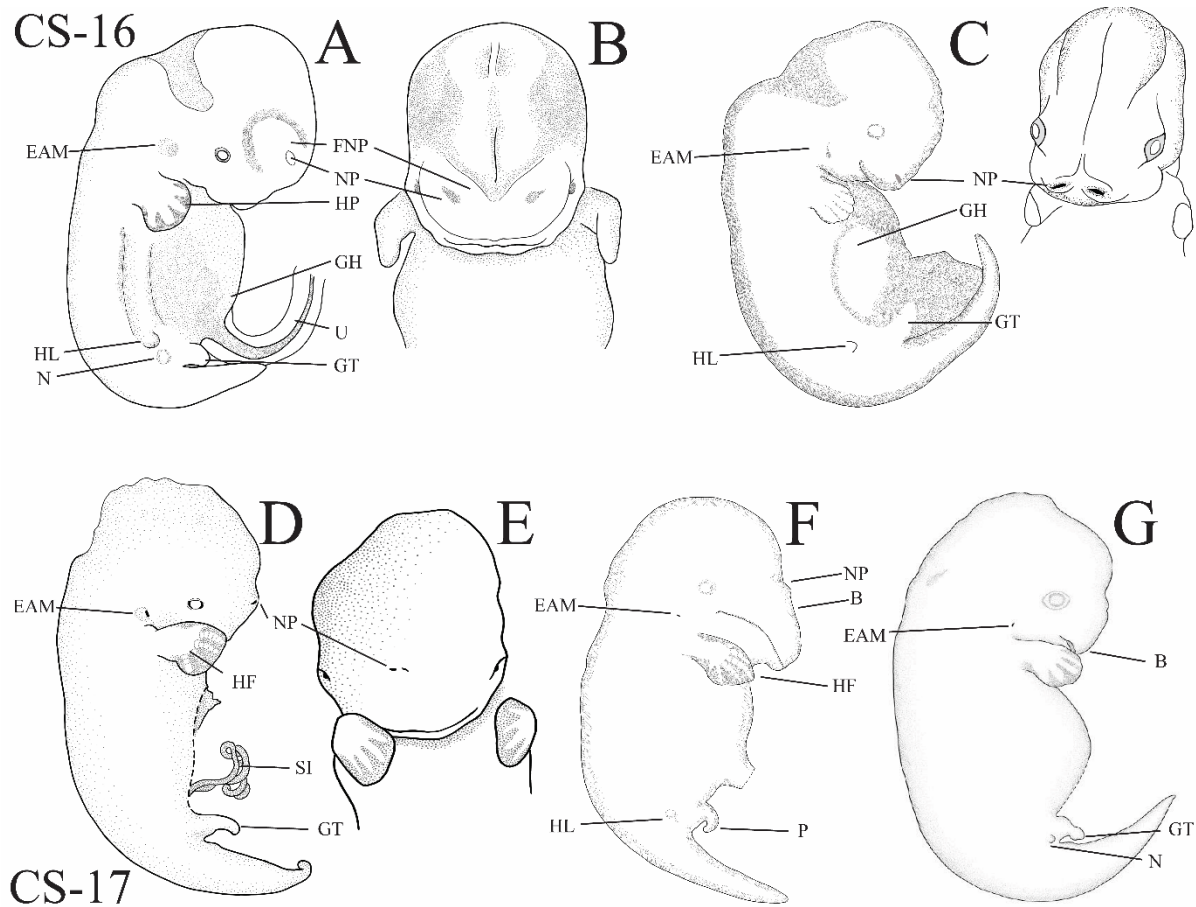
Figure 6: Embryos of *Delphinapterus* (**A, B, D, E**), *Balaena* (**F**) and *Stenella* (**C, G**) for Carnegie stages 16 and 17. All *Delphinapterus* specimens shown in left lateral and frontal view. All *Balaena* and *Stenella* specimens shown in left lateral view. **A, B**: NSB-DWM 2019LDL15F. **C**: LACM 94756. **D, E**: NSB-DWM 2013LDL6F. **F**: NSB-DWM 1999B7F, **G**: LACM 94673.

EAM: external acoustic meatus, FNP: frontonasal process, NP: nasal pits, HP: handplate, U: umbilicus, GH: gut herniation, GT: genital tubercle, HL: hindlimb, HF: hyperphalangeous flipper, SI: small intestine, P: penis, B: beak. Not to scale.

Stage 18: Carnegie stage 18 is defined in *Stenella* by digits II and III being equal in length. At this stage, the flipper takes on a hydrofoil shape and the digital rays are still cartilaginous with no evidence of joint formation. Our collection does not include *Delphinapterus* or *Balaena* specimens that display these combined features. This gap may suggest that variation in flipper development between *Stenella*

and the other taxa predates this stage, given that both *Delphinapterus* and *Balaena* embryos already

have asymmetry between digits II and III before this stage that is more prominent than the variation

seen in *Stenella*.

Stage 19: In *Stenella*, Carnegie stage 19 is defined by a digit II that is longer than digit III and the

emergence of a distinct beak (Thewissen and Heyning, 2007).

Delphinapterus— In these embryos (NSB-DWM 2009LDL17F, 2011LDL11F, 2009LDL9F), the

forelimb is distinctly angular, transitioning from a rounded handplate to a flipper (Figure 7A). Digit II

is both slightly longer and has more phalanges than digit III. There appears to be five phalanges in

digit III. The umbilical hernia is still present, although reduced in comparison to younger specimens.

The genital tubercle is present as a small protrusion. In all three specimens, the fluke shape is still

lanceolate in appearance. The dorsal and ventral keels of the tail and flukes begin forming. One

specimen (NSB-DWM 2009LDL17F) has a prominent external acoustic meatus on the lateral aspect of

the head (Figure 7B**)** while the other two specimens have small prominences posterior to the meatus.

The eye is pigmented, and the eyelids are visible but not fused. A small beak is forming. The left and

right nasal prominences are located near the midline and are separated by a thin strip of tissue.

Balaena— The *Balaena* forelimb is well-developed, with obvious digit asymmetries and

hyperphalangy (Figure 7C). Digit III is longer than digit II, with four phalanges in digit II and five

phalanges in digit III. Specimen NSB-DWM 2018G3F has visible paired protrusions next to the penis as

discussed in detail in **chapter 4**. This embryo also has moderate cervical flexion. The umbilical hernia

of this specimen is almost entirely retracted into the body wall. The flukes are still diamond-shaped in

appearance, although they are markedly wider than in earlier Carnegie stages. There is a small process posterior to the external acoustic meatus (Figure 7D). The eyelids are visible and unfused. The two nasal pits are unfused and bilaterally symmetrical. The rostrum is elongated. There is no indication of either tooth or baleen formation.

Comparisons with *Stenella*— All features listed in *Delphinapterus* are also present in the *Stenella* embryos (Figure 7E) except for the phalangeal counts within the hyperphalangeous flippers. *Delphinapterus* phalangeal counts are 1/5/4/3/3. The *Stenella* embryos show a more extreme form of hyperphalangy in digit II, with phalangeal counts of 1/7/4/2/1. Additionally, though both odontocete taxa demonstrate emergence of the beak at this stage, the protrusion of the beak is less prominent in the *Delphinapterus* embryos than the *Stenella* specimens, consistent with postnatal morphology.

The *Balaena* specimen shows distinct heterochronic differences with the odontocetes. The eyelids and fluke morphology of NSB-DWM 2018G3F suggest that this specimen is in stage 17 and the presence of hindlimbs in this specimen is comparable to a CS 16 *Stenella* or *Delphinapterus* embryo. However, digit III is longer than digit II in *Balaena*, in contrast to the defining characteristic of this stage for *Stenella*. NSB-DWM 2018G3F shows a distinctly elongated rostrum, which would suggest that this embryo is in the CS 19 category. The ontogenetically younger *Balaena* embryo NSB-DWM 1999B7F also has a long rostrum, indicating that this feature appeared at an earlier stage. We place *Balaena* into this stage based on the exclusion of defining features for Carnegie stages 20, 21, 22, or 23, which are found in ontogenetically older *Balaena* embryos and fetuses.

Stage 20: Stage 20 captures the transition from embryonic to fetal development in *Stenella*, as indicated by retraction of the umbilical hernia and fusion of the eyelids (Thewissen and Heyning, 2007).

Delphinapterus— In the *Delphinapterus* stage 20 specimens (Table 1), the forelimb has a clear flipper shape with prominent hyperphalangy (Figure 7F). Digits II and III are almost equal in length in some specimens, (NSB-DWM 2017LDL3F, 2014LDL4F), although digit II is slightly longer than digit III for the other *Delphinapterus* specimens in this stage. Despite variation in digit length, digit II consistently has more phalanges than digit III. As one example, NSB-DWM 2009LDL12F has eight phalanges in digit II and six phalanges in digit III. The embryos no longer exhibit significant cervical or lumbar flexion in the trunk and minimal ventral flexion at the tail base. Gut herniation is now fully retracted into the abdomen. The flukes change shape during this stage; smaller CS 20 specimens have a spade-shaped fluke while the larger specimens have a heart-shaped morphology. The fluke notch becomes apparent in larger embryos at this stage. Unlike previous stages, fluke width is greater than fluke length in the largest specimens (NSB-DWM 2014LDL4F, 2014LDL5F) when measured from the fluke notch to the peduncle (the base of the fluke). Posterior to the external acoustic meatus is a small protrusion from the head (Figure 7G). Fusion of the two nasal prominences is apparent at this stage, with only one slit visible on the surface. The blowhole has migrated caudally in comparison to the earlier stages of *Delphinapterus* specimens and is located towards the crown of the head. The upper and lower eyelids are partially to fully fused.

Balaena— The forelimbs of both *Balaena* specimens (NSB-DWM 1999B6F, 2016B9F) have an adult-like flipper, with hyperphalangy and a hydrofoil shape (Figure 7H). Digit II has three phalanges,

a reduction in phalangeal count by one compared to the CS 19 *Balaena* specimen (NSB-DWM 2018G3F). Cervical flexure in these stage 20 specimens is greatly reduced, though the neck is still slightly bent. The umbilical hernia is fully retracted. These specimens have an elongated rostrum, eye pigmentation, and eyelids. The nasal pits are symmetrically paired at the midline (Figure 7I). The oral cavity and rostrum are longer than in stage 19. Baleen is not present in either specimen.

Comparisons with *Stenella*— The differences between *Stenella* (Figure 7J) and *Delphinapterus* are similar to the morphological disparities seen between post-natal specimens. The flippers of *Delphinapterus* are more rounded and mediolaterally wider than the pointed, narrow *Stenella* flippers. Additionally, the differences in beak shape observed in stage 19 are even more prevalent at stage 20. Both *Balaena* and *Stenella* specimens have elongated rostra. In contrast, the *Delphinapterus* specimens have a comparatively short beak. The flukes of *Stenella* at this stage are diamond-shaped in smaller specimens while the largest CS 20 specimens have spade-shaped flukes. In contrast, *Delphinapterus* have spade- and heart-shaped flukes while the *Balaena* specimens have diamond- and club-shaped flukes (Figure 11). At this stage, the flukes of *Stenella* are less developed than the flukes of the Arctic taxa.

Balaena at this stage have an elongated curved rostrum, which differs from the *Stenella* embryos. The nasal pits of both odontocete taxa are fused in the midline to form the blowhole, while the *Balaena* specimens maintain two distinct pits. This is a common feature of mysticetes and represents a divergence between the toothed and baleen whales (Klima, 1999).

Fetal Specimens: In the Carnegie system for *Stenella*, the differentiation between fetal stages 21, 22, and 23 are the emergence of tactile hairs, eyelid separation, and skin pigmentation, respectively (Thewissen and Heyning 2007). It is important to note that the features defining fetal stages 21 and 22 emerge within a short developmental window. Thus, many *Stenella* are simply defined as Carnegie stage 21/22 to accommodate the extensive overlap.

Delphinapterus— These *Delphinapterus* specimens (NSB-DWM 2012LDL3F, 2014LDL7F, 2012LDL10F, 2019LDL11F, 2012LDL9F, 2016BDL3F, 2012BDL1F) cannot be assigned to stages 21-23 due to the lack of hairs, eyelid separation, or skin pigmentation (Figure 7K, 7L). The features that define these fetal stages in *Stenella* are not found in any of the largest *Delphinapterus* in our collection. These differences may be due to heterochronic shift of all three traits within these whales, or these features may occur in *Delphinapterus* fetuses that are developmentally older than the ones within our collection. All flipper and facial traits remain similar between stage 20 and these larger *Delphinapterus* specimens. Fetal specimen NSB-DWM 2012LDL10F has seven phalanges within digit II and five phalanges for digit III, which is a reduction in one phalanx per digit compared to stage 20 *Delphinapterus* specimen NSB-DWM 2009LDL12F. The other difference is a change in fluke shape (Figure 9A). Although not described in Thewissen and Heyning (2007) as differential criteria, stages 20 and 21 *Stenella* embryos have differently shaped flukes. *Stenella* stage 20 specimens have heart-shaped flukes while stage 21/22 specimens have triangular-shaped flukes, suggesting that there is a transition in fluke shape through these fetal stages (Figure 9A).

Balaena— *Balaena* fetuses are not significantly different in morphology between stage 20 and 21 (Figure 7M). One specimen in our collection represents stage 21, DWM-NSB 2000B3F (Figure 7M).

This specimen is nearly identical to the stage 20 *Balaena* specimens. The flipper is hyperphalangeous, with five phalanges on digit III. The flukes are more developed, achieving a triangular-shaped morphology in stage 21, and the body has pigmentation. The major morphological transition left between this stage and birth is the development and emergence of baleen. Thewissen et al., (2017) classifies these fetal *Balaena* with baleen as stage 23 (NSB-DWM 2007B16F, 2009KK1F, and 2015B9F). The animals listed in that study are approximately four times larger than this stage 21 *Balaena* fetus.

Flipper Size- *Delphinapterus* and *Balaena* whale embryos display segmentation of their digital rays and hyperphalangy at an earlier Carnegie stage than *Stenella*. At stage 17, both *Delphinapterus* and *Balaena* embryos have clearly defined digital rays and individual phalanges are readily identifiable (Figures 6D, 6F). Phalangeal segmentation is not observed in *Stenella* until Carnegie stage 19 (Cooper et al., 2017), though stage 18 embryos show length asymmetries between digits II and III (Figures 6G, 7E). Despite the later onset of phalangeal segmentation in *Stenella*, this taxon has more phalangeal segments in the longest digit than either *Balaena* or *Delphinapterus* (Figure 5).

At CS 20, both Arctic taxa have 5-6 phalanges in their longest digit ray, digit II in *Delphinapterus* and digit III in *Balaena* (Thewissen et al., 2021a), while a similarly staged *Stenella* fetus has eight phalanges in digit II (Cooper et al., 2007a, 2017) (Figure 8A). As such, the *Stenella* flipper is proportionally longer proximodistally and anteroposteriorly thinner than the other fetal cetacean specimens at CS 20. *Delphinapterus* and *Balaena* have similar flipper growth trajectories despite differences between digit II and digit III as the longest digit. *Stenella*, having extreme hyperphalangy, has a growth trajectory that is markedly different from the other cetaceans (Figure 8A).

Fluke Size- During embryonic development, all three taxa initiate fluke growth at approximately the same Carnegie stage. Cetacean fluke growth proceeds from a small, diamond-shaped outgrowth through a series of intermediate shapes before arriving at taxon-specific morphologies. Our data suggest that *Delphinapterus* initiates fluke growth and then gradually increases fluke width relative to tail length, where tail length is defined by the distance from the genitals to the tip of the fluke notch (Figure 9). In contrast, *Stenella* has a more elongate tail relative to fluke width for initial stages of fluke growth but attains rapid lateral fluke outgrowth in the early fetal period. *Stenella* is the only taxon to achieve an adult-like fluke early in the fetal period. Both odontocete taxa initiate small lateral fluke outgrowths around Carnegie stage 17 and then show a rapid transition from this diamond-shaped morphology to a spade- or heart-shaped intermediate morphology.

Fluke ontogeny for *Balaena* is not completely documented within specimens available to us, although several insights can be gleaned. At Carnegie stage 20, the two specimens have nearly identical tail length but differently shaped flukes (Figure 9A, B). DWM-NSB 2016B9F has a total length of 122.6 mm, genital to fluke notch length of 24.8 mm, fluke width of 8.7 mm, and a spade-shaped fluke. DWM-NSB 1999B6F has a total length of 166 mm, genital to fluke length of 25.6 mm, a fluke width of 16.68 mm, and a heart-shaped fluke. It appears that fluke growth increases with total body length, although the tail length remains relatively stable. While all three taxa initiate fluke outgrowth at Carnegie stage 17, the taxon-specific differences in lateral outgrowths become readily apparent (Figure 9A).
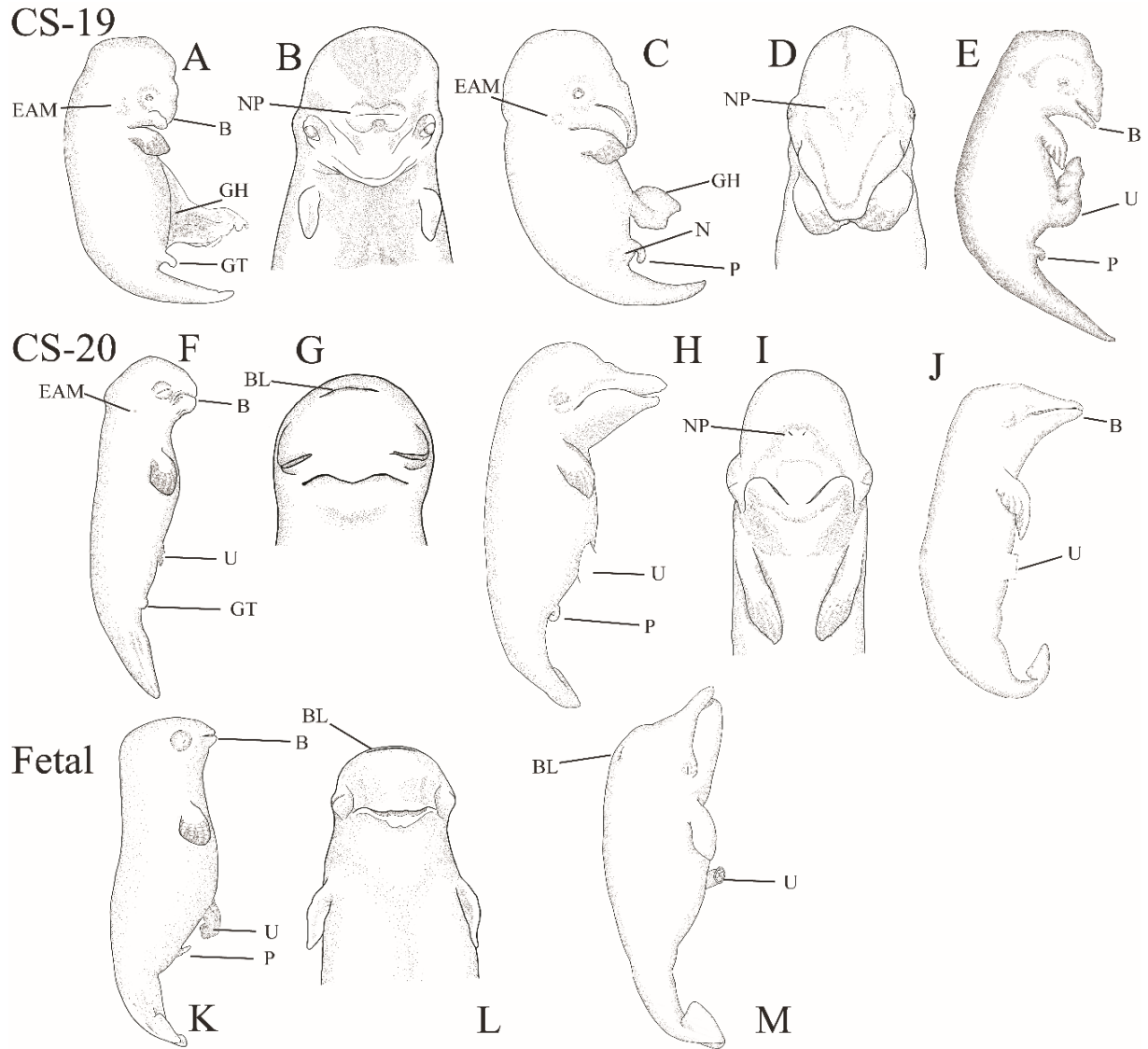
Figure 7: Embryos and fetuses of *Delphinapterus* (**A, B, F, G, K, L**), *Balaena* (**C, D, H, I, M**) and *Stenella* (**E, J**) for stages 19, 20, and fetal. All *Delphinapterus* and *Balaena* specimens shown in left lateral and frontal view. All *Stenella* specimens shown in left lateral view. **A, B**: NSB-DWM 2009LDL17F. **C, D**: NSB-DWM 2018G3F. **E**: LACM 94743. **F, G**: NSB-DWM 2009LDL12F, **H, I**: NSB-DWM 2015B9F, **J**: LACM 95014. **K, L**: NSB-DWM 2012LDL10F, **M**: NSB-DWM 2000B3F. EAM: external acoustic meatus, B: beak, BL: blowhole, NP: nasal pits, GH: gut herniation, GT: genital tubercle, N: nipple, U: umbilicus, P: penis. Not to scale.
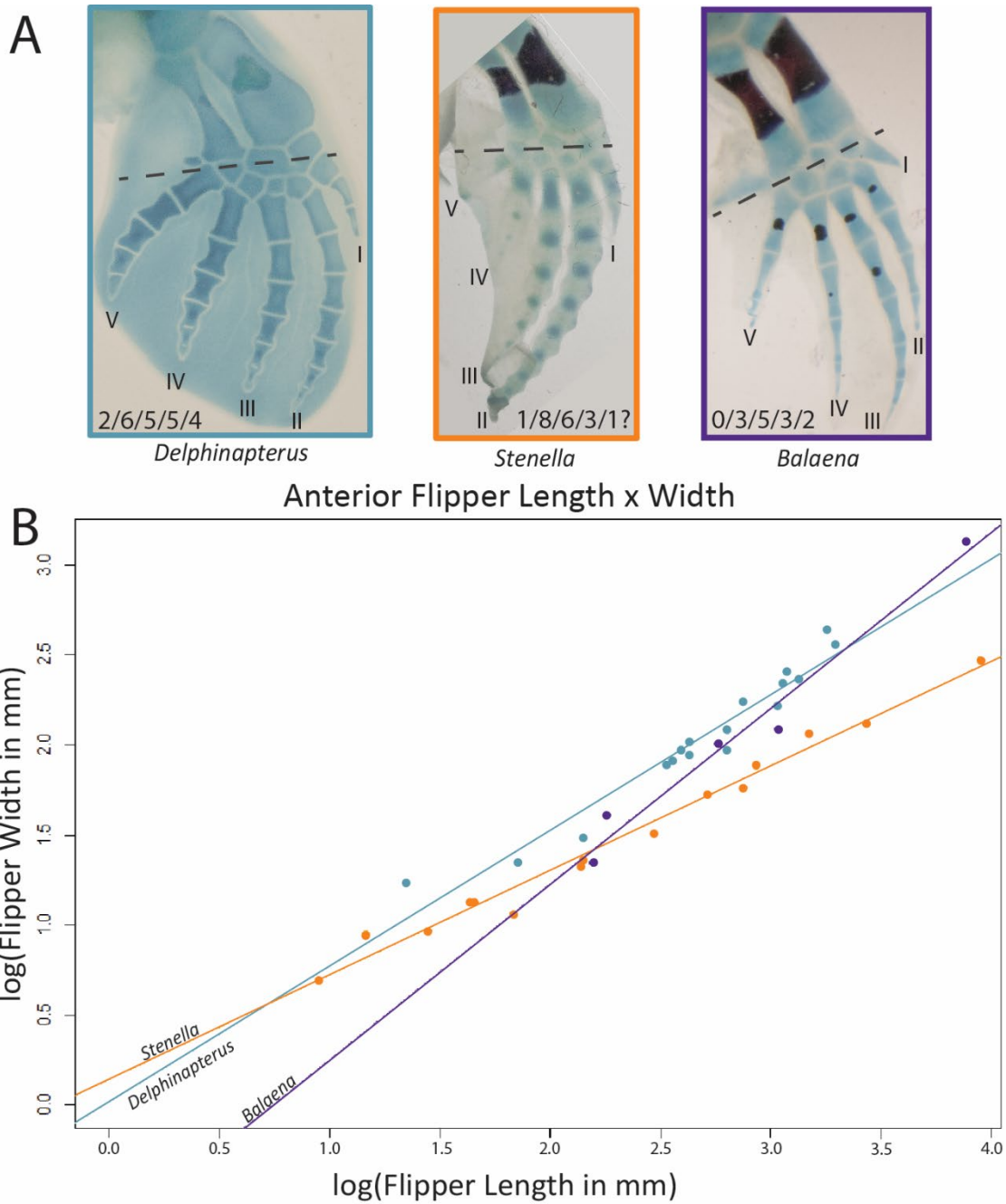
Figure 8: **A**: Flippers of CS 20 NSB-DWM 2012LDL9F *Delphinapterus* (left, blue), CS 20 LACM 90310 *Stenella* (middle, orange), and CS 21 NSB-DWM2000B3F *Balaena* (right, purple). Cartilage is stained with alcian blue, and bone is stained with alizarin red. **B**: Graph shows relationship between anterior flipper length, from axilla to leading edge, and flipper width, taken at the midcarpal joint. Dashed lines in the photos (**A**) represent plane of measurement, digits indicated by roman numerals. Scalebar equals 0.5 cm.
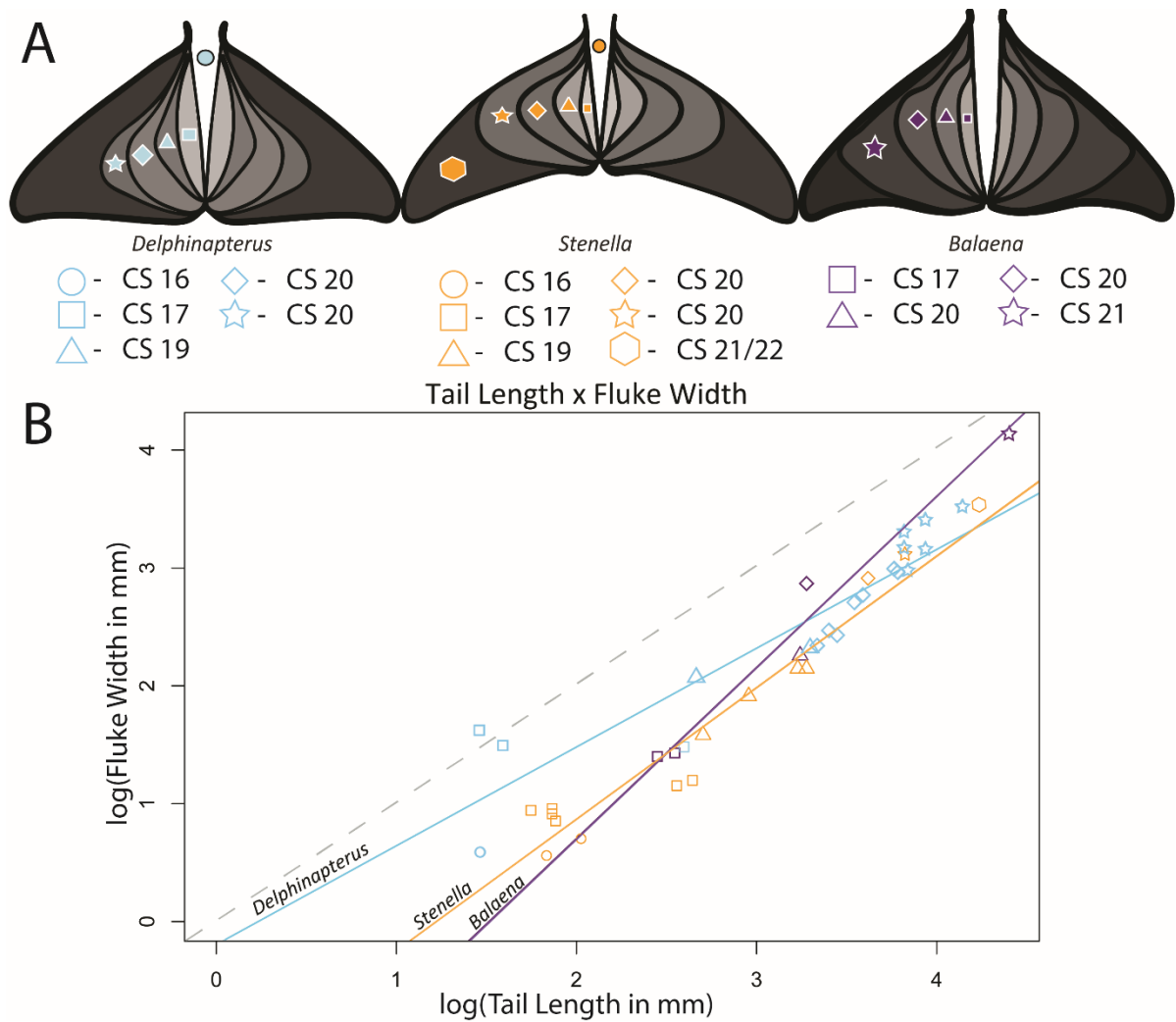
Figure 9: **A**: Diagrams of ontogenetic fluke growth morphologies for *Delphinapterus* (left), *Stenella* (middle), and *Balaena* (right). Shapes embedded within fluke illustrations correspond to intermediate growth morphology plotted on graph. **B**: Measurements, taken to the nearest millimeter, include tail length from genital tubercle to fluke tip, and maximum width of fluke. Dashed line shows isometry. Diagrams not to scale.

Discussion

Presomitic *Delphinapterus* Specimen (NSB-DWM 2017LDL21F) – This specimen is

ontogenetically younger than any staged *Delphinapterus* embryos. However, when compared to other

cetacean embryos, NSB-DWM 2017LDL21F is more developed than the *Balaenoptera acutorostrata*

morula described in Asada et al., (2001), which may be one of the youngest cetacean embryos described.

The fetal membranes appear similar to the supporting membranes in humpback whale (*Megaptera novaeangliae*) embryos shown in Stump et al. (Stump et al., 1960). Both our *Delphinapterus* specimen and the *Megaptera* supporting membranes referenced in Stump et al., (1960) are long and thin, with two projections from a centralized region where the embryo is contained. However, these specimens are remarkably different in structure despite similarities in fetal membrane morphology. The *Megaptera* specimen from Stump et al. (1960) already appears to be post-somitic whereas this *Delphinapterus* specimen shows no indications of somitogenesis. In a typical mammalian embryo at the gastrulation or neurulation stage, we would expect to find structures such as a primitive streak, notochord, or neural tube. However, none of these morphological characteristics are readily found in NSB-DWM 2017LDL21F.

Given the unusual appearance of this specimen, we hypothesize that NSB-DWM 2017LDL21F is an aberrant embryo that would have eventually been incompatible with life. There is considerable evidence that *Delphinapterus* have a synchronized mating schedule (Steinman et al., 2012). The narrow window of early development showcased by the embryos and fetuses collected from the harvests in Point Lay, Alaska, between Carnegie stages 16 and 21, are consistent with a constrained breeding season. Our presomitic specimen is clearly younger than other embryos collected from Point Lay, which further supports our conclusions that this embryo had likely ceased development prematurely.

Externally, the specimen showed clear bilateral symmetry with a number of structures resembling a potential stomodeum (Figure 4D) or notochord (Figure 4E). However, virtual segmentation and histological sectioning of the specimen do not reveal any cell types associated with these structures. Furthermore, there is clear differentiation of some tissues within the histological sections, however, the relationships of these cell types do not indicate any organized organ primordia. For example, we see a potentially cardiogenic region based on the presence of red blood cells and mesenchymal tissue (Figure 5C). However, that morphology does not appear to match cardiac primordia from similarly staged pig embryos (Patten, 1931). Furthermore, at approximately this gestational age in humans, the embryo and fetal membranes are similar in size (O'Rahilly and Müller, 2001). In this specimen, the fetal membranes were several times larger than the embryo. This suggests that the development of this *Delphinapterus* embryo was arrested while the membranes continued to grow.

Staging System— Our analysis of cetacean embryos reveals developmental variation between *Delphinapterus*, *Balaena*, and *Stenella* (Figure 10). Some features, such as the blowhole, display embryonic timing differences between odontocetes and mysticetes. While the developing nasal cavities initiate as paired processes during development in all cetacean taxa, eventually the two nares will fuse in the midline in odontocetes, forming one blowhole. For *Balaena* and other mysticetes, the nares remain separated by a septum throughout life. There is a fair body of evidence suggesting that odontocetes and mysticetes have differential patterns of development that lead to two separate mechanisms of blowhole orientation within the skull (Kellogg, 1928; Oelschläger, 1989; Armfield et al., 2011; Moran et al., 2011; Roston and Roth, 2021).

Other features, such as rostrum formation, do not follow systematic divisions and thus may represent areas of heterochronic development. Both *Balaena* and *Stenella* develop an elongate, prominent rostrum by Carnegie stage 18, whereas in *Delphinapterus* the oral cavity remains comparatively short (Figure 10). The most prominent morphological changes that contribute to the Carnegie staging system are within the flipper, hindlimb bud, and fluke.
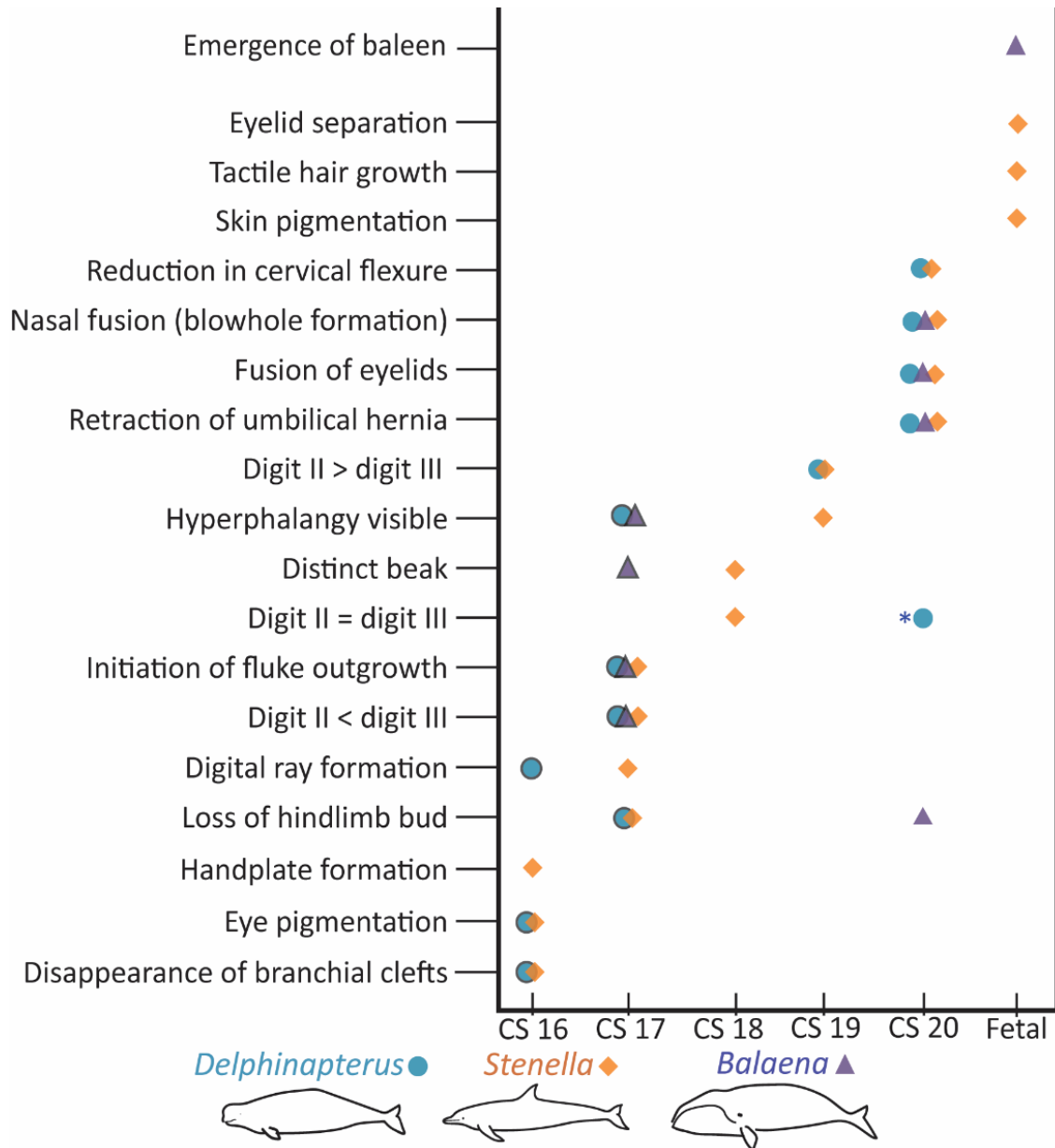
Figure 10: Heterochronic development between *Stenella*, *Delphinapterus*, and *Balaena*. Symbols indicate the presence of specific characters within these taxa. Outlined points indicated traits identified in one specimen. If no point is shown that trait was not able to be identified in our collection either due to developmental variation or sampling bias. * - Only occurs in some of the CS 20 *Delphinapterus* specimens, the flipper typically maintains digit II > digit II in both phalangeal count and absolute length.

Flipper – The most prominent difference between these taxa is the variation in the longest digit of the flipper and the degree of hyperphalangy on each digit (Table 2).

	Delphinapterus	*Stenella*	*Balaena*
CS 16	Digital rays, no segmentation	Handplate	Unknown
CS 17	?/5/3/5/2	Digital rays, no segmentation	0/4/5/4/3
CS 18	N/A	Digital rays, no segmentation	N/A
CS 19	?/6/5/5/3?	1/7/4/2/1?	0/3/5/4/3
CS 20	2/6-8/5-6/5/4	1/8/6/3/1?	0/3/5/3/2
Adult	0-3/6-8/5-7/5-6/4-6	1/7-9/4-6/1-2/0-1	0-2/3-4/4-5/3-4/2-3

Table 2: Summary of phalangeal counts for relevant Carnegie stages. Counts are read from anterior to posterior. Adult data for *Delphinapterus* (Kükenthal, 1889; Kleinenberg, 1969), *Stenella* (Sedmera et al., 1997b; Fedak and Hall, 2004; Cooper et al., 2017), and *Balaena* (Fedak and Hall, 2004; Cooper et al., 2007a; Thewissen et al., 2021b) is published elsewhere. Question mark indicates uncertainty of phalangeal formula at that particular Carnegie stage.

The longest digit for *Delphinapterus* and *Stenella* is digit II; this digit also has the greatest number of phalanges in prenatal and postnatal individuals. In contrast, digit III is the longest digit in the mysticete *Balaena*. This variation in longest digit length between odontocetes and mysticetes has been previously documented in post-natal individuals (Cooper et al., 2007). *Delphinapterus* has a hyperphalangeous phenotype on all digits except for the reduced digit I. In contrast, *Stenella* shows extreme hyperphalangy on digit II and hyperphalangy on digit III but reduced phalangeal numbers on digits IV and V compared to the mammalian standard of 2/3/3/3/3. Depending on the individual, a *Balaena* specimen will consistently have hyperphalangy of digit III, but may not have a hyperphalangeous phenotype on digits II or IV.

The adult *Delphinapterus* flipper phalangeal formula has a variable range of 0-3/6-8/5-7/5-6/4-6 (Kükenthal, 1889; Kleinenberg, 1969). The prenatal specimens mentioned in this study have

phalangeal counts ranging 0-2/6-8/5-6/5/4. The adult *Balaena* phalangeal formula is 0-2/3-4/4-5/3-4/2-3 (Fedak and Hall, 2004; Cooper et al., 2007a; Thewissen et al., 2021b). Prenatal *Balaena* from this study show a phalangeal count of 0/3-4/5/3-4/2, which matches the adult condition. In contrast to the Arctic whales, *Stenella* demonstrates a more hyperphalangeous phenotype. The adult phalangeal formula for *Stenella* is 1/7-9/4-6/1-2/0-1 (Cooper et al., 2017). This count is greater than the number of phalanges found in the prenatal specimens on digits II and IV, which have a formula of 1/7-8/4-6/2-3/1. In adult cetaceans, several interphalangeal joints can form, and phalanges can remain cartilaginous, which may contribute to the variation in counts between prenatal and postnatal specimens seen here. These variations in number of phalanges and longest digit length are reflected in the growth trajectories of the flipper (Figure 8B) and may be related to differences in gene signaling related to hyperphalangy.

Previous developmental work has experimentally shown that the generalized tetrapod hand is modified into a hyperphalangeous flipper via several critical modifications to the typical genetic cascade directing limb development. One such modification is the continued expression of the protein FGF8, which is critical for maintenance of the apical ectodermal ridge (AER) that supports proximodistal growth of the embryonic limb. In comparison to a more typical mammalian limb found in mice, the *Stenella* forelimb shows prolonged FGF8 protein signaling, probably extending the length of the limb (Cooper et al., 2017). Additionally, WNT9A, an essential protein for phalangeal joint formation is expressed within the cetacean limb. Augmentation of this protein is implicated in the increased segmentation of digit primordia within *Stenella* (Cooper et al., 2017). While all extant cetacean taxa demonstrate hyperphalangy and probably have prolonged FGF8 and WNT9A signaling

compared to terrestrial, pentadactyl mammals, it is possible that protein signaling for FGF8 and WNT9A is reduced in *Balaena* and *Delphinapterus* with respect to the extreme hyperphalangy found in *Stenella*, given that both arctic taxa have fewer phalanges than *Stenella*.

The cetacean flipper initially evolved from a pentadactyl, weight-bearing limb in early, amphibious archaeocetes and with a change in ecological niche came drastic restructuring of the skeleton, including the manus and forelimb (**chapter 3**) (Gavazzi et al., 2020). Early amphibious fossil whales are hypothesized to have partial interdigital webbing on the limbs (Thewissen et al., 1996; Madar, 2007). By the emergence of *Dorudon*, a basilosaurid archaeocete from the Late Eocene epoch and the first pelagic archaeocete, the forelimb was completely encased in a soft-tissue flipper (Uhen, 2004), though there is no evidence of hyperphalangy. Some of the earliest evidence for hyperphalangy is in the 7-8 MYA mysticete fossil *Balaenoptera siberi* (Pilleri, 1990) from the Miocene epoch, though this does not preclude the possibility of an earlier evolutionary timepoint. Thus, interdigital webbing found around the cetacean digits and the emergence of hyperphalangy are evolutionarily distinct events despite developmental integration.

Hindlimbs— Extant cetaceans do not have externally visible hindlimbs; the structures formed by the temporary hindlimb buds are embedded within the body wall and the pelvis, which is not articulated to the vertebral column, supports the urogenital system. For the delphinoids, which include both *Delphinapterus* and *Stenella*, the hindlimb bud only forms a rudimentary pelvis and occasionally a cartilaginous femur (Amasaki et al., 1989; Sedmera et al., 1997a). In *Balaena,* other elements of the hindlimb can also form, with both femora and tibiae present in the body wall (Struthers, 1881; Thewissen et al., 2021b)

Both *Delphinapterus* and *Stenella* maintain external hindlimb buds through Carnegie stage 16 (Figure 10). The *Stenella* hindlimb buds regress fully by stage 17 and are no longer visible externally. It is unclear if *Delphinapterus* retains hindlimb buds into stage 17; there is no evidence of hindlimbs in NSB-DWM 2013LDL6F, though the abdominal wall is damaged. In contrast, *Balaena* embryos retain hindlimb buds for a prolonged period and the hindlimb buds clearly persist through stage 19 (Figure 11). The hindlimb bud of NSB-DWM 2018G3F (CS 19) is elongated with a small epithelial protrusion on the end which may be an indication of an apical ectodermal ridge, the genetical signaling center for limb outgrowth.

Developmentally, the persistent presence of an apical ectodermal ridge (AER), the region which drives proximodistal limb growth, and the associated signaling factors, would promote continuous cellular differentiation that led to the development of more elaborate hindlimb structures (Richardson et al., 2004, 2009; Tabin and Wolpert, 2007). In *Stenella*, cessation of SHH signaling from the zone of polarizing activity (ZPA), a region that determines anteroposterior limb asymmetries, is implicated in the truncation and termination of hindlimb development (Thewissen et al., 2006). Because *Balaena* embryos clearly demonstrate the prolonged presence of hindlimb buds in comparison to other cetacean taxa, it is likely that this taxon extends the timeframe of AER expression, allowing for the formation of more hindlimb structures compared to other cetaceans. Furthermore, given that hindlimb loss has likely only evolved once in the cetacean lineage (Sedmera et al., 1997a; Uhen, 2004; Thewissen et al., 2006), this aberrant SHH signaling found in *Stenella* is possibly involved in hindlimb truncation in all of Cetacea, though this hypothesis has yet to be tested empirically in other taxa.

Early amphibious archaeocetes primarily relied on hindlimb dominated swimming via pelvic paddling or pelvic oscillation (Thewissen and Fish, 1997; Bebej and Smith, 2018). The pelvis was fully articulated to the vertebral column in early fossil cetaceans like *Ambulocetus*, *Remingtonocetus*, and many protocetids (Thewissen et al., 1994; Gingerich et al., 2001, 2009; Bebej et al., 2012; Uhen, 2014). There is evidence that some protocetids, such as *Aegicetus* and *Georgiacetus*, lack sacroiliac articulation (Hulbert, 1998; Uhen, 2008; Gingerich et al., 2019), however, both of these animals still retained elaborate, functional hindlimbs. *Dorudon* and *Basilosaurus*, in contrast, had greatly reduced hindlimbs compared to their overall body size. Their hindlimbs did not articulate to the vertebral column and probably did not serve a functional role during locomotion (Gingerich et al., 1990; Uhen, 2004).
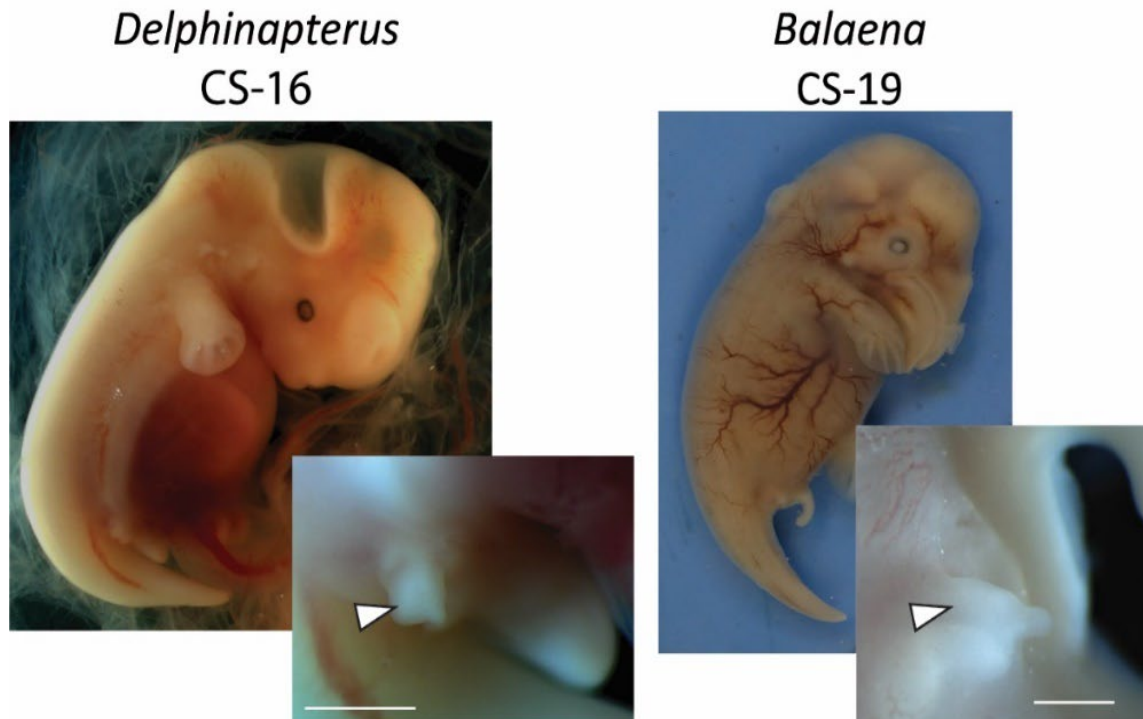
Figure 11: Photographs of CS 16 *Delphinapterus* (NSB-DWM 2019LDL15F - left) and CS 19 *Balaena* NSB-DWM 2018G3F - right) embryos. Hindlimbs (white arrows) are visible in both of these specimens. Scalebar equals 0.5 mm.

Fluke— All modern cetaceans have lunate shaped flukes, the main organ necessary for propulsion during locomotion. All three taxa analyzed here initiate fluke development at approximately the same Carnegie stage. However, the growth rates of the flukes vary between all three species, and taxon-specific variation quickly becomes apparent. The postnatal shape of the flukes is tailored for efficiency during swimming behaviors related to locomotion and feeding (Ayancik et al., 2020).

The genetics of cetacean fluke development are currently not understood. It has been hypothesized that flukes share common protein signaling with limb buds (Thewissen, 2018). However, no data supporting or refuting this hypothesis have been published and new evidence of protein

signaling driving outgrowth and patterning of the fluke is presented in chapter 6. Elucidating the mechanisms of fluke outgrowth in one taxon would likely be applicable to both extant and fully aquatic fossil cetaceans given that flukes likely developed once within the evolution of Cetacea, concurrent with the reduction and internalization of the hindlimbs.

The evolution of the flukes cannot be tracked directly, as soft tissue is not preserved within the fossil record. Instead, the development of the flukes within the archaeocetes is investigated via skeletal traits. (Uhen, 2004) proposed that fluke presence is correlated with the presence of a ball vertebra, which is convex on both the proximal and distal vertebral bodies. It is found in the first fully aquatic basilosaurid, *Dorudon atrox* (Uhen, 2004) but tails for many earlier cetaceans are not well preserved. Details of osteological correlates of fluke evolution are discussed in **chapter 5**.

Conclusion

Our objective for this chapter was to set a conceptual framework for detailed comparisons of embryogenesis in three cetacean taxa: *Delphinapterus* and *Balaena* to the previously described *Stenella*. Further elucidation of the phenotypes described here included a description of hindlimbs in chapter 4, an investigation of protein signaling driving fluke development in chapter 6 and a quantitative analysis of the osteological characters associated with vertebral and fluke evolution were included in chapter 5.

While *Delphinapterus* generally follows the *Stenella* based staging system with a few notable variations, identification of early *Balaena* exposes heterochrony between odontocetes and mysticetes.

The two smallest *Balaena* specimens in our collection, NSB-DWM 1999B7F and NSB-DWM 2018G3F

display hyperphalangy (a CS 19 trait for *Stenella*), hindlimb buds, (CS 16), elongate rostra (CS 19), and

small fluke outgrowths (CS 17). Thus, trying to bin these mid-to late embryos into the existing

Carnegie staging system proves challenging. Some Carnegie stages, such as CS 18, which is defined by

digit II = digit III, are not applicable for any of the *Balaena* specimens that we examined and only

further highlight the differences in morphology observed between the odontocetes and mysticetes.

Lastly, the heterochrony among bowhead whale embryos compared to the odontocetes also has

implications for fetal growth, which is used for inferences about gestation length and mating period in

Balaena (e.g., (Reese et al., 2001; Christiansen et al., 2022). Though embryonic length measurements

are not an integral component of the Carnegie staging system, our limited bowhead data set illustrates

overlap in morphological features at variable embryo length (see also Thewissen et al., 2021a). Further

research is needed to resolve developmental chronology and associated length variation for mid to late

bowhead whale fetuses. Chapter 4 describes the cartilaginous anlagen found in the developing

hindlimbs of *Balaena* fetuses.

　　　　Some of the most striking morphological changes during cetacean development center around

the flippers, hindlimbs, and flukes. *Delphinapterus* and *Balaena* flippers are similar to each other

morphologically while *Stenella* demonstrate a more extreme form of hyperphalangy. Hindlimb bud

development is exceptionally prolonged in *Balaena* compared to the odontocete taxa. The

hypermorphosis of the hindlimb bud in *Balaena* compared to the odontocetes is directly reflected in

the extensive post-natal skeletal morphology (see discussion in **chapter 4**). The flukes of all three taxa

initiate around the same Carnegie stage. However, the growth patterns vary. *Delphinapterus* flukes

grow at a consistent pace, whereas *Stenella* flukes appear to transition between intermediate fluke

shapes quickly, especially between a spade-shaped morphology and the adult-like fluke. The *Balaena*

fluke growth trajectory has the steepest growth rate of any taxon based on our current, albeit

incomplete, dataset.

This study furthers the field by incorporating two additional taxa into the Carnegie staging

system that was initially only developed for *Stenella*. This work therefore lays a conceptual framework

to test hypotheses of heterochrony and interspecific variation among cetaceans. The integration of

cellular and molecular data will further enrich our understanding of cetacean ontogeny and evolution,

as seen in **chapters 4** and **6**.

CHAPTER 3 CARPAL MORPHOLOGY AND FUNCTION IN THE EARLIEST CETACEANS

This chapter was originally published in The Journal of Vertebrate Paleontology by Taylor and Francis

and has been reprinted here with permissions.

Introduction

Cetaceans (whales, dolphins, and porpoises) have a dramatic evolutionary history, moving

from an initially terrestrial to a fully aquatic niche. This transition involved major modifications to the

generalized mammalian bodyplan to accommodate life in the seas, including modifications to the

vertebral column and pelvis (Buchholtz, 2007; Uhen, 2014; Moran et al., 2015; Bebej and Smith, 2018),

loss of hindlimbs and emergence of fluke-powered locomotion (Fish, 1998; Bejder and Hall, 2002;

Uhen, 2004; Thewissen et al., 2006; Geisler, 2019), and emergence of a dorsopalmarly flattened

forelimb embedded within a soft-tissue flipper (Richardson and Oelschläger, 2002; Uhen, 2004;

Cooper et al., 2007a, 2018; Sears et al., 2018). Specifically, this transition occurred during the Eocene

epoch, and whales from this period document these major skeletal changes related to the shift from a

semi-terrestrial to a fully-aquatic environment (Thewissen et al., 1996; Gingerich et al., 2001, 2009;

Madar, 2007; Houssaye et al., 2015; Lambert et al., 2019; Vautrin et al., 2019) (Fig. 1). Prior to the

colonization of the sea, the earliest archaeocetes occupied shallow waters, probably returning to land

for shelter and reproduction (Thewissen et al., 2009a).

Evidence of adaptations for aquatic life became more pronounced within the fossil record over the span of approximately eight million years. The forelimb transformation included a shift from a cylindrical carpus to a mediolaterally flattened carpus in cross-section. The cylindrical carpus is optimal for weight-bearing locomotion on land, whereas a flattened carpus would reduce drag on the appendage in the water, depending on the angle of attack (Figure 12). Further adaptations, such as maintenance of interdigital webbing and hyperphalangy, also evolved to facilitate forelimb-based paddling and steering during swimming (Cooper et al., 2017). In modern cetaceans, the carpus is immobile within the flipper, and the whole forelimb functions as a control surface during locomotion (Fish and Lauder, 2006; Cooper et al., 2007a, 2008; Weber et al., 2009).

As evidenced by fossil remains, the earliest archaeocetes, the pakicetids, had weight-bearing limbs and utilized a digitigrade posture for terrestrial locomotion (Thewissen et al., 2001b; Madar, 2007). Their skeleton is systemically pachyostotic, resulting in most postcranial bones displaying thickened cortices, indicating some early adaptations towards an aquatic niche (Gray et al., 2007); Madar, 2007). This pachyostotic phenotype acts as ballast to counteract body-buoyancy and is found in extant water-dwelling taxa such as *Hippopotamus* (Gray et al., 2007; Thewissen et al., 2007). Only two carpals, the pisiform and unciform, are described for pakicetids (Madar, 2007), so little could be said about the overall wrist morphology. Here we describe an additional element, the trapezium, and suggest that the previously described unciform in Madar (2007) is instead a lunate.

Ambulocetus, a moderately complete and well-preserved archaeocete, is inferred to have had a more plantigrade forelimb posture and spent more time in the water hunting and swimming than pakicetids (Thewissen et al., 1996). *Ambulocetus* demonstrates numerous anatomical adaptations for

both terrestrial and aquatic locomotion, including large hindfeet for propulsion within the water and evidence of powerful back musculature. These features are consistent with pelvic paddling and caudal undulation as a mode of straight-line swimming (Thewissen et al., 1994; Thewissen and Fish, 1997; Buchholtz, 1998; Madar et al., 2002a), though Bebej and Smith (2018) found evidence of a dorsoventrally stable vertebral column in *Ambulocetus*, suggesting a reliance on hindfoot based locomotion. The forelimb shows reduced pronation/supination, as well as large insertions for musculature that supported flexion and extension of the cubital joint (Thewissen et al., 1996). Increased flexion and extension power may have compensated for the inability to rotate the forelimb during terrestrial and aquatic locomotion. The carpus of *Ambulocetus* as known from the fossil record is nearly complete, with only partial loss of the lunate and cuneiform. Conversely, no carpal elements are currently known for the remingtonocetids. It is likely that this group still relied on hind-limb powered locomotion over tail-based locomotion; analysis of *Remingtonocetus* lumbar vertebrae indicates that this taxon relied on pelvic paddling for swimming, similar to *Ambulocetus* (Bebej et al., 2012; Bebej and Smith, 2018).

Protocetids are also described as semi-aquatic, and different taxa within the group are inferred to employ different locomotor patterns (Gingerich, 2003). There is a considerable amount of forelimb material described for this family, particularly for *Maiacetus* (Gingerich et al., 2009), *Rodhocetus* (Gingerich et al., 2001), *Peregocetus* (Lambert et al., 2019), and the newly published Senegalese protocetid (Vautrin et al., 2019). The carpi of these protocetids appear as dorsopalmarly flattened in modern cetaceans, and likely serves as a swimming adaptation. The limb morphology of both *Rodhocetus* and *Peregocetus* suggests that both taxa engaged in pelvic paddling or caudal undulation,

similar to *Ambulocetus* (Gingerich et al., 2001; Lambert et al., 2019), although there is also evidence suggesting that protocetids had more dorsoventrally flexible lumbar region of the vertebral column than *Ambulocetus*, and thus possibly utilized a more tail-based locomotor pattern than earlier archaeocetes (Bebej and Smith, 2018). There is also suggestion that the Senegalese protocetid utilized forelimbs for power during swimming in addition to pelvic paddling, which is a locomotor pattern not inferred for any other protocetid (Vautrin et al., 2019).

Late-Eocene basilosaurids, such as *Dorudon*, were obligatorily aquatic with a body plan more similar to modern cetaceans, including dramatically reduced hind-limbs that were not functional in locomotion, soft-tissue flippers, and short tail vertebrae to accommodate flukes (Uhen, 2004). See discussion of vertebrae and flukes in chapter 5. The carpus of *Dorudon* is dorsoventrally flattened and mediolaterally expanded, with the trapezoid and magnum fused. The pisiform is robust and lies in plane with the rest of the carpals (Uhen, 2004). *Cynthiacetus*, another basilosaurid, shares morphological similarities to *Dorudon* (Martínez-Cáceres et al., 2017). This taxon is hypothesized to have seven carpals, with trapezoid-magnum fusion, and appears to be dorsopalmarly flattened. The pisiform and trapezium of *Cynthiacetus* are not currently known (Martínez-Cáceres et al., 2017). For *Zygorhiza*, there is only one carpal element known, making functional interpretations difficult. It is either an unciform (Kellogg, 1936) or a lunate (Gingerich and Smith, 1990). This transition from land to sea also affected changes within the vertebral column for dorsoventral undulation and tail-powered locomotion, which further de-emphasized the importance of the limbs as the source of power during swimming (Buchholtz, 1998; Gingerich, 2003; Bebej and Smith, 2018).

Cetaceans share a common ancestor within terrestrial artiodactyls (Gatesy, 1998; Gingerich et al., 2001; Thewissen et al., 2001b, 2007). Of particular interest is the raoellid *Indohyus*, which has several post-cranial elements preserved. The cuboid tarsals of *Indohyus* are similar to other artiodactyls, which may have functioned to reduce mediolateral movement and enhance flexion and extension (Cooper et al., 2012). Limb bones of *Indohyus* were osteosclerotic, with a highly reduced medullary cavity (Thewissen et al., 2007; Cooper et al., 2012; Madar, 2007). This is similar to pachyostotic adaptations in the pakicetid skeleton.

Modern artiodactyls have derived appendicular skeletons for unguligrade postures and locomotion. The carpals of an artiodactyl are generally cuboidal or rectangular in shape, stacking in a serial pattern. As in the tarsals, this morphology facilitates dorsoventral flexion but greatly limits all mediolateral movement and stabilizes the foot (Yalden, 1971; Clifford, 2010). This highly canalized morphology is present in the earliest artiodactyls. Some of the earliest primitive Eocene artiodactyls, such as *Messelobunodon* and *Diacodexis*, show evidence for cursorial locomotion adaptations within the carpals that are common amongst more derived taxa (Rose, 1982; Franzen, 1983; Thewissen and Hussain, 1990). *Diacodexis pakistanensis* is an early Eocene taxon with a complete but poorly preserved carpus that reduced pronation/supination in the forelimb, reduced the pollex, and had paraxonic digits (Thewissen and Hussain, 1990). *Indohyus,* another terrestrial taxon, has reduced pronation and supination at the elbow, a double-trochleated astragalus, and reduced first digits like other fossil artiodactyls (Thewissen et al., 2007; Cooper et al., 2012b).

This chapter leverages the abundant evidence of cetartiodactyl fossil forelimbs to investigate morphological shifts along the land-to-water transition. Whereas the hindlimb has been lost in

obligatorily aquatic cetaceans, there is a continued presence of a forelimb in all cetartiodactyls, making the carpus an important region of study. It is our goal to elucidate the relationship between carpal form and function in Eocene cetartiodactyls. To achieve this, we utilized micro-CT scans to reconstruct the carpus of *Ambulocetus natans* (Thewissen et al., 1994, 1996) and identified several new carpals for *Indohyus* and *Pakicetus*. We utilized carpal data from *Ambulocetus* to compare with modern and fossil cetaceans, Eocene artiodactyls, and mesonychids. Mesonychids are fossil ungulates that were previously thought to be the closest ancestor to Cetacea, although now known to have no special relationship with cetaceans (Geisler and Theodor, 2009; Thewissen et al., 2009b). We choose to include mesonychids as a point of comparison with Cetacea based on their known carpal morphology for multiple fossil taxa and unguligrade posture for comparison with the artiodactyl carpus, which is derived for cursorial locomotion. Information on forelimb morphology for the mesonychids (Scott, 1888; Rose and O'Leary, 1995), *Messelobunodon* (Franzen, 1983), *Diacodexis* (Thewissen and Hussain, 1990)*, Maiacetus* (Gingerich et al., 2009)*, Peregocetus* (Lambert et al., 2019)*, the Senegalese protocetid (Vautrin et al., 2019), *Dorudon* (Uhen, 2004)*, and modern cetaceans (Cooper et al., 2007a) was taken from previously published data. Only one carpal element has been previously described for *Indohyus*, the magnum (Cooper et al., 2012b), and we describe two additional carpals for this study. We also discuss the evolutionary and locomotor significance of these elements.
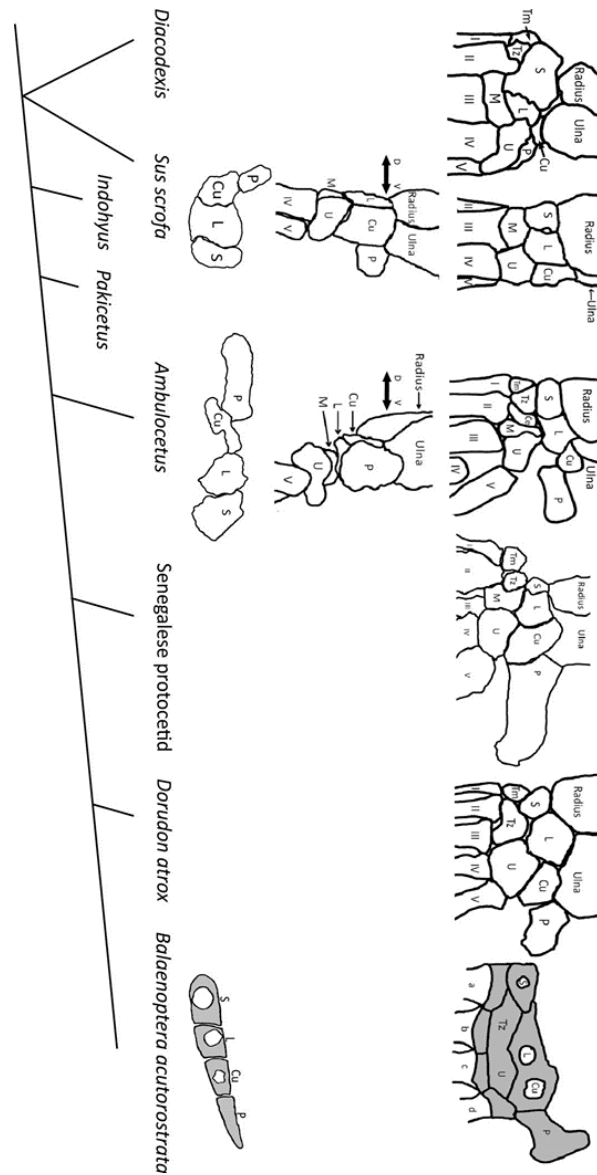
Figure 12: A truncated phylogeny of Cetartiodactyla based on Thewissen et al. (2007) with taxa referenced in this study. The outline of *Dorudon* has been mirrored from the original image, a right carpus, for standardization across the taxa. Gray represents cartilage and white represents bone. All outlines are provided in dorsal view (top row). Lateral views of the same wrist are provided for some taxa (middle row). The bottom row shows the proximal carpal row in cross-sectional view. Information on *Diacodexis* (H-GSP 300-5023) from Thewissen and Hussain (1990), on the Senegalese protocetid (SNTB 2011-11) from Vautrin et al. (2019), on *Dorudon* (UM 101222) from Uhen (2004), and on the minke whale from Cooper et al. (2007a). Abbreviations: **Ce**, centrale; **Cu**, cuneiform; **D**, dorsal; **L**, lunate; **M**, magnum; **P**, pisiform; **S**, scaphoid; **Tm**, trapezium; **Tz**, trapezoid; **U**, unciform; **V**, ventral. **I–V** correspond to digit numbers.

Methods

Materials from *Ambulocetus natans* (H-GSP 15807), and pakicetid taxa *Pakicetus* and *Ichthyolestes* (H-GSP 30169, 96570, 96581) are part of the collections of the Howard University-Geological Survey of Pakistan (H-GSP). Pakicetid material reported here was found in the Ganda Kas Area of the Kala Chitta Hills in Punjab, Pakistan. At H-GSP locality 62 (33° 38' N, 72° 11.25' E), where all postcranial fossils were found, 61% of the recovered dental specimens are attributed to pakicetids, and so we expect a similar ratio for postcranial elements as well (Thewissen et al., 2001b). There are three species of pakicetids at this locality, from small to large body size: *Ichthyolestes pinfoldi*, *Pakicetus attocki,* and *Nalacetus ratimitus*. Pakicetids represent a discrete size range within that faunal assemblage and do not overlap with other mammalian groups. Anthracobunids, a fossil group of stem perissodactyls (odd-toed ungulates) found at this locality (Cooper et al., 2014b) are larger than both *Pakicetus* and *Nalacetus*, while raoellids recovered from this region are significantly smaller than *Ichthyolestes* (Thewissen et al., 2001b; Madar, 2007; Cooper et al., 2014b). Isotopic analysis of some postcranial elements recovered from this locality confirms cetacean identity (Thewissen et al., 2001b), although no such analysis was carried out on the bones described herein. It is likely that these carpals are from either *Pakicetus* or *Nalacetus*, and not *Ichthyolestes*, based on the size differences between previously identified *Ichthyolestes* limb bones and the new carpals (Thewissen et al., 2001b).

Indohyus materials (RR) are part of the collections of the Obergfell-Ranga Rao Trust of the Geosciences (Dehradun, India). All specimens were collected at a single locality (33° 14.5' N, 74° 22.5' E) in the state Jammu and Kashmir in India. This locality is called Sindkhatudi and is near the village of Kalakot. Faunal lists were presented by (Kumar, 1998) and Thewissen et al. (Thewissen et al.,

58

2001a). Hundreds of vertebrate fossils have been collected at this locality, and the vast majority of the identifiable specimens are jaws of *Indohyus*. A few taxa are similar in size to *Indohyus*, but these are exceedingly rare. The hyaenodontid *Paratritemnodon indicus* was based on one specimen described by Ranga Rao (1973), with two others referred to by Kumar (1992). The raoellid *Khirtharia inflatus* was based on two specimens by (Ranga Rao (1972), with Sahni and Khare (1972) adding two more, and there is an undescribed dichobunid that is larger than *Gujaratia pakistanensis* and possibly referred to as *Haqueina haquei* (one specimen, Sahni and Khare, 1972). The tapiroid *Sastrilophus dehmi* was based on two specimens by (Sahni and Khare, 1971). Approximately twenty specimens of the derived tapiroid *Kalakotia* have been described (Ranga Rao, 1972; Sahni and Khare, 1972; Kumar and Sahni, 1985). The most complete survey of *Indohyus* specimens is published by Thewissen et al. (2020), which describes well over 100 specimens of dental and cranial elements of *Indohyus* and did not include fragmentary specimens such as isolated teeth or postcranial material.

Evidence from dental remains indicate that *Indohyus* is by far the most common taxon in the fossil assemblage. This implies that most postcranials recovered will pertain to *Indohyus*. Morphological evidence supports that the carpals described herein do not pertain to *Kalakotia* or *Sastrilophus*, based on comparisons with the tapiroid *Karagalax* (Maas et al., 2001). Furthermore, the trapezoid described here for the first time directly articulates with the magnum previously attributed to *Indohyus* in Cooper et al. (Cooper et al., 2012b). Specimens used here are currently housed at the Northeast Ohio Medical University (NEOMED), Rootstown, Ohio, but will be returned to their repository.

All identified carpal and zeugopodial elements of these specimens were imaged on a micro-CT scanner (Scanco Medical, Viva70) at 70 kVp, with a voxel range of 20.4 – 40 microns. Scanned fossil data was virtually segmented from the matrix in Avizo2019.1 (Thermo Fischer Scientific) and reconstructed in Maya 2019 (Autodesk). The carpus of *Ambulocetus* is nearly complete, although part of the lunate and cuneiform are missing. The relationships of the species are shown in Figure 12. The carpal nomenclature used within this text, from proximal row to distal row, are: scaphoid, lunate, cuneiform, pisiform, trapezium, trapezoid, centrale, magnum, and unciform.

Results

***Ambulocetus* Pisiform** – The carpus of *Ambulocetus* was collected with most bones *in situ*. The pisiform of *Ambulocetus* (H-GSP 18507.3413) has been previously described in (Thewissen et al., 1996) (Figures 13, 14). It is approximately 44 mm long and robust. Its distal end is cranially curved and craniocaudally flared. There is a large surface for attachment of the flexor carpi ulnaris muscle. Proximally, the pisiform has two articular facets with a slight ridge between. These facets are oriented craniocaudally. The pisiform is oriented in plane with the rest of the carpus and laterally projecting from the wrist (Figure 13). In cross section, the shaft of the pisiform is rounded. Previously, Thewissen et al. (1996) suggested that the pisiform had contacted the ulna. Based on micro-CT reconstruction we now hypothesize that the pisiform articulates with the cuneiform proximally and with the unciform distally.

***Ambulocetus* Centrale** – The *Ambulocetus* carpus is unusual in having an os centrale (H-GSP 18507.3418, Thewissen et al. 1996). The os centrale of *Ambulocetus* is the smallest of carpal elements,

craniocaudally long, and mediolaterally flattened compared to other carpals. The os centrale articulates predominantly with the trapezoid and magnum; it also slightly contacts the lunate and the scaphoid in the proximal row, as well as metacarpals II and III.

Ambulocetus **Trapezium** – First described by Thewissen et al. (1996), the trapezium of *Ambulocetus* (H-GSP 18507.3414) was found *in-situ* and articulated with the trapezoid and scaphoid. The trapezium is roughly pyramidal in shape. Superiorly, there is a broad, slightly sloping surface for articulation with MC I and a smaller, concave groove for MC II. The articular surface for MC I is medially deviating from MC II. There is an articulation with the scaphoid along a small inferior medial portion of the trapezium, which is reflected by a groove in the scaphoid. The entire length of the medial aspect of the trapezium is in direct contact with the trapezoid. The lateral face of the trapezium is notched, with the notch oriented towards the scaphoid. This unique notch does not articulate with any other skeletal element.

Ambulocetus **Metacarpal I** – MC I (H-GSP 18507.3421) was described by Thewissen et al. (1996) and is the shortest of the metacarpals; it is also mediolaterally flattened and dorsoventrally expanded. There is a broad, slightly convex surface on the proximal end to articulate with the trapezium. The corresponding surface on the trapezium slightly offsets MC I from the rest of the metacarpals, suggesting some medial deviation of digit I from the rest of the digits. A small shallow pit on the proximal end of MC I also articulates with MC II.
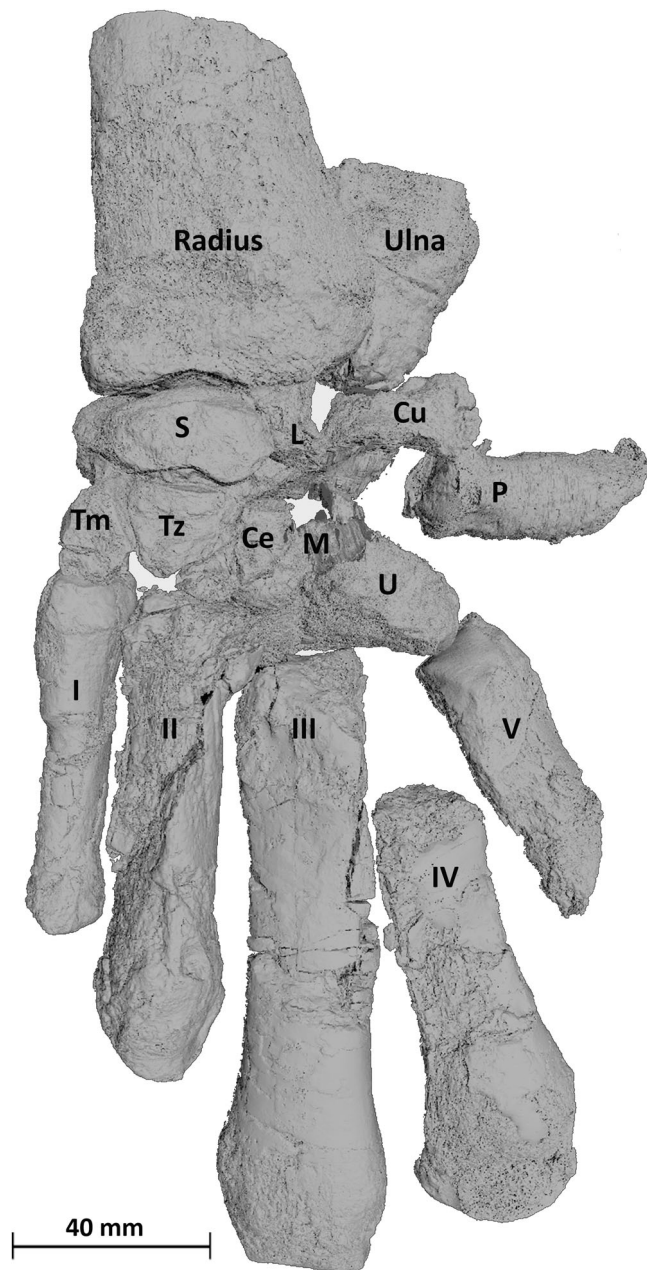
Figure 13: Virtual reconstruction of the left *Ambulocetus* hand in dorsal view. Abbreviations: **S**, scaphoid; **L,** lunate; **Cu**, cuneiform; **P**, pisiform; **Tm**, trapezium; **Tz,** trapezoid; **Ce**, centrale; **M**, magnum; **U**, unciform.

Pakicetid Pisiform – This pisiform (H-GSP 30169) was previously described by Madar (2007). It is 17 mm long and the distal end is absent (Figure 14). The bone is long and curved, similar to *Ambulocetus*. In addition, it is mediolaterally compressed, and the shaft is ovoid in shape. The proximal surface is divided into cranial and caudal facets by a sharpened ridge. The cranial facet is deeply angled towards the manus, while the caudal facet is more rounded. This facet morphology is consistent with a posteriorly-oriented pisiform, similar to most terrestrial mammals. We lack contextual information from a distal ulna, unciform, or magnum to concretely determine articular relationships. The pisiform is usually robust and prominent in the archaeocete carpus; however, this pisiform is small in comparison to the remaining pakicetid carpals described here. We suspect that this pisiform is from the pakicetid *Ichthyolestes* instead of *Pakicetus*, as it was attributed in (Madar, 2007).

40 mm
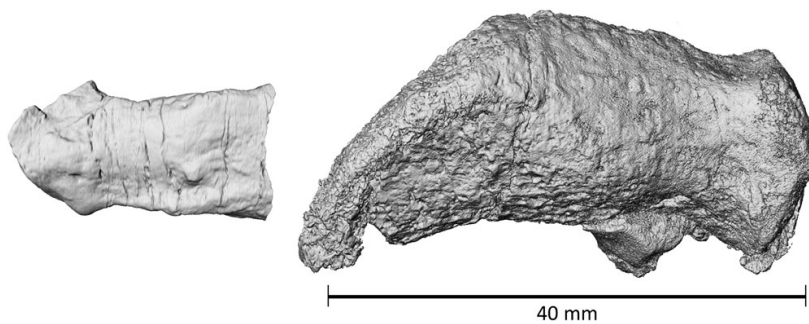
Figure 14: Lateral view micro-CT images of the left pakicetid pisiform (H-GSP 30169) (**left**) and the left *Ambulocetus* pisiform (H-GSP 18507.3413) (**right**). In both taxa the articular surfaces are oriented craniocaudally; in *Ambulocetus* those articular surfaces are canted at an angle to face more mediolaterally than *Pakicetus*, suggesting rotation of the pisiform.

Pakicetid Trapezium – The pakicetid trapezium (H-GSP 96570) has not been described (Figure 15A).
It is 10 mm wide mediolaterally, 13.4 mm deep dorsoventrally, and 11 mm tall proximodistally. The
trapezium is overall triangular or pyramidal in shape. The caudal aspect of the trapezium is expanded
and wider than the proximal region. There is a concave facet for MC I; this facet is surrounded
mediolaterally by two ridges. There is a facet for the trapezoid, with a ridge that is inferior and dorsal
to the articular facet. The middle of the medial aspect has a shallow pit, likely for additional contact
with the trapezoid. The articular surface for the scaphoid is crescent-shaped on the cranial surface of
the bone. The scaphoid surface is only present on the medial third of the proximal surface of the
trapezium, with a ridge separating this articular surface from the rest of the bone.

Pakicetid Lunate – Madar (2007) previously described this bone (Figure 15B, H-GSP 96581) as a
magnum. After further analysis, we propose that this carpal is the left lunate of a pakicetid based on
articular facets for the scaphoid, cuneiform, trapezoid, radius, and ulna. This carpal is larger than both
the trapezium and pisiform. The dimensions are 12.4 mm wide, 22 mm deep, and 14 mm tall. The
lateral aspect of the carpal is dominated by a curved, convex facet for the scaphoid. There are also two
small, recessed areas dorsally and ventrally on the lateral facet for articulation with the trapezoid.
Caudally, there is a rounded facet for contact with the magnum; this face is separated from a surface
for the trapezoid by a small crest. On the cranial side, there is a large surface for contact with the
radius and a smaller triangular surface for the ulna. These two ulnocarpal and radiocarpal facets are
separated by a sharp ridge. The ulnar facet is also bordered by two facets for articulation with the
cuneiform.

Indohyus **Trapezium** – We identified the right trapezium for *Indohyus* (RR 3), a previously undescribed carpal (Figure 15C). The trapezium for *Indohyus* is only 5 mm wide, 6 mm deep, and 6.6 mm tall. It is generally triangular with a large concave articular surface for the trapezoid that dominates the proximal and medial aspect of the bone. The *Indohyus* trapezium articulates strongly with MC I, trapezoid, and scaphoid. There is a rounded facet for MC I on the caudal surface. This facet is slightly laterally and posteriorly displaced, suggesting an offset MC I. There is no evidence of an articular surface for MC II. The lateral surface has a large, rounded facet for the trapezoid, with a small region on the superior aspect of the bone that is not in direct contact with the trapezoid. The cranial surface is diminished and separated into two rounded ridges, which also articulate around the trapezoid. There is a small, flattened area between these two ridges that may serve as an articular surface for the scaphoid, although the contact between these two bones was likely small.

Indohyus **Trapezoid** – The *Indohyus* trapezoid (RR 48) is described here for the first time (Figure 15D). This trapezoid is from the right carpus. This carpal is unusually shaped with a large expanded caudal portion that tapers proximally. The medial face is craniocaudally linear, while the lateral side of the trapezoid tapers from distal to proximal. The trapezoid is 7.5 mm wide, 6.2 mm deep at the widest part, 4 mm at proximal depth, and 6.7 mm tall. The anterior ridge of the trapezoid articulates within the trapezium facet. The facet is distally expanded and proximally reduced. There is a crest between dorsal and ventral surfaces on the anterior side, which is located between the two ridges found on the trapezium. Laterally, the trapezoid has an articular surface for the magnum that is proximodistally oblique. This surface is generally smooth and flattened, with a small protuberance in the center of the surface, and articulates with RR 250, the *Indohyus* magnum described by (Cooper et al., 2012b). MC II

65

is not preserved from *Indohyus,* so the articular relationship with the trapezoid is not known. There is a small protuberance on the caudal edge of the trapezoid that articulates with MC III. The cranial surface of the trapezoid is flat and triangular, with a small crest that sits between the two ridges of the trapezium. Dorsally on the cranial surface, there is a small, flattened area that is angled away from the flattened surface. We were unable to determine if this is due to postmortem damage or an articular region for the scaphoid.
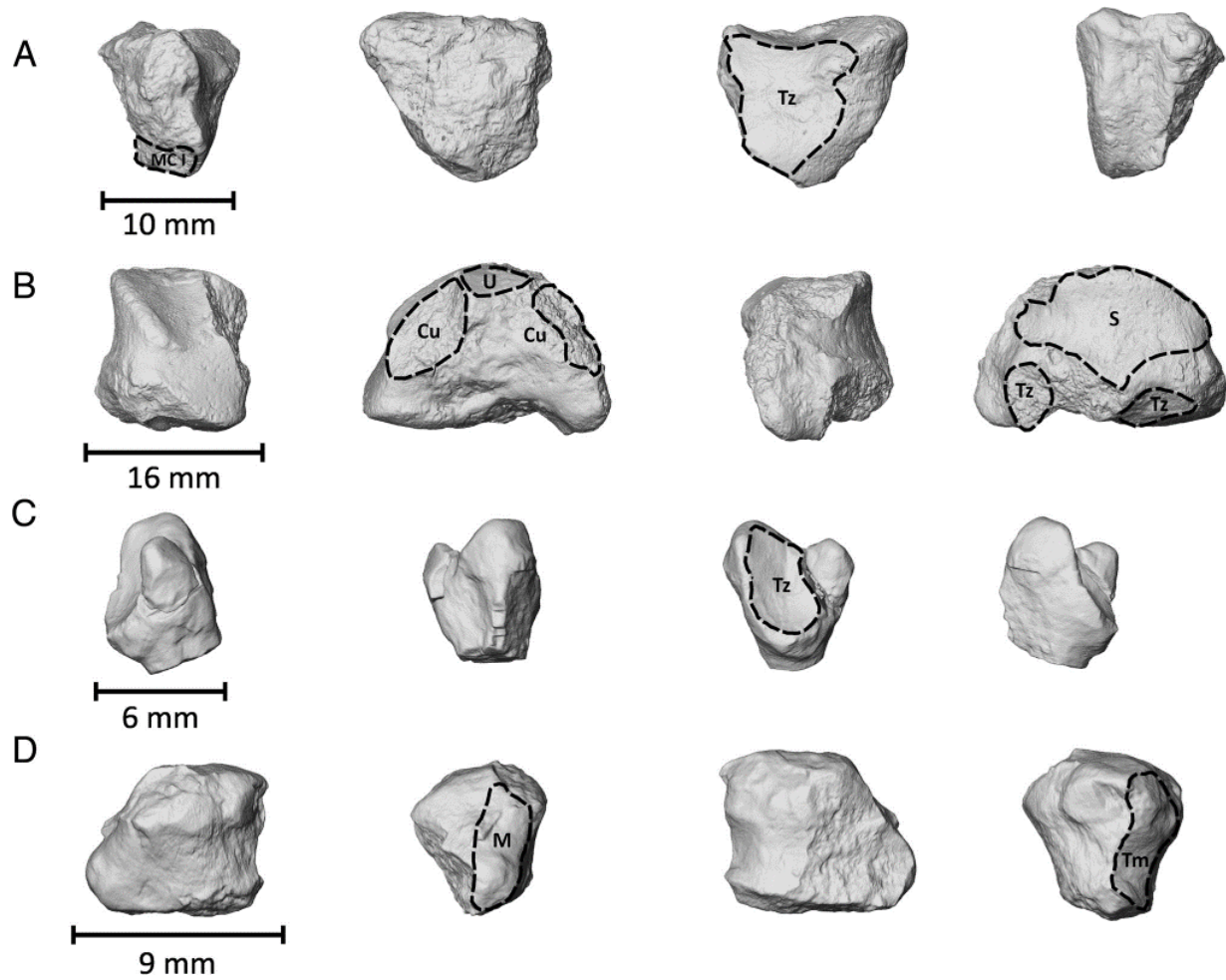
Figure 15: micro-CT data of the newly identified carpals. All are shown in dorsal (left column), lateral (middle left column), palmar (middle right column) and medial (right column) views. A, left *Pakicetus* trapezium (HGSP 96570). **B**, left *Pakicetus* lunate (HGSP 96581). **C**, right *Indohyus* trapezium (RR 3) **D**, right *Indohyus* trapezoid (RR 48). Articular facets on each carpal are highlighted by the dashed lines; labels indicate element that contacts facet. Abbreviations: **MC I**, metacarpal I; **Tz**, trapezoid; **Cu**, cuneiform; **U**, unciform; **S**, scaphoid; **M**, magnum; **Tm**, trapezium. Individual scalebars are shown.

Discussion

The early evolution of cetacean wrist is characterized by a shift from the highly specialized,

cylindrical wrist to a mediolaterally flattened carpus (Figure 12). The artiodactyl forelimb is optimized

for movement in the flexion-extension plane at all joints of the wrist and digits (Yalden, 1971; Clifford, 2010). A small degree of ulnar deviation occurs in conjunction with flexion, but this movement cannot happen in isolation. Modern artiodactyls are unable to perform any noticeable degree of rotation or radial deviation at the wrist joint (Yalden, 1971; Clifford, 2010). Early taxa such as *Diacodexis* had more flexibility within the wrist and were likely capable of these deviation and rotation movements to some degree (Rose, 1982; Thewissen and Hussain, 1990). In Eocene whales, the carpus is clearly not constrained to movement solely in the flexion-extension plane. Even the earliest semi-aquatic cetaceans demonstrate the capacity for moderate ulnar deviation and abduction of the digits. Rotation of the forelimb, however, is highly limited in some archaeocete taxa, like *Ambulocetus* (Thewissen et al., 1996). While the dichobunids display a more flexible forelimb than many other artiodactyls, the early cetacean hand demonstrates an even greater capacity for deviation and abduction than previously seen within Cetartiodactyla.

These modifications to the archaeocete wrist for increased flexibility and power coincide with dorsoventral flattening of the hand skeleton embedded within a cambered flipper. Along with these broad, sweeping changes, there are several carpal-specific modifications that potentially facilitated the shift from a terrestrial habitat to an aquatic one. Particularly, the transition from limb to flipper includes lateral rotation of the pisiform and alignment of digit I with the rest of the carpus.

Lateral Rotation of the Pisiform – The pisiform serves as an attachment point for the flexor carpi ulnaris, allowing for flexion and adduction of the ulnocarpal joint (Lewis et al., 1970; Cooper et al., 2007b). Early in cetacean evolution, the pisiform transitions from a ventrally projecting orientation to a lateral one. A posterior position within the carpus is the common pisiform morphology found in

most terrestrial taxa, including Eocene artiodactyls *Messelobunodon* and *Diacodexis* (Franzen, 1983; (Thewissen and Hussain, 1990)). A pisiform is not known for *Indohyus*. The pakicetid pisiform was likely posteriorly oriented, as the proximal facets strongly resemble those of an artiodactyl. It is unsurprising that pakicetids would maintain a posteriorly oriented pisiform, given that they are the most terrestrial of the cetaceans. A shift in pisiform orientation occurs early in cetacean evolution with *Ambulocetus* and coincides with the increased reliance on aquatic locomotion over terrestrial locomotion. A laterally oriented pisiform is also reported in the Senegalese protocetid (Vautrin et al., 2019), *Basilosaurus* (Gingerich and Smith, 1990), and *Dorudon* (Uhen, 2004). No information on the pisiform is provided for *Rodhocetus* (Gingerich et al., 2001) or *Peregocetus* (Lambert et al., 2019). In contrast, *Maiacetus* (GSP-UM 3551) is reported to have a ventrally projecting pisiform (Gingerich et al., 2009). All other known archaeocete wrists for which a pisiform is known, aside from the pakicetids and possibly *Maiacetus*, have a laterally oriented pisiform. Extant cetaceans appear to maintain a laterally orienting pisiform, although the carpus may not ossify in baleen whales (Cooper et al., 2007a). Interestingly, the flexor carpi ulnaris is conserved in modern cetaceans, while other forelimb and intrinsic hand muscles show variability between taxa (Cooper et al., 2007b).

While the lateral orientation of the pisiform remains constant across semi-aquatic and aquatic archaeocetes except for pakicetids and possibly *Maiacetus*, the articular relationships of the pisiform are not conserved. Our new interpretation of the *Ambulocetus* wrist suggests that the pisiform of *Ambulocetus* articulates with both the unciform and cuneiform, having no contact with the ulna. This morphology is hypothesized for *Pakicetus* as well (Madar, 2007). The articular relationships of the *Maiacetus* pisiform are unclear. Little information is provided on individual carpal elements within

Gingerich et al. (2009), and the provided illustrations of the *Maiacetus* specimen (GSP-UM 3475a) do not appear to align with other publicly available information on that taxon. This specimen was not available for study by us at the time of data collection. The illustration (GSP-UM 3475a) in (Gingerich et al., 2009) indicates that all carpals are known for *Maiacetus* and suggests that the pisiform articulates between the cuneiform and unciform, which is the same morphology found in *Ambulocetus*. However, the 3D cast of *Maiacetus* (GSP-UM 3551) that is publicly available online (https://umorf.ummp.lsa.umich.edu/wp/specimen-data/?Model_ID=1340) shows the pisiform articulating with the cuneiform and radius. While sexual dimorphism within a taxon can affect the allometry of carpal bone relationships, there are no documented cases of variation in carpal articulations within a single taxon.

In comparison, the wrist of *Dorudon*, which is both published in Uhen (Uhen, 2004) and available online (https://umorf.ummp.lsa.umich.edu/wp/specimen-data/?Model_ID=1339) is visually identical in the photographs and the 3D rendering. The *Dorudon* pisiform articulated with the ulna and the cuneiform (Uhen, 2004). The Senegalese protocetid (Vautrin et al., 2019) shares this morphology with *Dorudon*. The pisiform articular relationships in modern cetaceans are highly variable, with no discernable pattern within or between odontocete and mysticete taxa (Cooper et al., 2007a). Once the cetacean forelimb became immobile within the flipper, the articular relationship of the pisiform to the rest of the wrist would have become less important. While pisiform articular patterns change throughout archaeocetes, a mediolateral pisiform that is in plane with the rest of the carpus is found in all cetaceans except for the pakicetids and potentially *Maiacetus*. A distal shift of the pisiform to lose contact with the ulna may have increased the range of ulnar deviation within those

70

taxa. However, the benefits of that flexibility may not have been enough to remain fixed throughout archaeocetes.

The transition from a ventrally projecting pisiform to a laterally oriented pisiform in plane with the carpus is the most dramatic carpal modification in the cetacean wrist. Not only is this morphology consistent across nearly all Eocene fossil taxa discussed here but is also present in all modern cetaceans analyzed in (Cooper et al., 2007a). The modern cetacean carpus is immobile and a laterally oriented pisiform in plane with the rest of flipper is maintained. Furthermore, while the neuromuscular anatomy affiliated with the carpus varies widely, the flexor carpi ulnaris is consistently found attached to the pisiform in modern taxa (Cooper et al., 2007b). Given that this morphology is only known in semi-aquatic and aquatic species, the change in bone arrangement was likely correlated with increased swimming efficiency by drag reduction and use of the forelimb as a control surface.

Digit I Deviation – The trapezium is an attachment point for the abductor pollicis brevis and flexor pollicis brevis muscles. The abductor pollicis brevis both abducts and extends digit I; the flexor pollicis brevis flexes and medially rotates digit I. Both muscles belong to the lateral volar aspect of the hand and are critical for digit I flexibility. MC I of *Ambulocetus* articulates with the trapezium and MC II. It is suggested that *Ambulocetus* was capable of moderate pollical deviation (Thewissen et al., 1996). Pentadactyl artiodactyls, such as *Diacodexis*, have a posteriorly displaced digit I with respect to the rest of the hand (Thewissen and Hussain, 1990). *Ambulocetus* maintains this morphology.

Messelobunodon has a highly reduced MC I, approximately half the size of MC III and MC IV (Franzen, 1983). The trapezium is not visible in *Messelobunodon,* but trapezium shape would likely reflect this MC I diminution. The trapezium solely articulates with the MC I in *Diacodexis*, which also

has a reduced MC I (Thewissen and Hussain, 1990). Given the overall reduction in size of both MC I and the trapezium, it is unlikely that either taxon utilized pollical deviation during locomotion. This is unsurprising, given that the artiodactyl wrist predominantly functions in flexion with highly reduced capabilities for deviation and rotation (Yalden, 1971). The articular surface for MC I of *Indohyus* appears to be posteriorly displaced from the other digits, similar to other early pentadactyl Eocene artiodactyls (Figure 15D). Digit I was likely reduced in comparison to the other four digits and posteriorly displaced from the rest of the hand. The trapezium of *Ambulocetus* has an articular surface that is dorsoventrally deep and spans the majority of the distal surface. MC I is within the same plane as the other digits, although medially displaced compared to MC II – V, and the robusticity of the trapezium indicates a larger surface for attachment of lateral volar musculature. The pakicetid trapezium shares many of these features found in *Ambulocetus*, suggesting that the MC I may have also been medially displaced in pakicetids, which would allow for more independent movement of digit I (Figure 15A).

While the pakicetids are the most terrestrial of the archaeocetes, this may suggest that subtle modifications to the wrist already conferred some advantages for moving through water. The scaphoid, trapezoid, and MC I were not recovered for the pakicetids, so the overall relationship of trapezium size to the rest of the carpals is unknown. The trapezium in *Maiacetus* appears to articulate with MC I and then traverses both the proximal and distal carpal row to directly contact the radius (Gingerich et al., 2009). This is the only known instance of this particular morphology in archaeocetes. Functional interpretations of this unique morphology are difficult, given that a singular carpal element stacking between the radius and MC I would greatly inhibit radial deviation. However, the 3D scan of

the *Maiacetus* cast (UMMP VP 118197) that is available publicly does not have this morphology. There are four carpals in the distal row of the right limb, with the trapezium articulating between the scaphoid and MC I. The cast and illustration are based on two different specimens; however, carpal articular relationships are invariant within a taxon. The trapezium on the cast represents a typical articular relationship that is observed in other archaeocete taxa, such as *Ambulocetus.* The Senegalese protocetid appears more similar to *Ambulocetus* and *Pakicetus* than to *Maiacetus* as presented in Gingerich et al. (2009), with a trapezium that articulates with MC I and possibly with MC II (Vautrin et al., 2019). The MC I of *Dorudon* is in line with the rest of the digits, articulates exclusively with the trapezium, and shows no medial deviation. At this point, the forelimb was likely embedded in a soft-tissue flipper and did not require pollical deviation during swimming like many of the semi-aquatic Eocene whales. It does not appear that many extant taxa have a trapezium (Cooper et al., 2007a). Instead, digit I (or the anteriormost digit in tetradactylous mysticetes) frequently articulates with the scaphoid. Additionally, nearly all modern cetaceans examined in Cooper et al. (Cooper et al., 2007b) display reduced manus musculature.

Centrale – Although the functional implications of the centrale are currently unknown, the complex evolutionary history of this carpal is worth noting. The centrale is absent in dichobunids; neither *Diacodexis* nor *Messelobunodon* has a centrale (Thewissen and Hussain, 1990); Franzen, 1983), nor do any modern artiodactyl taxa. The centrale appears and disappears throughout the archaeocete lineage with it being present in first in *Ambulocetus* between the trapezoid and magnum. *Basilosaurus isis* has a centrale (Gingerich and Smith,1990), but *Dorudon* does not (Uhen, 2004) and it is unlikely that *Cynthiacetus* possessed a centrale either (Martínez-Cáceres et al., 2017). The bone is absent in most

protocetids such as *Rodhocetus* (Gingerich et al, 2001), *Peregocetus* (Lambert et al., 2019), and the Senegalese protocetid (Vautrin et al., 2019).

In addition to an inconsistent evolutionary history within cetaceans, the articular relationships of the centrale vary greatly. A centrale is found in the mesonychids *Mesonyx* and *Pachyaena* (Scott, 1888; O'Leary and Rose, 1995; Rose and O'Leary, 1995). The *Pachyaena* centrale is reduced in size and located between the proximal and distal carpal rows, articulating with the trapezoid, magnum, lunate, and scaphoid (Rose and O'Leary, 1995). The *Mesonyx* centrale articulates between the trapezium, trapezoid, and scaphoid (Scott, 1888). *Ambulocetus* has a centrale that articulates between the trapezoid and magnum (Thewissen et al., 1996). The *Basilosaurus* centrale is hypothesized to articulate with the scaphoid (Gingerich and Smith, 1990). Although these taxa all possess a centrale, the articular relationship between the centrale and the rest of the carpals varies greatly and shows no obvious patterning or clear functional benefit.

In summary, this chapter categorizes and compares changes within the archaeocete wrist. This study shows that during the Eocene epoch, during the cetacean land-to-sea transition, the pisiform underwent lateral rotation until it was positioned to lie in plane with the rest of the carpus; this change occurred between the pakicetids and ambulocetids. A laterally projecting pisiform is maintained in all other fossil and modern cetaceans, except for possibly *Maiacetus*, and likely facilitated increased ulnar deviation in semi-aquatic taxa and increased surface area for the flipper of fully aquatic taxa. For comparison, two fossil pinnipeds, *Pliophoca etrusca* (Berta et al., 2015a) and *Enaliarctos mealsi* (Berta and Ray, 1990), have laterally oriented pisiforms, making these taxa examples of convergent evolution that further suggests the importance of this morphological shift for

aquatic locomotion. Conversely, the functional importance of the centrale in *Ambulocetus* is difficult to discern, though the emergence and loss of this carpal throughout the evolutionary history of Cetartiodactyla is worth noting. In addition to the presence of a centrale, *Ambulocetus* exhibits a deviating first digit and robust trapezium. The trapezium is an attachment point for several palmar muscles. This increased musculature, in addition to pollical deviation, indicates that *Ambulocetus* has a robust first digit that helped power the autopod. It is possible that the ability to maintain a medially deviated thumb in abduction during swimming would increase the overall surface area of the hand and increase the thrust generated during a paddling downstroke, much like the laterally oriented pisiform. Other Eocene whales display a digit I that is in plane with the rest of the hand, which highlights an overall flattening of the forelimb into a paddle-like morphology and eventually the formation of a flipper (Uhen, 2004). While this movement of digit I was functionally relevant to the limb to flipper transition, the lateral rotation of the pisiform likely played a greater role during this shift.

The shift from a posteriorly oriented pisiform in mesonychids and Eocene artiodactyls to a laterally-oriented pisiform in all cetacean taxa except for pakicetids and possibly *Maiacetus* suggests that this modification is important for swimming and other aquatic behaviors. A robust, laterally oriented pisiform would increase power for ulnar deviation. As the carpus became immobile within the flipper approximately 40 million years ago (Uhen, 2004), a laterally projecting pisiform would also increase surface area of the soft-tissue flipper for the displacement of water during steering. In addition, the reorientation of the pisiform would increase streamlining of the forelimb to reduce drag on the appendage and energy consumption, thus permitting greater swimming speeds. As Eocene

whales became more competent in the water and shifted reliance from the hind-foot to the tail for

power during locomotion, these other adaptations may have become less critical for locomotion. While

many amphibious archaeocetes are interpreted as hind-limb powered swimmers (Thewissen et al.,

1994; Gingerich et al., 2001, 2009; Bebej and Smith, 2018; Lambert et al., 2019), there is some

evidence to suggest that the Senegalese protocetid used the forelimb for propulsion (Vautrin et al.,

2019). The Senegalese protocetid also demonstrates a massive pisiform that dominates in size over

every other carpal, affording this specimen tremendous strength in flexion and adduction, which

supports the reconstruction of a forelimb-powered protocetid. Further recovery and identification of

more archaeocete carpals will only improve our understanding of the relationship between form and

function in the cetacean wrist.

CHAPTER 4 EMBRYOLOGY OF THE CETACEAN HINDLIMBS

Introduction

As part of their evolutionary transition from land-to-sea, cetaceans (whales, dolphins and porpoises) have undergone significant reduction of the pelvic girdle and hindlimb to vestigial structures embedded within the body wall. Furthermore, the pelvis was decoupled from the vertebral column and the small hindlimbs were no longer functional during locomotion. Fossil evidence shows that these changes occurred throughout the Eocene epoch and are found in concert with the shift from foot-powered to tail-powered locomotion. Extant cetaceans often lack hindlimb structures and retain only rudiments of a typical mammalian hindlimb. Nearly all modern odontocetes have only a simple pelvis that sits along the anterolateral body wall, fully embedded within the surrounding soft tissues and isolated from other skeletal elements. Occasionally, a cartilaginous femur is also found articulated with the odontocete pelvis (Amasaki et al. 1989; Sedmera et al. 1997a) Most mysticetes and the sperm whale (*Physeter macrocephalus*) have a small femur in addition to the rudimentary pelvis (Table 3). The balaenids, the bowhead whale (*Balaena mysticetus*) and the right whale (*Eubalaena glacialis*) have been reported to possess elaborate hindlimbs, with the presence of the pelves, femora, and occasionally tibiae (Struthers, 1881; Thewissen et al., 2021b). There are rare examples of cetaceans that develop fully robust hindlimbs that protrude from the body wall (Andrews, 1921; Ogawa and Kamiya, 1957; Thewissen et al., 2009a) although these are considered anomalous.

Determining the exact homology of the cetacean hindlimb and girdle is challenging given that these structures are highly modified and no longer resemble skeletal structures necessary for terrestrial locomotion. Furthermore, these simple hindlimbs may remain cartilaginous and not undergo ossification well beyond the juvenile or subadult period. Thus, documenting the identity or presence of a hindlimb within any given taxon is further complicated by the difficulty of visualizing or retrieving a small cartilage node from within the anterolateral body wall.

			Pelvis	Femur	Patella	Tibia	Citations
Mysticeti	Balaenidae	E. glacialis (right whale)	x	x	x	x	Struthers 1881, Andrews 1907
		B. mysticetus (bowhead)	x	x	x	x	This study, Struthers 1881, Kükenthal 1914, Thewissen et al. 2021, Cooper et al. 2023
	Balaeonpteridae	B. musculus (blue whale)	x	x			Struthers 1893
		B. physalus (fin whale)	x	x			Hosokawa 1951
		B. acutorostrata (minke)	x	?			Hosokawa 1951*, Omura 1980, Miyakawa et al. 2016
		B. borealis (sei whale)	x	x			Hosokawa 1951
		M. noveangeliae (humpback)	x	x			Kükenthal 1914
Odontoceti	Physeteridae	P. macrocephalus (sperm whale)	x	x			Kükenthal 1914
	Delphinidae	S. attenuata (pan-tropical spotted dolphin)	x				This study, Sedmera et al. 1997, Thewissen et al. 2006
	Monodontidae	D. leucas (beluga)	x				This study, Kleinenberg 1969

Table 3: Summary of cetacean hindlimb development and the degree of hindlimb remnants present in each taxon. * - Hosokawa 1951 reports that the minke whale does not possess a femur, however, both Miyakawa et al. 2016 and Omura 1980 provide evidence for either a cartilaginous or partially ossified femur.

Hindlimb evolution – The evolution of swimming behaviors in archaeocetes (ancient whales) generally follows a pattern from foot-powered locomotion and a rigid spine to tail-powered locomotion facilitated by a highly flexible vertebral column. During the Eocene epoch (~50-42 mya) the first whales (pakicetids, ambulocetids), were amphibious taxa with rigid lumbar vertebrae and robust hindlimbs for locomotion on land and in the waters (Thewissen et al., 1994, 2001b; Thewissen and Fish, 1997; Madar, 2007; Bebej et al., 2012; Bebej and Smith, 2018). Evidence from the lumbosacral vertebral column and hindlimbs indicate that *Ambulocetus* likely swam using pelvic paddling (Thewissen et al. 1994, Thewissen et al. 1996), meaning that the feet were the primary propulsors and the robust, compressed tail was used for stabilization (Thewissen and Fish, 1997). Swimming efficiency in the pakicetids and *Ambulocetus* was also enhanced by interdigital webbing between the fingers and toes, which increased the surface area of the hands and feet to facilitate a larger volume of water displacement during the stroke phase of swimming (Thewissen et al., 1996, 2001b; Thewissen and Fish, 1997; Madar, 2007; Gavazzi et al., 2020). This early adaptation to life in the seas is maintained in more derived archaeocetes and is elaborated in fully-aquatic fossil cetaceans where the entire forelimb is encased within the soft-tissue flipper.

The next lineage of fossil whales, the remingtonocetids, have a more gracile skeleton and flexible vertebral column morphology, which suggests a greater reliance on spinal undulation over pelvic paddling during swimming, though the known hindlimb bones for these taxa show that they were still capable of terrestrial locomotion (Thewissen et al., 2009a; Bebej et al., 2012; Bebej and Smith, 2018).

A lineage of later diverging whales, called protocetids, retained connection between the vertebral column and pelvis. This highly diverse group has taxa demonstrating skeletal traits related to both hindlimb-dominated pelvic paddling [*Peregocetus*, (Lambert et al., 2019), *Maiacetus* (Gingerich et al., 2009), *Rodhocetus* (Gingerich, Ul Haq, et al., 2001), and *Natchitochia* (Uhen, 2014)] and pelvic undulation [(Gingerich et al., 2019) and *Georgiacetus* (Hulbert, 1998)]. The two latter taxa have pelves that are disarticulated from the vertebral column, which is considered a critical step towards the tail-based undulatory locomotion of fully-aquatic cetaceans (Thewissen and Fish 1997). However, both taxa maintained fully developed hindlimbs, suggesting that pelvic decoupling may have preceded hindlimb reduction in archaeocetes.

The first fully aquatic cetaceans, the basilosaurids, had examples of both allometric hindlimb reduction and the developmental loss of hindlimb structures. Both *Dorudon* and *Basilosauris isis* had a reduced pelvis and small hindlimbs that likely did not contribute to locomotion, and *B. isis* reduced both digits I and V to vestigial structures (Kellogg, 1936; Gingerich and Smith, 1990; Gingerich et al., 1990; Uhen, 2004). The pelvis of the basilosaurids still had a pubic symphysis, meaning that the two sides of the pelvis still contacted each other within the body wall (Uhen, 2004). These highly reduced hindlimbs would not have been capable of supporting terrestrial locomotion (Cooper et al. 2023) and one hypothesis suggests that these small limbs may have been used during copulatory behaviors (Gingerich et al. 1990).

Unlike the exceptional preservation of pelvic girdles seen in Eocene cetaceans (basilosaurids, ambulocetids, and remingtonocetids), few pelvic and hindlimb elements are known for Miocene and Oligocene mysticetes. Some Miocene taxa (*Mauicetus*) have a rudimentary femur that articulated with

the pelvis (Fordyce et al., 2000) while others still have a tibia present (Gol'din, 2014). There is currently no evidence of tarsal, metatarsal, or pedal phalanx formation in any fully aquatic fossil cetaceans after the basilosaurids, which suggests that these hindlimb structures were likely vestigial, did not form during development, and did not function in locomotion, similar to modern mysticetes and the sperm whale.

Hindlimb development in prenatal cetaceans - Previous investigations into the development of hindlimb buds in embryonic and fetal cetaceans has primarily focused on the transient nature of the structure (Ogawa 1953, Guldberg and Nansen, Sedmera 1999). Initially, hindlimb buds are prominent structures that protrude from the body wall, but these buds are reabsorbed in the developing body in later stages, and timing of limb bud loss differs between odontocetes and mysticetes (**chapter 2**, Gavazzi et al. 2023). The hindlimb buds of the bowhead whale (*B. mysticetus*) are retained for a comparatively longer period of developmental time than other cetaceans (Thewissen et al., 2021a; Gavazzi et al., 2023). This increase in developmental timing is likely to allow for the formation of more hindlimb structures in bowheads compared to other cetaceans. Bowhead whales are unusual in the amount of hindlimb present within the body wall – the femur and occasionally a cartilaginous tibia can be identified in adult bowheads (Struthers, 1881, 1893; Thewissen et al., 2021a, 2021b; Cooper et al., 2023). In addition to having more hindlimb structures than other whales, adult bowhead whales of both sexes also display allometrically larger pelvic and hindlimb elements compared to those of odontocetes, where the pelvis is sometimes smaller than a single vertebra (Struthers, 1881, 1893; Thewissen et al., 2021b, Cooper et al. 2023). Males typically display relatively larger pelves compared

to females, and the pelvis is highly asymmetrical (Struthers, 1881; Tarpley et al., 2021; Thewissen et al., 2021b; Cooper et al., 2023).

Thewissen et al., (2006) investigated protein signaling associated with outgrowth and subsequent regression of the hindlimb buds of embryonic specimens of the pantropical spotted dolphins (*Stenella attenuata*). Although the limbs showed protein staining patterns consistent with proximodistal outgrowth of the limb (i.e., fibroblast growth factors), these limb buds did not display the correct signaling associated with anteroposterior patterning of the limb (i.e., Sonic hedgehog (SHH). The early truncation of SHH signaling from the zone of polarizing activity (ZPA), a signaling center that dictates anteroposterior limb development, in the *Stenella* limb bud is likely to cause cessation and regression of the hindlimb. Knock-down and knock-out experiments in model animals have shown that a reduction in SHH expression leads to a limb that is allometrically smaller than the body and has often lost or reduced limb bones (Harfe et al., 2004; McGlinn and Tabin, 2006; Scherz et al., 2007; Tschopp et al., 2009; Lopez-Rios, 2016; Letelier et al., 2018). Cessation of this feedback loop has also been implicated in hindlimb reduction and digit loss in other vertebrates including squamates (lizards, snakes) (Cohn and Tickle, 1999; Infante et al. 2018), the emu (*Dromaius novaehollandiae*) (Newton and Smith, 2021), and artiodactyls (even-toed ungulates) (Cooper et al., 2014a), while comparatively prolonged timing and relocation of SHH signaling is found within the expansive bat wing (Weatherbee et al. 2006; Hockman et al., 2008).

The ontogeny of hindlimb loss in cetaceans is only known for a few taxa and the bulk of this knowledge comes from historical documentation that rely heavily on illustrations (Kükenthal, 1893, 1914; Guldberg and Nansen, 1894). Comparisons of cetacean hindlimb development between taxa are

few and far between, with one of the last systematic investigations occurring over a century ago

(Previous to Gavazzi et al. 2023 is Kükenthal, 1914). Here, I investigate the development of the

hindlimb in two taxa, the bowhead and the beluga whale. Hindlimb buds were visually identified in

three embryonic cetacean specimens and cellular analysis of the limb was examined in both bowhead

specimens. The potential presence of cellular markers of limb development such as the apical

ectodermal ridge are identified in both beluga and bowhead, and consideration is given to the genetic

cascades that may be pertinent to the formation of these vestigial structures.

Methods

Three embryos, one beluga and two bowheads, with distinct hindlimb buds were selected for

this study. Specimens were gathered during the Iñupiat subsistence harvests in collaboration with the

North Slope Borough Department of Wildlife Management (NSB-DWM), the Alaskan Eskimo Whaling

Commission, and the communities of Utqiaġvik and Point Lay, Alaska. The NSB-DWM ID system is

based on the year the animal was collected, an abbreviation to refer to the village in which the embryo

was recovered, and the number of animals caught that year. Within *Delphinapterus leucas*, the

addition of DL indicates the taxon to distinguish from *Balaena*. The addition of an F at the end

differentiates between the mother and 149 the fetus (F). Embryos were further classified into Carnegie

stages (CS) based on external morphological features (Gavazzi et al. 2023).

Hindlimbs were visually identified on all three specimens in Gavazzi et al. (2023) (**see chapter

2**) and photographed. The procedure included the identification of labioscrotal swellings and

mammary placodes, when applicable. The urogenital region of all embryos was dissected away from

the body wall. This region of interest was then dehydrated, processed, and embedded in paraffin wax. The tissue was then sliced into six-micron sections and mounted on glass slides. The beluga specimen was not histologically examined, as delphinoids only develop a rudimentary pelvis and occasionally a cartilaginous femur (Amasaki et al, 1989, Sedmera et al. 1997a).

Sections from each bowhead specimen were stained with a modified Mallory's trichrome designed for embryonic connective tissues (Everett and Miller 1973). This trichrome stain comprised of 1% aqueous aniline blue in 8% acetic acid, acid fuchsin, and 2% orange G in 8% acetic acid produces contrast between indigo mesenchyme and blue mature connective tissue. Additionally, metabolically active cells will stain orange within the cytoplasm. This feature of the modified Mallory's trichrome has been verified in fluke tissue from an embryonic beluga whale (**see Chapter 6**).

To secondarily validate our findings, we looked for the presence of a columnar epithelium covering the protrusions and the existence of cartilaginous condensations in the urogenital region. In many vertebrate taxa, the apical ectodermal ridge (AER) is formed by stratified columnar epithelium. However, presence of this cellular organization alone is not enough to determine the presence of an AER, as previous research has demonstrated the great diversity in AER morphology (Cooper et al. 2011). The cetacean flipper does not demonstrate a stereotypical AER at the cellular level, yet the presence of the protein FGF-8 is still detected in the distal limb bud epithelium (Cooper et al. 2017). Previous immunohistochemical and hematoxylin and eosin staining of *Stenella attenuata* hindlimbs suggest that an AER may be present during early stages of hindlimb development, and immunohistochemical staining has shown that this region secretes FGF-8 (Thewissen et al. 2006).

Results

        Beluga embryo NSB-DWM 2019LDL15F – The urogenital region of CS-16 NSB-DWM 2019LDL15F is accompanied by the presence of two hindlimb buds which sit lateral to the midline genital tubercle (Figure 16). In this beluga specimen, the hindlimb bud is a wide mound with a low slope. This structure is capped by a small epithelial protuberance, which may be the AER. There is a thickened structure visible within the semi-opaque limb bud. This curved process may be the cartilaginous anlage for the pelvis. The shape of this structure is similar to that found in bowhead specimen NSB-DWM 2018G3F (Figure 18), as both hindlimb buds have an epithelial projection from the distal edge of the organ. This is the only beluga in the collection that has a clearly identifiable hindlimb bud. Ontogenetically older animals do not have externally visible limbs, a feature that is shared with the spotted dolphin as discussed in **chapter 2** (Gavazzi et al. 2023).

        Paired labioscrotal swellings are visible medial to the hindlimb buds and attached to the genital tubercle. At this Carnegie stage, it is difficult to determine the sex of cetacean embryos.
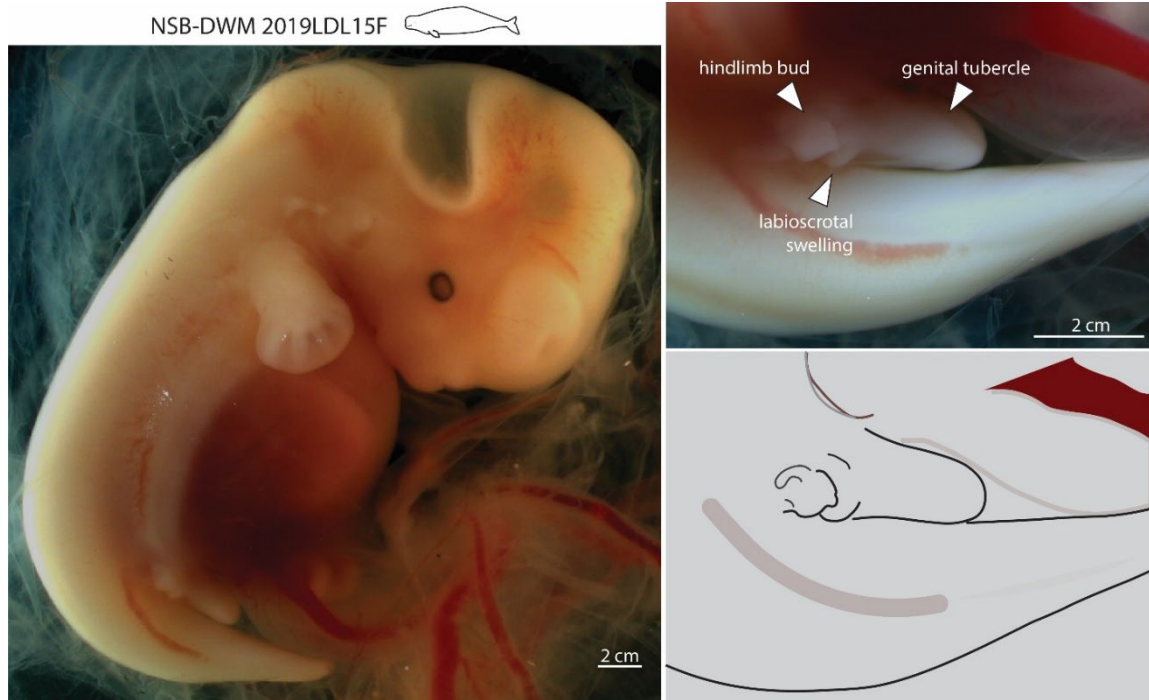
Figure 16: Photographs and illustration of NSB-DWM 2019LDL15F illustration depicting relevant anatomical features of the urogenital region.

Bowhead embryo NSB-DWM 1999B7F – This specimen is the ontogenetically younger of the two

bowheads in this study at Carnegie stage 17 (Figure 17) (**Chapter 2**, Gavazzi et al. 2023). These

hindlimb buds sit lateral to the penis in the midline of this specimen. This animal had low, circular

limb buds, however, there was no visible epithelial protuberance on this specimen. Histological

sections of this specimen reveal two conical projections from the body wall. Furthermore, our

histological data show that there is a cartilage node deep to each of these structures, which is

consistent with the presence of hindlimb elements within each of these hindlimb buds. The right

cartilaginous condensation sits superior to the cartilage on the left side. As this specimen was cut at an

oblique angle, it is likely that the right node is the early ossification center of the pelvis, and the left side node may be part of the developing femur.

There are two paired swellings visible between the hindlimb bud and the genitals akin to what I visually identified in the beluga specimen. Here, it is known that the sex of the specimen is male. At this age in other mammals, the testes are still embedded within the abdominal cavity and would not be visible externally (O'Rahilly and Muller 2001), so these protrusions are potentially either urogenital folds, which will form the prepuce, or rudimentary mammary glands. Histologically, there is neither evidence of developing testes nor the mammary placode, which initiates breast and nipple organogenesis. Due to the age of the specimen, the epithelium is almost completely removed from this animal, which prevents analysis of the proteins associated with the morphologies present.
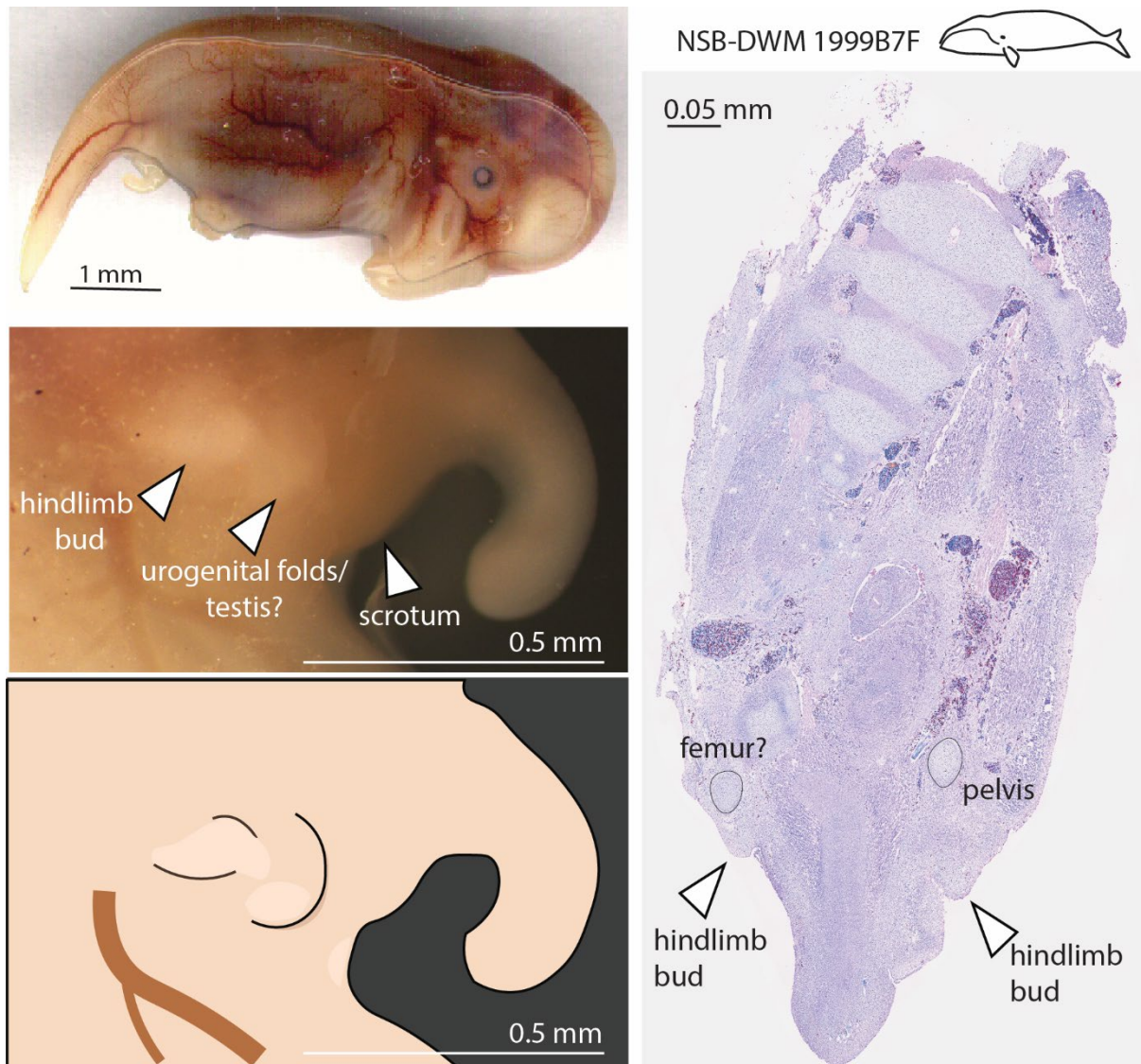
Figure 17: Left: Photographs and illustration of CS 17 NSB-DWM 1999B7F depicting relevant anatomical features of the urogenital region. **Right**: Oblique histological section of 1999B7F stained with a modified Mallory's trichrome. Hindlimb buds are indicated with arrows.

Bowhead embryo NSB-DWM 2018G3F – The largest and ontogenetically oldest bowhead (CS 19) in the collection has large, ovoid limb buds (Figure 18A, B, C). Cartilaginous condensations can be seen through the semi-opaque skin, forming a hook or c-shaped anlage. At the distal tip of the hindlimb bud is a thin projection of tissue (Figure 18B, C) similar to what is seen in NSB-DWM 2019LDL15F.

This tissue may be part of the AER, supporting the proliferation of hindlimb tissues. Medial to the hindlimb bud is a second rounded protrusion. This bump is a thickened region of tissue and may be part of the mammary placode. The scrotum sits in the midline, just below the penis.

Histological sections show that within the hindlimb buds are several cartilaginous condensations within the anterior body wall (Figure 18D). The pelvis sits closest to the midline and is separated by a thin slip of connective tissue from the other cartilages in the section. The cartilages closes to the hindlimb bud are part of the developing femur. On the right side of the embryo there is a second cartilage visible, though it is difficult to determine whether this is a continuation of the developing femur or a separate condensation that may be a primordium for the tibia. The distalmost cartilage appears to protrude externally from the abdominal wall into the mesenchymal limb bud, a feature which was not seen in the other bowhead embryo (NSB-DWM 1999B7F). The unfortunate loss of the epithelial tissue surrounding the urogenital region in this specimen precludes a deeper investigation of the apical ectodermal ridge and the proteins involved in bowhead limb development and differentiation.

Histological evaluation of this bowhead did not reveal regions of differential cellular tissue between the penis and the hindlimb buds, contrary to visual observations of the urogenital region. At this stage of development in other mammals, the testes have not fully descended into the scrotum and will not be visible externally (O'Rahilly and Muller 2001). The cranial view of the urogenital region (Figure 18) shows the presence of the developing epithelium that will encase the penis and become the prepuce, which initially derives from the urogenital folds.
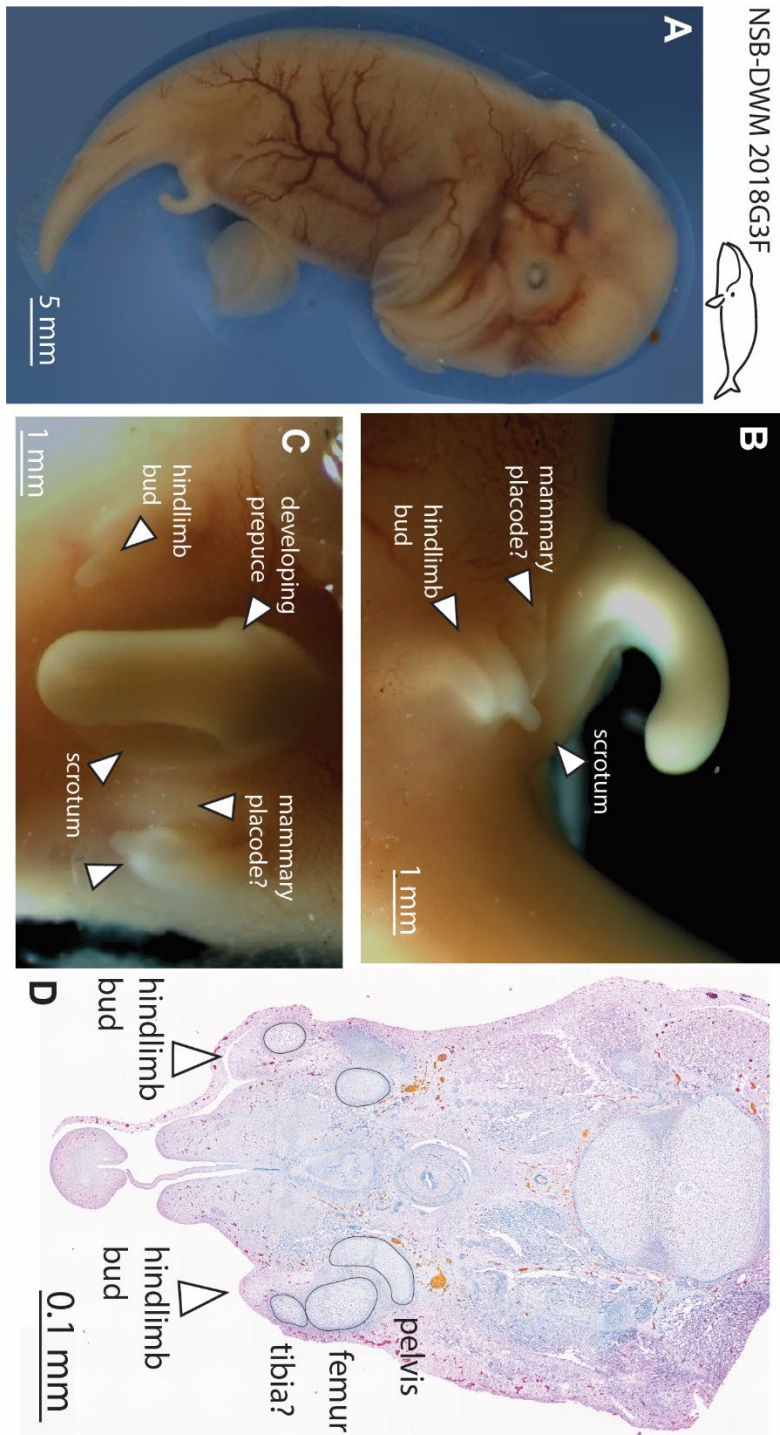
Figure 18: A, B, C: Photographs of the CS-19 bowhead specimen NSB-DWM 2018G3F, including detailed images of the urogenital region in lateral (**B**) and cranial (**C**) views. **D**: A transverse histological section through the urogenital region of the specimen stained with a modified Mallory's trichrome. The cartilages and their corresponding hindlimb buds are outlined**.**

Discussion

Hindlimb bud morphology in cetaceans - Hindlimb buds have been documented in the embryos of numerous cetacean taxa throughout the 19th, 20th, and 21st centuries (Guldberg and Nansen, 1894; Kükenthal, 1914; Ogawa, 1953; Sedmera et al., 1997a; Thewissen et al., 2006; Gavazzi et al., 2023). Historically, there was heated debate surrounding the presence of cetacean hindlimb buds, as some of the earliest research on these transient structures misidentified the transient hindlimb as a mammary gland (Kükenthal, 1893). The identity of the hindlimb buds has been thoroughly settled via photography and histology since that time, though the mammary glands still remain greatly understudied (Anderssen, 1918).

In the studies the describe cetacean embryonic development, there is a noted discrepancy in descriptions of the overall morphology of the hindlimb bud. Some taxa, particularly dolphins and porpoises, appear to have a hindlimb bud that is conical in appearance (Figure 19, left center) (Guldberg and Nansen, 1894; Kükenthal, 1914; Sedmera et al., 1997a). This hindlimb bud is morphologically distinct from the wide, low hindlimb bud seen in the beluga (Figure 19, right center) and the ovoid limb bud of the bowhead whale (Figure 19, right) (Thewissen et al., 2021a). Kükenthal, (1914) depicts several small embryos of True's porpoise (*Phocoenoides dalli truei*) with large, flattened hindlimb buds similar in appearance to terrestrial mammals (Figure 19, left). These four distinct morphologies all correspond to four separate genera within Cetacea, but there is not enough data currently to speculate on how the variation within hindlimb morphology may relate to phylogeny. This may be related to relaxation of selection pressures on the hindlimb bud, but more molecular evidence of hindlimb development in these taxa would be needed to support this claim.

Previous work on key features of the tetrapodal limb bud, such as the apical ectodermal ridge (AER) which drives proximodistal limb outgrowth, have shown that cellular and morphological variation in the AER do not appear to impact limb development so long as the correct molecular signals are being expressed (Lewandoski et al., 2000; Moon and Capecchi, 2000; Moon et al., 2000; Boulet et al., 2004; Cooper et al., 2011).

It is worth noting that these images from the spotted dolphin, beluga, and bowhead all correspond to roughly the same Carnegie stages (CS 16 for odontocetes, CS 19 for bowhead), which uses the morphology of the hindlimbs as a key identifier of relative ontogenetic age (see also chapter 2). The features present on this illustrated True's porpoise specimen, such as a hand plate and presence of the pharyngeal arches, suggest that it is roughly a Carnegie stage 14 or 15 which would make that embryo approximately the same relative ontogenetic age as well (Thewissen and Heyning, 2007). Therefore, the morphology indicated in the drawing is roughly contemporaneous with the other odontocetes. All four of these embryos can be generally categorized in the mid-embryonic phase of development. For an in-depth discussion of embryonic heterochrony in cetaceans, see **chapter 2**.
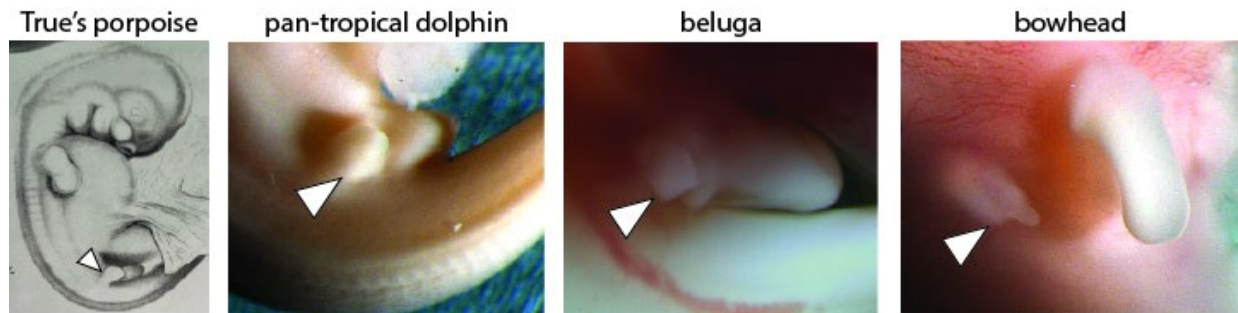
Figure 19: Images of hindlimbs in four taxa depicting various hindlimb bud morphologies reported in cetaceans. Drawing of True's porpoise from Kükenthal, (1914). Photographs from a CS 16 pan-tropical dolphin (Natural History Museum of Los Angeles County specimen 98808), a CS 16 beluga (NSB-DMW 2019LDL15F), and a CS 18 bowhead (NSB-DWM 2018G3F) (Gavazzi et al. 2023).

Variation in hindlimb rudiments – The variability in external hindlimb bud morphology does not appear to correspond to the differences in hindlimb development. Aside from the sperm whale, all odontocetes only retain a vestigial, highly reduced pelvis. The difference in external hindlimb bud morphology between these taxa may not translate to a significant modification in gene expression patterns, as these disparate bud shapes all produce morphologically similar skeletal traits.

For the cetaceans that do maintain some hindlimb rudiments, it has been previously hypothesized that the hindlimb buds will persist for an ontogenetically extended period of time to allow for the formation of these skeletal traits (e.g., femur and tibia) (Gavazzi et al., 2023). It has been shown in mouse models that earlier perturbations to the limb bud result in greater phenotypic changes than later shifts in gene expression (Agarwal et al., 2003; McGlinn and Tabin, 2006; Kozhemyakina et al., 2014). As the bowhead hindlimb is externally visible for an ontogenetically longer period than in the spotted dolphin or beluga (see **chapter 2**), it is likely that active gene expression in that bowhead limb is continuing as well. There are a few critical datasets showing that SHH and the

94

regulatory genes associated with this morphogen are altered to reduce expression in cetacean hindlimbs (Thewissen et al., 2006; Sun et al., 2022). Given that hindlimb loss only occurs once within the fossil record (Gingerich et al., 1990; Uhen, 2004; Thewissen et al., 2009a), it is likely that SHH is a key regulator of hindlimb formation across all of Cetacea and that the degree of SHH expression, or lack thereof, partially dictates the degree of hindlimb or pelvic development.

Recent studies have shown that there are cetacean-specific modifications to enhancers associated with the transcription factor TBX4 (Liang et al., 2022), which is crucial for the early specification of the hindlimb field in concert with other transcription factors such as PITX1 (Logan and Tabin, 1999; Duboc and Logan, 2011). This data, along with assessment of numerous limb-related genes (Sun et al., 2022) corroborates the protein signaling data found in Thewissen et al. (2006) as *TBX4* is an upstream regulator of SHH expression. In addition to SHH, Sun et al. (2022) also reports modifications to the expression patterns of BMP4, BMP7, FGF-8, FGF-10, and PITX1. These genes are critical for hindlimb development in quadrupedal mammals and have been hypothesized as additional key proteins involved in cetacean pelvic and hindlimb reduction (Thewissen et al., 2006; Gol'din, 2014; Thewissen, 2018), though these signaling factors have yet to be tested using immunohistochemistry or other gene expression assays.

Anatomical investigation of the cetacean pelvis reveals left-right asymmetry between the two isolated sides and significant sexual dimorphism related to these two bony elements (Simões-Lopes and Gutstein, 2004; Dines et al., 2014; Cáceres-Saez et al., 2015; Miyakawa et al., 2016; Cooper et al., 2023). Previous work on left-right asymmetry in the spines of stickleback fish (*G. aculeatus*) and the sirenian (*T. manatus*, *D. dugong*) pelves revealed that these taxa have modified PITX1 expression

(Shapiro et al., 2006; Chan et al., 2010; Nganvongpanit et al., 2020). Furthermore, mouse models with reduced PITX1 expression have smaller hindlimbs and/or asymmetry in the pelvis (Thompson et al., 2018). As mentioned previously, PITX1 works in tandem with TBX4 to initially specify and pattern the limb region as a distinct morphological and developmental entity from the flank of an embryo (Logan and Tabin, 1999). It is reasonable to infer that the modified PITX1 expression reported in the cetacean genome is also contributing to left-right asymmetry in the pelvis (Liang et al., 2022; Sun et al., 2022).

Among cetaceans, the balaenids (bowheads and right whales) have comparatively robust hindlimbs with a cartilaginous or ossified femur, occasional tibia, and rarely a metapodial (Struthers, 1881, 1893; Thewissen et al., 2021b). The purpose for this distinction from other cetaceans is currently unknown, though the additional hindlimb elements function as a greater surface area for attachment of urogenital musculature and the penis (Struthers, 1881; Thewissen et al., 2021b). Bowheads have a dynamic mating behavior where both the male and female will rotate and the penis must arch over several meters to locate the vagina (Slijper, 1966; Tarpley et al., 2021; Cooper et al., 2023), which would require robust musculature for control and movement of the penis during reproduction. There are currently no experimental or correlation studies that track pelvis size and shape to mating behaviors.

It is also possible that there is a lack of developmental constraint on the hindlimb, which would allow for a greater degree of developmental plasticity and variation. If this were the case, however, we would expect to see a greater degree of intraspecies variation. In the cetacean flipper, which has the potential to develop more than three phalanges (hyperphalangy) on one or more digits, there are a range of phenotypes and phalangeal counts found within most taxa. As one example, most

sperm whales have between three and six phalange on their second digit (Cooper et al., 2007a). While

skeletal elements may ossify or remain cartilaginous at differing rates, this does not translate into the

same level of intraindividual variation as seen in the cetacean flipper. There are some notable

exceptions, though, where aberrant hindlimbs will highly developed skeletons that project from the

body wall have been reported (Andrews, 1921; Ogawa and Kamiya, 1957; Thewissen et al., 2009a),

suggesting that the hindlimb buds are capable of creating a fully realized hindlimb with a femur, tibia,

and some metapodials/pedal phalanges.

This chapter provides morphological and cellular insight into the hindlimb buds of two

cetacean taxa, belugas and bowhead whales. While belugas, like nearly all other odontocetes, only

form a rudimentary pelvis, the hindlimbs of the bowhead are some of the most elaborate found in

modern cetaceans. While the exact mechanism for this variation is not currently known, bowhead

embryos clearly demonstrate robust hindlimb buds that persist for an ontogenetically longer period

than other cetaceans (**chapter 2**) (Gavazzi et al., 2023) and gene expression research suggests that

expression of the morphogenetic protein SHH may be a key determinant of limb development in

cetaceans (Thewissen et al., 2006; Liang et al., 2022; Sun et al., 2022).

CHAPTER 5 CAUDAL TAIL MORPHOLOGY IN TWO ARCTIC CETACEANS

Introduction

The body plan of cetaceans (whales, dolphins, and porpoises) is unique among mammals in that soft-tissue flukes at the distal end of tail produce lift-based propulsion via dorsoventral undulations. Flukes are supported along the midline by spinal tendons and caudal vertebrae, and the fluke blades are made entirely of soft tissues. The core of these lateral projections are comprised of two differentially arranged dense irregular connective tissue, the outer ligamentous layer and inner core layer, and are covered by a smooth epithelium (Sun et al., 2011; Gough et al., 2018). Compared to other caudal vertebrae, the centra of odontocete (toothed whale) fluke vertebrae are dorsoventrally compressed and mediolaterally wide (Figure 20, purple) (Slijper, 1961; Buchholtz, 1998, 2007). These vertebrae anchor epaxial and hypaxial tendons that facilitate generation of thrust during swimming, and these forces are then propagated via the tail flukes (Felts, 1966; Fish et al., 2006; Sun et al., 2010, 2011; Ayancik et al., 2020). Some studies of odontocetes and rorquals (balaenopterids, like humpback and blue whales) have reported that the vertebra closest to the point of fluke insertion onto the tail is highly spherical and is described as a 'ball' vertebra (Watson and Fordyce 1993). This single vertebra, the ball vertebra, differs in shape from adjacent vertebrae and is considered an osteological correlation for the insertion of the fluke blades onto the narrowest point of the tail, called the peduncle. (Figure 20, pink) (Rommel, 1990; Watson and Fordyce, 1993; Fish et al., 2006).

Post-thoracic vertebrae are morphologically similar in appearance within extant cetaceans, which hinders the identification of disarticulated vertebrae (De Smet, 1977; Buchholtz, 2007; Buchholtz and Gee, 2017). Changes in centrum proportions and the identification of the 'ball' vertebrae are standard approaches to the identification of fluke vertebrae in cetacean spinal reconstructions.
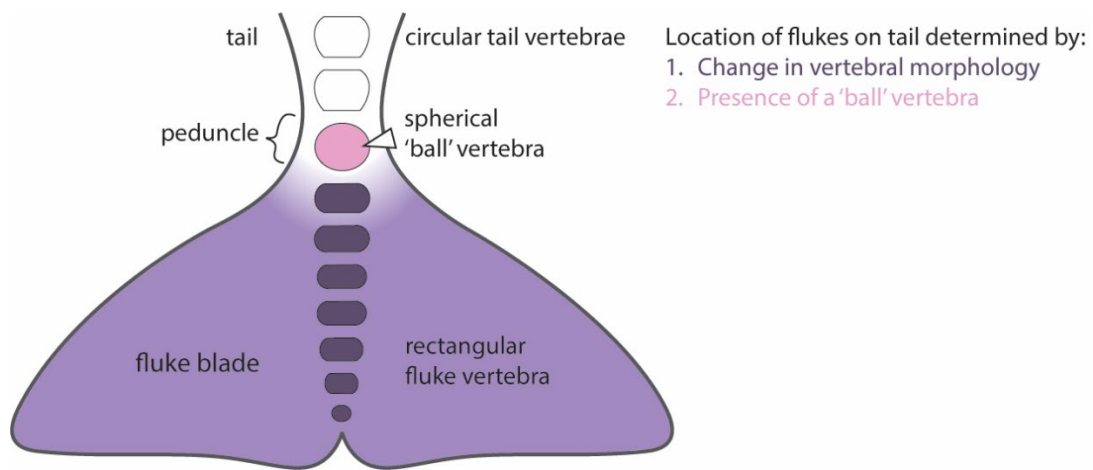
Figure 20: Illustration of tail depicting both the soft-tissue and skeletal features associated with the flukes as described by literature (Roux, 1883; Ryder, 1885; Slijper, 1961; Felts, 1966; Watson and Fordyce, 1993; Buchholtz, 1998; Fish et al., 2006).

Tail morphology in aquatic tetrapods

Aquatic and secondarily aquatic tetrapods utilize the tail for oscillation, undulation, or stabilization during swimming, and modern taxa are often used as proxies to infer archaeocete (ancient cetacean) swimming behaviors (Thewissen and Fish, 1997; Buchholtz, 1998; Fish, 1998). To accommodate the distinct suite of traits necessary for life in the water, the tail is frequently modified

via skeletal and soft-tissue adaptations. There are several major categories of tail adaptations, or lack thereof, in aquatic tetrapods: a.) narrow elongate tails with few specializations are found in the raoellid *Indohyus* or the pakicetids, the earliest cetaceans (Figure 21A) (Fish, 1984; Madar, 2007), b.) dorsoventrally or mediolaterally compressed tails as found in the archaeocete *Ambulocetus* (Figure 21B) (Fish, 1994; Thewissen and Fish, 1997), c.) the triangular/lunate tails of dugongs and fully aquatic cetaceans (Figure 21C, 2D) (Ayancik et al., 2020; Felts, 1966; Fish, 1998; Fish et al., 2006; Ryder, 1885; Sun et al., 2010), and d.) the rounded tail paddles of manatees (Figure 2E) (Buchholtz et al., 2007; Kojeszewski & Fish, 2007).

Fluke evolution in cetaceans

Within the fossil record of Cetacea, the transition from limb-powered to tail-powered locomotion involves reduction of the hindlimb (Gingerich et al., 1990; Uhen, 2004), disarticulation of the sacroiliac joint to uncouple the pelvis from the spine (Hulbert, 1998; Martínez-Cáceres et al., 2017; Gingerich et al., 2019; Cooper et al., 2023), increasing flexibility in the lumbus (Thewissen and Fish, 1997; Bebej and Smith, 2018) and outgrowth and elaboration of the soft-tissue flukes. The loss of sacroiliac articulation and reduction in hindlimb length appears to be evolutionarily concurrent with the emergence of the flukes in basilosaurid archaeocetes from the late Eocene epoch (Uhen, 2004). Distal tail elements are infrequently recovered and as such, identification of more anterior caudal vertebrae, sacral vertebrae, and the pelvis are used as proxy to determine the degree of tail usage in archaeocete locomotion, which in turn estimates the likelihood of soft-tissue tail modifications in a given taxon (Thewissen et al., 1996; Gingerich et al., 2009, 2019; Lambert et al., 2019). All current

fossil evidence suggests that flukes evolved once within Cetacea and that this likely occurred within

early basilosaurids (Gingerich et al., 1990; Fish, 1998; Uhen, 2004; Buchholtz, 2007).

A

Pakicetus

B

Ambulocetus

C

Dorudon

D

common dolphin

E

manatee
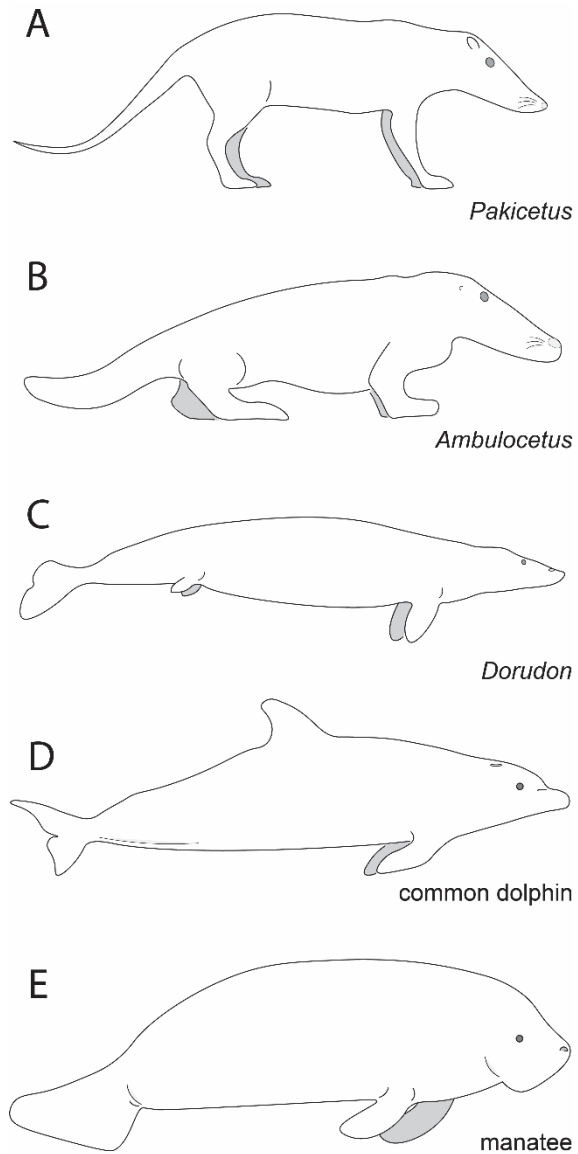
Figure 21: Images of representative taxa depicting modifications to the tail for aquatic locomotion. Early fossil cetaceans (A, B) show minor changes to the tail while fully aquatic fossil (C) and extant cetaceans (D) and sirenians, such as the manatee (E) have dramatically changed the structure of their tails for swimming.

The initial cetacean bodyplan in the most terrestrial of the archaeocete taxa, the pakicetids, has

no morphological adaptations for aquatic behaviors in the pelvis or the tail (Figure 21A). The four

sacral vertebrae are tightly fused to each other and to the ilium (Thewissen et al., 2001b; Madar,

2007). Caudal vertebrae of *Nalacetus* and *Pakicetus* are not unique in external morphology but have

minerally dense bone, a reduced medullary cavity (osteosclerostic), and thickened cortices

(hyperostotic) that serve as bony ballast and counter overall body buoyancy in the water (Madar,

2007). The tail, if used in swimming, likely served a stabilization function. One of the first amphibious

cetaceans, *Ambulocetus natans*, was primarily a foot-powered swimmer with a large, robust tail and

rigid spine (Figure 21B) (Thewissen et al., 1994; Thewissen and Fish, 1997). As seen in other early

archaeocetes, the pelvis of *Ambulocetus* is comprised of four ossified sacral vertebrae and an

articulated ilium (Madar et al., 2002b). Five caudal vertebrae are known for *Ambulocetus* with large

attachment sites for intrinsic spinal musculature, which suggests active use of the tail during

swimming for stabilization. It is unlikely that *Ambulocetus* had soft-tissue flukes. Later diverging

remingtonocetid archaeocetes had a more flexible lumbus than earlier archaeocetes, but still likely

relied on pelvic paddling as their primary form of aquatic locomotion (Bebej et al., 2012; Bebej and

Smith, 2018). For an in-depth review of fossil whales, their shifting locomotor behaviors in the water,

and the relevant skeletal morphologies see **chapters 3 and 4**.

Protocetid archaeocetes are a diverse group that capture a wide range of skeletal morphologies

in the pelvic and caudal region. None of these taxa have direct evidence for the presence of flukes,

though there is secondary evidence for highly aquatic behaviors within other regions of the body that

would potentially correlate to modified tail anatomy (see **chapters 3 and 4** for detailed reviews). Most

protocetid taxa have four sacral vertebrae, and there is frequently some degree of fission between these bones. For example, *Maiacetus* has fusion between three of the four sacral vertebrae. The fourth sacral vertebra is only fused to S3 via the transverse processes, not the centrum (Gingerich et al. 2009). One well-preserved taxon, *Peregocetus*, has caudal vertebrae that are morphologically reminiscent of modern semi-aquatic animals with dorsoventrally compressed tails (Lambert et al., 2019). Some taxa (*Natchitochia, Georgiacetus, Protocetus*) have either a reduced sacral count or lack sacral fusion (Hulbert, 1998; Uhen, 1998). For many of these specimens there are few caudal vertebrae, so little is known about the tail. In the protocetid *Aegicetus*, the sacral vertebrae are unfused and there is no evidence in the tail vertebrae for attachment of soft-tissue fluke (Gingerich et al., 2019), which suggests that decoupling of the spine from the vertebral column may precede the evolution of the soft-tissue flukes.

The pelvic and spinal diversity found within the protocetids is not reflected within the basilosaurids. All basilosaurids are obligatorily aquatic and have spines more akin to modern cetaceans; the pelvis is disarticulated from the spine, the hindlimbs are highly reduced, and the posterior caudal vertebrae are dorsoventrally compressed with a rectangular appearance (Gingerich et al., 1990; Uhen, 2004; Martínez-Cáceres et al., 2017). *Dorudon*, a basilosaurid archaeocete, has no easily identifiable sacral vertebrae. The pelvic bones are completely disarticulated from the spine and there is no evidence of fusion between any of vertebrae from this region (Uhen, 2004). Instead, Uhen (2004) suggested that the last four lumbar vertebrae may represent the sacral region based on presence of thickened transverse processes. These are also the last four vertebrae within the spine that lack associated chevron bones, which is a common feature used to identify anterior caudal vertebrae

(Buchholtz, 1998; Buchholtz and Gee, 2017). In *Dorudon*, there is a shift within the distal tail region from craniocaudally elongate and morphologically circular vertebrae to rectangular vertebrae with laterally expanded centra (Uhen, 2004), which is the same morphological change identified in the fluke vertebrae of modern odontocetes (Buchholtz, 1998). This change in tail morphology is some of the earliest evidence in the fossil record for the formation of soft-tissue flukes (**Figure 21C**).

Examination of fluke homology and evolution is hindered in both modern and fossil contexts by the reliance of secondary and tertiary means for investigation of this novel appendage. As a soft-tissue structure, the flukes are not preserved in skeletal or fossil remains. Furthermore, the two common metrics utilized to identify fluke vertebrae, 1) mediolaterally wide and dorsoventrally short vertebrae and 2) identification of a 'ball' vertebra, have been primarily tested using odontocete skeletal collections alone without direct reference to the overlying soft-tissues. The first publication describing the 'ball' vertebrae does not have baseline metrics to more accurately assess the curvature of particular vertebrae associated with the peduncle (Watson and Fordyce, 1993). Both centrum measurements and the identity of the 'ball' vertebrae are primarily, though not exclusively, tested on odontocete taxa with different ecologies and life histories from many mysticetes, including the bowhead whale. To better understand the relationship of the known hard-tissue materials to the soft-tissue flukes, here I test the accuracy of these two metrics, centrum proportions and the identity of a 'ball' vertebra, for fluke vertebra identification in an odontocete, (beluga), and a mysticete, (bowhead) whale tail. These two whales have different evolutionary histories, locomotor patterns, and diet, which may impact their skeletal morphologies. Through dissection, I investigated the relationship of vertebral measurements and metrics directly against the overlying morphology.

Methods

The caudal soft-tissue and in-situ vertebrae were removed from one beluga (*Delphinapterus leucas*) (**Figure 22**, NSB-DWM 2021LDL9) and one bowhead whale (*Balaena mysticetus*) (**Figure 23**, 2021B11). These specimens were collected with permission from the subsistence hunters of Point Lay and the whaling captains of Utqiaġvik, Alaska in collaboration with the North Slope Borough Department of Wildlife Management and the Alaskan Eskimo Whaling Commission. Without their generosity and guidance, this work would not be possible. The flukes of two of the whales were removed for subsistence (aqikkak) and cut marks indicating fluke insertion onto the tail were visible. NSB-DWM 2021B11 was estimated to be a two-year old bowhead whale and 2021LDL12 was a light grey subadult beluga whale.

The *in-situ* tails were flensed and macerated to extract the vertebrae from overlying tissue. Both specimens were photographed throughout the maceration process to record the relationship between soft- and skeletal tissues. After skeletonization, the beluga tail vertebrae were measured with digital calipers and microCT scanned (Scanco Medical, Viva70) at 70 kVp with a voxel size of 40 microns. The bowhead vertebrae with measured to the nearest mm with vernier calipers and CT scanned (GE BrightSpeed 1) with a voxel size of 0.8 mm.

Linear measurements of centrum width (CW), height (CH), and depth (CD) were recorded to the nearest 0.1 mm. (Figure 24) The relationship between centrum width and centrum height was additionally plotted as a ratio of CW/CH where vertebrae that are wider than they are tall exceed a value of 1.0. To assess curvature of the caudal vertebrae, mid-sagittal slices were extracted in Avizo (ThermoFisher) and imported to ImageJ (National Institute of Health) where roundness and

circularity were calculated. Roundness is a measurement of the area of the sample calculated as a

variable between 0.0 and 1.0, where 1.0 is a complete circle. Circularity is a measurement of the object

perimeter that calculates the amount of deviation from an idealized circle from 0.0 to 1.0 with 1.0 as a

perfect circle.

Figure 22: Photographs of beluga vertebrae (*D. leucas,* NSB-DWM 2021LDL9) in cranial and lateral view. Star indicates vertebra closest to the soft-tissue peduncle and insertion of fluke blades onto the tail.

Figure 23: Photographs of bowhead vertebrae (*B. Mysticetus*, NSB-DWM 2021B11) in cranial and lateral view. Star indicates vertebra closest to the soft-tissue peduncle and insertion of the fluke blades.

Results

Beluga whale (*Delphinapterus leucas,* NSB-DWM 2021LDL9) – Measuring the CW, CH, and CD of the vertebrae shows a clear separation in overall length from the tail vertebrae to the caudal fluke vertebrae (Figure 24A). At caudal vertebra 4 (Ca 4), the width of the vertebrae becomes proportionally longer than the height of the vertebrae, giving them a highly rectangular appearance. The shift in proportions is not only identified via caliper measurements but is also visually distinct. This ratio of centrum width over centrum height continues to increase caudally before reducing at the terminal vertebra, which is a small and nodular bone (Figure 24B). The craniocaudal depth of the vertebrae decreases slowly with no major or sudden transitions in the dataset. This shift in proportions correlates to the attachment of the fluke blades, which occurred between Ca3 and Ca4. The first five vertebrae were associated with chevron bones.

Neither roundness nor circularity demonstrated significant differences across the tail to fluke boundary. Roundness of the epiphyses increased through the beluga tail, decreasing sharply at the terminal vertebra, while circularity remained constant throughout the sequence. The dataset shows no clear evidence for a ball vertebra within the beluga tail.

Bowhead whale (*Balaena mysticetus,* NSB-DWM 2021B11) – Within the bowhead tail, separation of centrum metrics is less defined than in beluga. Within this vertebral sequence, the centrum width and centrum height are nearly equal for Ca3, Ca4, and Ca5 (Figure 24C). The first vertebra to exceed centrum width over centrum length is Ca4. This vertebra was anterior to the insertion of the flukes, which occurred along the span of Ca5.

The shape descriptors for the bowhead (NSB-DWM 2021B11) follow a similar trajectory as the

beluga (NSB-DWM 2021LDL9) (Figure 24D). Roundness gradually increases throughout the vertebral

sequence before shifting between the penultimate and the terminal vertebra. Circularity remained

generally consistent throughout the vertebrae. Once again, there is no clear indicator for the presence

of a ball vertebra within this dataset.
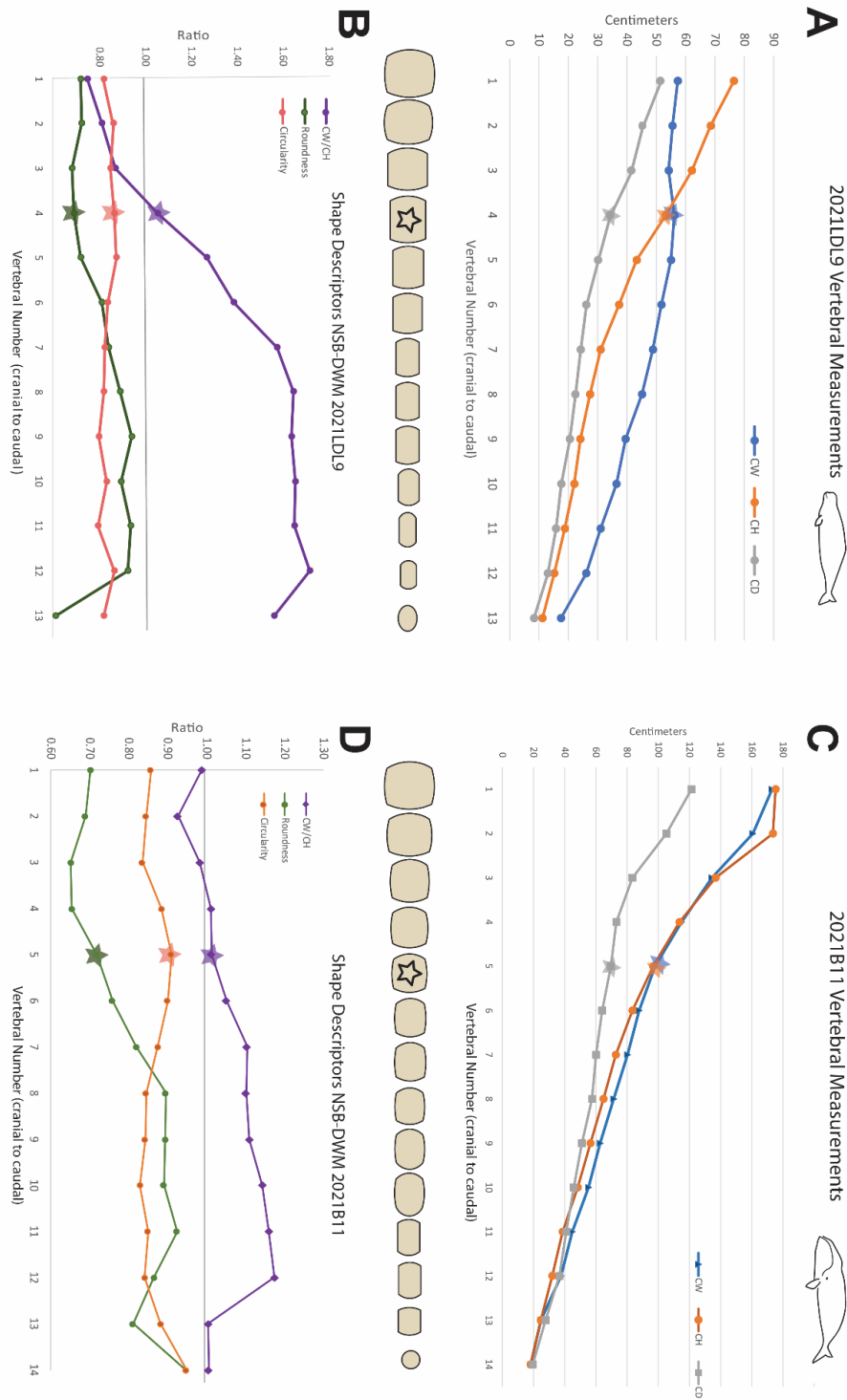
Figure 24: Measurements of subadult beluga NSB-DWM 2021LDL9 (A, B) and ingutuk bowhead NSB-DWM 2021B11 (C, D). The star symbol indicates the vertebra closest to the soft-tissue peduncle. Centrum height (CH), centrum width (CW) and centrum depth (CD) were measured with digital calipers to the nearest .1 mm. CW > CH in the fluke vertebrae, calculated as a ratio in B and D. Degree of roundness and circularity were calculated in ImageJ via digitization of a midsagittal view through each vertebra (B, D). A measurement of 1.0 = perfect circle and 0.0 = oblong ellipse.

Discussion

Through the measurement of one odontocete (beluga) and one mysticete (bowhead) tail, the beluga vertebrae show the expected shift in centrum proportions. The difference in shape between tail and fluke vertebrae is stark enough that the two can be differentiated visually and is clear within the dataset as well (Figure 22, 24A, B). The bowhead measurements do not clearly conform to the commonly utilized metrics for identifying fluke vertebrae within the tail. Ca3, Ca4, and Ca5 are all similar in appearance and show little variation in shape difference. The caudal width to caudal height ratio does not change at the first fluke vertebrae. Additionally, some studies have relied on the presence or absence of chevron bones within the tail as a proxy to identify the fluke region of the tail (Roux, 1883; Ryder, 1885; Felts, 1966; Buchholtz, 1998). Here, the chevron bones terminate at the peduncle. Thus, the bowhead tail does not fit the hypotheses surrounding fluke identification by vertebral elements alone and in the absence of chevron bones should be interpreted cautiously. The overall shift from circular to squared vertebrae can identify the relative location of the flukes on the bowhead tail, but specific locations for fluke attachment or the peduncle cannot be determined.

For both taxa, a ball vertebra is not readily apparent by eye alone, nor do the metrics circularity or roundness indicate a specialized vertebra (Figure 22, 23, 24B, D). Measurements of vertebral perimeter (circularity) and overall area (roundness), taken from isolated midsagittal slices through the micro-CT data, do not set any particular vertebra apart from the rest of the spinal column (Figure 25). While the original definition of the 'ball' vertebra is based entirely on visual identification (Watson and Fordyce, 1993), the dataset here does not provide any evidence to support the presence of an overtly spherical vertebrae at the peduncle nor within the flukes.
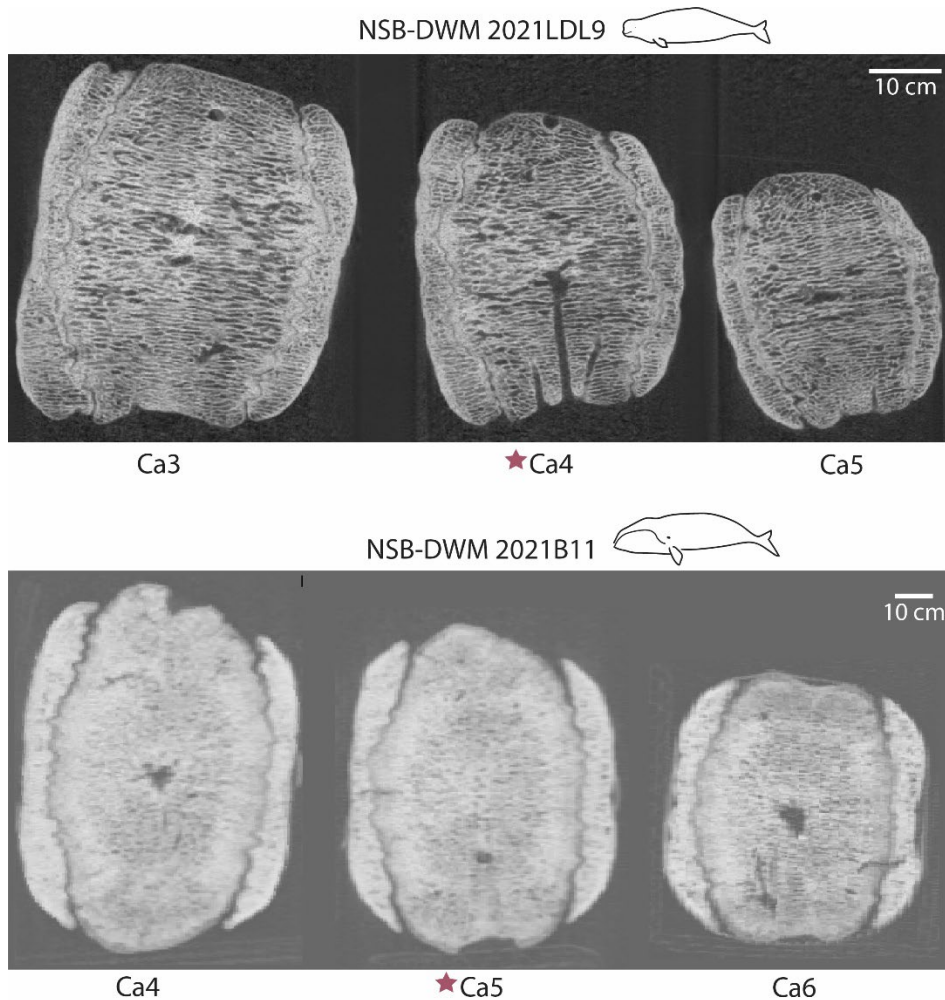
Figure 25: Mid-sagittal cross sections through the vertebral column. The star symbol indicates the vertebra closest to the soft-tissue peduncle. NSB-DWM 2021LDL9 vertebrae were scanned at a resolution of 0.04 mm voxels and NSB-DWM 2021B11 vertebrae were scanned at a resolution of 0.8 mm voxels.

When comparing the bowhead vertebral series to the current methods used to identify fluke

vertebrae, there are a few variables that may explain the difference between our expected outcomes

and the data presented here. First, this dataset for the bowhead may be confounded by the unusual

ontogeny of this animal. Bowheads are the longest-lived mammals known, with an estimated lifespan

>200 years (George et al., 1999, 2016; Keane et al., 2015). These whales maintain a substantial amount of calcified cartilage around their vertebrae and do not close the epiphyses of their long bones (Thewissen et al., 2021b). It is currently unknown how these unusual skeletal phenotypes may have impacted the data provided here, as measurements of the cartilage encasing the vertebrae were not taken. The contributions of supporting adnexa to the vertebrae within the flukes is largely unknown and warrants further investigation using ontogenetically older specimens.

Both the beluga and bowhead tail have unfused epiphyses. For other mammals, this skeletal phenotype is indicative of sub-adult status. There are many cetaceans, including the two taxa referenced here, that may not fuse their epiphyses at all throughout the lifespan or do so well after sexual maturity (Moran et al., 2015; Thewissen et al., 2021b). In Watson and Fordyce (1993), the minke whale (*Balaenoptera acutorostrata*) vertebral column had unfused epiphyses along the spine and was noted to be an immature female. Minke whales are known to fuse the epiphyses of their vertebrae (Kato, 1988), which suggests that the minke whale specimens used to determine the existence of a 'ball' vertebrae may not be representative of other cetacean vertebral morphologies.

The differences in vertebral shape within the bowhead may also be related to locomotor behavior. The centrum ratio and ball vertebra methods were both generated using predominantly, though not exclusively, odontocete specimens (Ryder, 1885; Felts, 1966; Rommel, 1990; Watson and Fordyce, 1993; Buchholtz, 1998). Odontocetes, particularly dolphins, have dynamic swimming and feeding behaviors that are drastically different from the deliberate ram-feeding in balaenids (Fish and Rohr, 1999; Simon et al., 2009; Goldbogen et al., 2017; Tanaka et al., 2019). In Watson and Fordyce (1993), the ball vertebra is identified in the mysticete minke whale (*B. acutorostrata*). While there are

no testable metrics given for the ball vertebra in this taxon, there is also a difference in locomotor

capabilities between the minke whale and other mysticetes. The fastest swimming speeds relative to

body size for baleen whales are found in the rorquals, including the minke whale (Heide-Jørgensen et

al., 2001; Goldbogen et al., 2012, 2017). The rapid relative locomotion of the minke whale, in contrast

to the slower bowhead, places different stresses and strains upon the fluke vertebrae. The variance

between the data reported in Watson and Fordyce (1993) and here may be related to the differential

strains placed upon the fluke vertebrae and thus the remodeling, or lack thereof, of this peduncular

vertebra to resemble a ball.

Overall, the data presented here indicate the need for a better framework to identify the

peduncular vertebra. Neither measurement nor dissection revealed the presence of a rotund vertebra

at the insertion of the flukes, calling into question the efficacy of this identification metric in modern

and fossil contexts. If continued identification of the peduncular vertebra is desired, then centrum

measurements are currently the most effective tool in ontogenetically older animals. However, even

these measurements are not infallible, as shown in the bowhead dataset. There are three vertebrae, Ca

3, 4 and 5 that are nearly equitable in centrum measurements (Figure 24C) and the identification of

the first fluke vertebra can easily change based on the inherent variation in slight caliper shifts.

Further investigation of older bowhead specimens will reveal if this lack of shape separation is

common to the taxon or a product of young age.

Despite the conflicting data found for the bowhead, it is my opinion that the use of centrum

measurements as a proxy for the soft-tissue flukes should continue to be the standard within the field.

The efficacy of this proportional relationship, where centrum width exceeds centrum height, has been

demonstrated across a wide number of odontocete taxa and in the fossil record (*Dorudon*) (Buchholtz

1998, Buchholtz et al. 2007, Uhen 2004). However, the presence of a 'ball' vertebra could not be

detected. Evaluation of the vertebra located closest to the peduncle did not reveal any metrics that

readily identify this element as a 'ball' vertebra, visually or via measurements of epiphyseal facets in

either the beluga or the bowhead. The use of this metric to identify the flukes is not consistent across

Cetacea. Ontogenetically young cetaceans or samples from taxa with less dynamic swimming

behaviors, like the bowhead, do not display the same suite of vertebral traits that have been

documented in delphinoids and some of the rorquals (Kato, 1988; Moran et al., 2015; Thewissen et al.,

2021b). Identification of fluke vertebrae in extinct and extant cetaceans is better quantified via

centrum proportions, and the field should continue to use measurements of caudal width and height

for vertebral identity.

CHAPTER 6 PROTEIN SIGNALING AND DEVELOPMENT OF THE TAIL FLUKE IN THE

EMBRYONIC BELUGA WHALE (*DELPHINAPTERUS LEUCAS*)

Introduction

The soft-tissue flukes of cetaceans (whales, dolphins, and porpoises), found at the caudalmost region of the tail, are the main propulsive organ and have functionally replaced hindlimbs (Thewissen and Fish, 1997; Fish, 1998; Fish et al., 2006). These soft-tissue elaborations of the tail are one of the most visually striking modifications found on the cetacean body, and flukes serve as one of the key evolutionary adaptations critical for their successful colonization of the seas. Flukes dramatically increase the surface area of the tail, have a cambered cross-section, and function to generate lift-based propulsion. They are an altogether novel paired appendage and are a key evolutionary adaptation that has afforded cetaceans efficient means to propel themselves in a fluid habitat.

Among mammals, functions of the tail are varied and diverse; many long-tailed taxa use them for counterbalance [e.g., arboreal primates, (Young et al. 2015)] or to dynamically reposition the body during locomotion [e.g., cats (Wada et al., 1993), kangaroos (O'Connor et al., 2014)]. Some chiropterans (bats) display a thin tail membrane that connects the tail and hindlimbs that is used as a net to capture insects and sweep prey into their mouths (Swartz et al., 1996). The tail also acts as a means for socialization and communication via position and movement (Hickman, 1979). The most extreme variations in tail elaborations are seen in marine mammals.

Aquatic and semi-aquatic mammals include a host of taxa with unusual tail phenotypes including beavers, manatees, and dugongs (sirenians), and cetaceans. Manatees, evolutionary relatives of elephants, underwent a land-to-sea transition during the Eocene epoch and independently evolved flippers, lost hindlimbs, and modified the tail into a broad, rounded structure that acts as a propulsor. The close relative to the manatee, the dugong, is fascinating in that it evolved a fluke shaped like that of a cetacean fluke with paired triangular outgrowths (Buchholtz et al., 2007; Kojeszewski and Fish, 2007). While the manatee tail encompasses the entirety of the caudal vertebral column, cetacean and dugong flukes emerge from the distal point of the tail as soft-tissue outgrowths. Both the paddle and the flukes are used to propagate and direct the undulatory forces of the vertebral column (Felts, 1966; Fish, 1998; Fish et al., 2006; Sun et al., 2011; Ayancik et al., 2020).

The flukes of cetaceans are a relatively simple structure. Emerging from a hinge point on the tail known as the peduncle, two fluke blades are located lateral to the vertebrae with a notch in the midline (Figure 26A). The internal anatomy of the flukes is comprised of differentially arranged tissue layers: the thinner ligamentous layer of collagen, and the core layer, a dense fibrous tissue that is comprised of a meshwork of collagen fibers, making this region highly resistant to bending (Figure 26B) (Roux, 1883; Sun et al., 2011; Gough et al., 2018). These two tissue layers are supported by an elaborate vascular network. There are no muscles within the flukes, though epaxial and hypaxial tendons extend along the caudal vertebrae.

Developmentally, cetacean tails initially form in a manner that is similar to other mammals as a simple somite-driven structure. During the mid-embryonic phase (Carnegie Stage 16 – 17), the flukes initially bud off of the post-somitic tail of embryonic cetaceans and initially take on a lanceolate or

diamond-shaped appearance (see **chapter 2** for information on heterochronic fluke growth) (Ryder, 1885; Thewissen, 2018; Gavazzi et al., 2023). The outgrowths next take on a spade-like appearance before transitioning to a heart shape (Figure 26C). After this, the lateral outgrowths of the heart-like flukes continue expanding until forming triangular-shaped blade. The shape of the embryonic flukes through ontogeny has been documented elsewhere (Ryder, 1885) and can be used as a metric for estimating relative developmental age of cetacean embryos (Gavazzi et al., 2023). Fluke shape is established during prenatal development, and fully functional flukes are required for neonatal cetaceans to swim to the surface for air without assistance.

Molecular development of the fluke: While fluke anatomy has been documented (Roux, 1883; Ryder, 1885; Felts, 1966; Fish, 1998; Sun et al., 2010, 2011; Gough et al., 2018; Garten and Fish, 2020), nothing is known about the developmental genes that regulate the patterning and outgrowth of this appendage. The development of the flukes involves mesenchymal mesoderm with an overlying ectodermal epithelium, similar to other appendages such as limbs, fins, and the genital tubercle. It has been previously suggested that fluke development may be related to limb development ontogenetically (Ogawa, 1953) or at the molecular level (Thewissen, 2018).

Appendage patterning and outgrowth: Limb, fin, and genital development all share a common set of genetic cascades (Mercader, 2007; Seifert et al., 2009; Cohn, 2011; Yano and Tamura, 2013; Infante et al., 2018; Hawkins et al., 2021). Despite functional, morphological, and evolutionary divergences between these three structures, they are united as spatially asymmetrical structures that bud off of the body wall and form via a feedback loop between epithelium and underlying mesenchymal tissue. Extensive gene expression work using animal models has shown the functional connections between

the limb and fin paradigms (Wagner and Chiu, 2001; Abbasi, 2011; Yano and Tamura, 2013; Gehrke et al., 2015; Hawkins et al., 2021; Onimaru and Marcon, 2021) and the limb and genital tubercle (Haraguchi et al., 2001; Perriton et al., 2002; Yamada et al., 2006; Seifert et al., 2009; Armfield et al., 2016).

Limbs: To establish the proximodistal axis of the limb, the apical ectodermal ridge (AER) forms at the boundary between the dorsal and ventral surface of the primordial limb (Altabef et al., 1997). The AER secretes a number of fibroblast growth factors (FGFs) such as FGF-8 (Ahn et al., 2001; Boulet et al., 2004). FGF-8 from the AER creates a positive feedback loop with numerous signaling factors in the underlying mesenchymal mesoderm, including FGF-10 (Agarwal et al., 2003; Berenguer and Duester, 2021). This FGF signaling is necessary for proximodistal limb formation (Lewandoski et al., 2000; Sun et al., 2002; Boulet et al., 2004; Yu and Ornitz, 2008). In close relationship with the AER is the zone of polarizing activity (ZPA). The ZPA specifies the anterior-posterior axis and is especially critical for appropriate digit formation later in limb development. The morphogen Sonic hedgehog (SHH) is critical as part of the causative mechanism for ZPA formation (Harfe et al., 2004; McGlinn and Tabin, 2006; Scherz et al., 2007; Amano et al., 2009; Bastida et al., 2009).

The dorsoventral axis of the limb is specified by wingless-type family member 7a (Wnt-7a) and LIM homeobox transcription factor 1 (Lmx1) on the dorsal aspect while the ventral side is specified by the transcription factor Engrailed-1 (En-1) (Parr and McMahon, 1995; Logan et al., 1997; Adamska et al., 2004; Lan et al., 2019). There is robust evidence suggesting that the midline of these conflicting dorsoventral signals indicates to the developing limb where the AER should begin to form (Altabef et

al., 1997; Rodriguez-Esteban et al., 1997; Kengaku et al., 1998; Pizette et al., 2001; Gorivodsky and Lonai, 2003).

Later in limb development, the interdigital tissues of the handplate are removed via apoptosis. It is during this period that the digits are sculpted from mesenchymal condensations and assigned a digital identity. Bone morphogenetic proteins (BMPs) are implicated throughout limb patterning as both upstream and downstream targets of the FGFs and SHH. In particular, BMPs are considered critical for the structuring of the digits (Selever et al., 2004; Bandyopadhyay et al., 2006). In animals that maintain webbed appendages, such as ducks, bats, and cetaceans, this BMP expression is modified and potentially reduced via expression of GREM and FGF (Hockman et al., 2008; Cooper et al., 2017), signaling factors that likely maintain the webbing between digits and prevent apoptosis.

Fins: Fin development shares numerous similarities with the tetrapod limb. In the early stages of the developing fin, FGF-8 is expressed within an AER, and SHH is secreted from a ZPA, similar to the limb bud (Dahn et al., 2007; Mercader, 2007; Yano et al., 2012; Letelier et al., 2018; Höch et al., 2021; Hawkins et al., 2022). It is only at later stages of fin development, including the transition from an AER to an apical ectodermal fold (AEF), that the paired fins begin to diverge from limb ontogeny morphologically and developmentally to promote growth of the pectoral fins (Grandel and Schulte-Merker, 1998).

The fins do not experience a major apoptotic event, however, there is evidence of a GREM-FGF-SHH feedback loop found in the formation and growth of the midline fins, suggesting that BMP is still critical to median fin development (Höch et al., 2021; Hawkins et al., 2022). Neither fins nor

genitals are dorsoventrally asymmetrical appendages, however, Wnt-7a can be found in the zebrafish pectoral fin (Norton et al., 2005).

Genital tubercle: Though classified as an appendage, genital development is considerably divergent from both the generalized limb and fin paradigms. The major organizing center of the genital tubercle is the distal urethral epithelium (DUE) (Haraguchi et al., 2000; Suzuki et al., 2003; Yamada et al., 2006; Seifert et al., 2009; Armfield et al., 2016). This epithelium primarily secretes SHH, as opposed to the FGFs found in the AER, and there are high levels of the morphogen found both within the DUE and along the midline of the genital tubercle. In the genitals, it is hypothesized the SHH patterns the appendage and promotes outgrowth (Haraguchi et al., 2001; Perriton et al., 2002; Cohn, 2011). FGF-10 expression has been reported within the genitals, but FGF-8 provides a more complex story. Data gathered from in-situ hybridization experiments shows that FGF-8 is expressed in a very small midline region within the DUE (Seifert et al., 2009; Armfield et al., 2016). However, subsequent examination of the genital tubercle using immunohistochemistry does not corroborate these results (Cohn, 2011) suggesting that the mRNA for this growth factor is not translated. This relationship requires further exploration to be fully understood.

As an appendage, the flukes originated long after Lower Cambrian fin evolution (Shu et al., 1999; Zhang and Hou, 2004; Morris and Caron, 2014), Devonian tetrapodal limb transition (Daeschler et al., 2006; Clack, 2009; Cloutier et al., 2020), and emergence of the amniote penis (Leal and Cohn, 2015; Gredler, 2016). With the first evidence for flukes in the Eocene (Gingerich et al., 1990; Uhen, 2004), the morphological and evolutionary novelty of the cetacean flukes compared to fins and limbs allows key insight into the pathways that drive novelty. Cetaceans have long been regarded as a model

organism for extreme mammalian evolution, and the last 15 years of molecular research has provided

a crucial understanding of the unique developmental processes that govern extremity development in

both generalized and highly derived mammals.

Cetacean limb development: Protein signaling during embryogenesis in cetaceans is best understood

in the pan-tropical spotted dolphin (*Stenella attenua*ta). The ontogeny of this taxon has been

documented and described from early somitogenesis to the fetal period (Štěrba et al., 2000; Thewissen

and Heyning, 2007). Gene expression hypotheses based on visual examination of *Stenella* embryos

(Richardson and Oelschläger, 2002) have been further tested via immunohistochemistry on both the

forelimb and hindlimb buds (Thewissen et al., 2006; Cooper et al., 2017). Immunohistochemical

studies demonstrate that cetacean limbs initially form using the common developmental signaling

cascade but diverge early in development to form cetacean-specific traits. Key proteins related to limb

development have been identified in *Stenella* at a similar developmental age to the beluga embryo

utilized for this study (Thewissen et al., 2006; Cooper et al., 2017; Gavazzi et al., 2023).

In the forelimb, *Stenella* maintains FGF-8 signaling in the AER for a prolonged period of time

when compared to mice and pigs, an artiodactyl relative of whales. Furthermore, where other

mammals express BMPs within the interdigital tissues to sculpt the acropodium, the interdigital zone

of the cetacean forelimb co-expresses FGF-8 and GREM to help maintain this webbing for the soft-

tissue flipper (Cooper et al. 2017). Concurrently, the hindlimbs of cetaceans initiate like a typical

mammalian limb bud except for a lack of SHH protein signaling from the ZPA. This aberration, which

would lead to the loss of anteroposterior axis specification and the requisite feedback loops necessary

to maintain limb proliferation, is implicated in the eventual cessation of limb cell proliferation in *Stenella* (Thewissen et al. 2006).

Speculation has suggested that the flukes have an intimate association with the regression of the hindlimb buds (Ogawa, 1953), and may develop using an appendage-like signaling regime (Infante et al., 2018; Thewissen, 2018), which here we test empirically. Using embryonic beluga whales (*Delphinapterus leucas*) as our model, we used immunohistochemistry to identify and localize some of the common protein signals associated with morphogenesis and outgrowth of appendages during embryonic development. Of the three appendages, we expect that cetacean fluke development most closely resembles the protein signaling patterns found in limb development. Fin development is restricted to non-tetrapodal taxa, and the formation of the limb from the fin suggests that the initial conditions needed to form a functioning fin are likely lost within tetrapods. The genital tubercle is different enough from the limb and fin that it has independently evolved distinct expression patterns after the initial exaptation of the signaling cascade. Logically, it seems unlikely that the flukes would then take signaling cues from this highly derived appendage.

Given the current fossil evidence of fluke evolution, it is reasonable to hypothesize that flukes evolved once within the cetacean lineage (Uhen, 2004; Buchholtz, 2007; Gingerich et al., 2019; Lambert et al., 2019). The data presented here provides some insight into the initial development of the flukes, informing our understanding of the fundamental building blocks necessary for the evolution of a novel appendage.
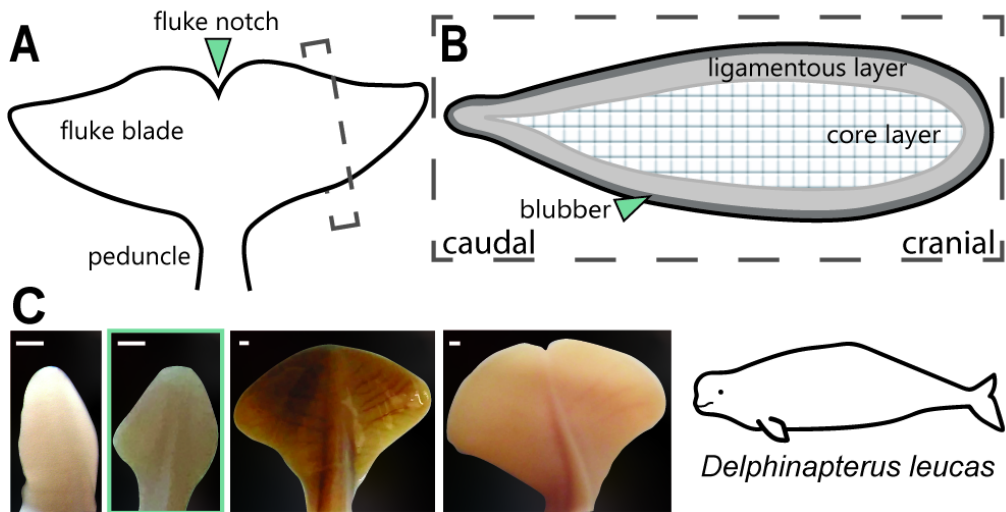
Figure 26: Identification of fluke anatomy and morphology using the beluga whale (*Delphinapterus leucas*) as the model taxon. A: Basic anatomy of cetacean flukes in adults. B: Internal morphology of the flukes of adult cetaceans in parasagittal section. C: Photographs of embryonic fluke outgrowth through ontogeny based on embryonic specimens (from left to right) Carnegie Stage (CS)-17 NSB-DWM 2013LDL6F, CS-19 2011LDL11F and fetal specimens NSB-DWM 2014LDL7F, 2012LDL10F. Blue box indicates morphology of sample selected for this study (NSB-DWM 2009LDL9F). Scalebar = 1 mm.

Methods

Three beluga embryos, NSB-DWM 2009LDL9F, 2014LDL7F, and 2012LDL10F were used for analysis. These beluga embryos were collected as part of the Iñupiat beluga harvest that occurs in Point Lay, Alaska, for both cultural and subsistence fulfillment (Frost et al., 2021; Suydam and George, 2021). These embryos correspond to Carnegie Stage 19, 20, and the fetal period as described in chapter 2 (Gavazzi et al., 2023). All three specimens were paraffin-sectioned for histology cranially to caudally. This sectioned fluke tissue was subjected to multiple histological stains and immunohistochemistry.

Hematoxylin and eosin, Mallory's trichrome – Two stains were used to identify cell types and internal morphology of the embryonic fluke tissue. Modified Harris hematoxylin in acetic acid and 1% eosin Y diluted in 95% ethanol were first used to identify basic tissue types. A modified Mallory's trichrome, taken from Everett and Miller (1973), provided additional information. This trichrome is adapted for embryonic tissue, which can be difficult to stain due to the undifferentiated state of many organs. The protocol uses 1% aqueous acid-fuscin red, 0.5% aniline blue in 8% acetic acid, and 2% orange G in 8% acetic acid to distinguish between tissue types. Red blood cells stain red, nuclei stain orange, undifferentiated connective tissue is blue while differentiated connective tissue is blue-purple. Muscle, epithelial tissue, and cytoplasm will stain purple. The protocol also states that highly proliferative and metabolically active cells will take on an orange hue throughout the entire cell, not just the nuclei.

Immunohistochemistry – To assess the importance of common embryonic proteins in fluke outgrowth, I performed a modified immunohistochemical (IHC) protocol that was used in other cetacean protein signaling research (Thewissen et al., 2006, 2017; Armfield et al., 2013; Cooper et al., 2017) on one beluga embryo, NSB-DWM 2009LDL9F. Primary antibodies were incubated overnight at 4°C, the secondary antibody was incubated for two hours at room temperature, and the avidin-biotin reagent was incubated for 90 minutes at room temperature. The tissue was exposed to 3,3′-Diaminobenzidine (DAB) for 8 minutes and then counterstained with 0.01% thionine for contrast. Concentrations of the antibodies were as follows: FGF-8 at 1:100 (Invitrogen: PA5-79295), FGF-10 at 1:750 (Invitrogen: PA5-88291), SHH at 1:100 (Invitrogen: PA5-19492), WNT-7A at 1:200 (Invitrogen: PA5-80231) and GREM 1:100 (Invitrogen: PA5-121945). The antibody for BMP4 (Invitrogen: PA5-

27288) was tested at the following concentrations: 1:50, 1:100, 1:200, 1:250, 1:500, 1:750, and 1:1000. No antigen binding and subsequent chromogen staining was detected at any of these concentrations.

Results

Hematoxylin and Eosin – Initial staining of the embryonic fluke tissue with hematoxylin and eosin (H&E) reveals cellular morphology that is generally similar to that described in adult cetaceans (Figure 27A) (Ryder, 1885; Fish, 1998). The cross-section in figure 27A shows that the prenatal flukes are predominately comprised of mesenchymal cells covered by a simple squamous epithelium. This mesenchyme and the corresponding extracellular matrix have two different orientations: the outer layer appears to span the tissue craniocaudally and the inner layer has a dorsoventral orientation. This differentiation roughly aligns with the ligamentous and core layers of the post-natal cetacean flukes (Sun et al., 2010; Gough et al., 2018). Within the flukes, there is a greater density of nuclei at the lateralmost edges, suggesting that this may be a highly proliferative area. At Carnegie Stage 19, the flukes are diamond-shaped and will transition to a spade shape thereafter (Gavazzi et al., 2023). The skin of the flukes is thin and there is no blubber. The vertebra is still a cartilaginous anlage surrounded by epaxial and hypaxial tendon precursors.

Modified Mallory's Trichrome – We stained two additional flukes with the modified Mallory's trichrome to assess development of the flukes at the cellular level. These three flukes, NSB-DWM 2009LDL9F (CS 19) (figure 27B), 2014LDL7F (CS 20), and 2012LDL10F (Fetal) (figure 28) had three different fluke morphologies from diamond-shaped to triangle-shaped, respectively.

Within the flukes of NSB-DWM 2009LDL9F, the presumptive ligamentous and core layers are highly contrasted with Mallory's stain. What we described as the ligamentous layer within the hematoxylin and eosin-stained section of the flukes appears to be subdivided into two different cell types (Figure 27C). Just deep to the skin, the lamina propria is comprised of purple cells, indicating a differentiated connective tissue, with little extracellular matrix. The deeper layer is orange-purple (L), which according to the protocol indicates highly active and proliferative cells. It is possible that these layers are the precursors to the blubber (b) and ligamentous layer (L), respectively. Both of these cell layers are superficial to the core layer (Co). The core layer has purple staining mesenchymal tissue with long extracellular projections running dorsoventrally. Furthermore, there is a greater density of connective tissue cells in the ligamentous layer than the core layer overall, contributing to the darker staining pattern. At the lateral edge of the fluke, there are a high number of orange-purple cells, indicating that this region is one of increased cellular activity (Figure 27D). The skin of the flukes is purple and all nuclei of the stratum basale (S) are orange-purple, which is indicative of differentiated tissue and a stratum basale that is synthesizing elevated levels of mRNA and protein. Throughout the connective tissue, erythrocytes can be seen via their bright red staining.

The NSB-DWM 2014LDL7F flukes (Figure 28A) are highly vascularized with blood vessels visible throughout the tissue. In the central portion of the fluke, differentiation of the core layer has been initiated. There is additionally a dark blue/purple band of tissue just deep to the first layer of connective tissue, which also suggests differentiation of the mesenchyme. The skin of this specimen had peeled away prior to fixation, so the degree of epithelial proliferation or staining is unknown. As

previously found in NSB-DWM 2009LDL9F, there is a highly dense region of nuclei at the lateral edge of the fluke blade, suggesting that this region is still proliferating.

NSB-DWM 2012LDL10F (Figure 28B, 28C) shows a similar pattern to Figure 28A with differentiation at the innermost core layer in the fluke blades. The tissue just deep to the epithelium has a blue hue, suggesting further differentiation of these tissues. The skin in a more cranial section of the flukes is red (Figure 28B) but shows evidence of differentiation more caudally (Figure 28C). Though this specimen is similar in morphology to the perinatal fluke shape, the lateral edges of this tissue are still densely packed with nuclei and appear to maintain a state of high proliferation when compared to the rest of the connective tissue in these sections.
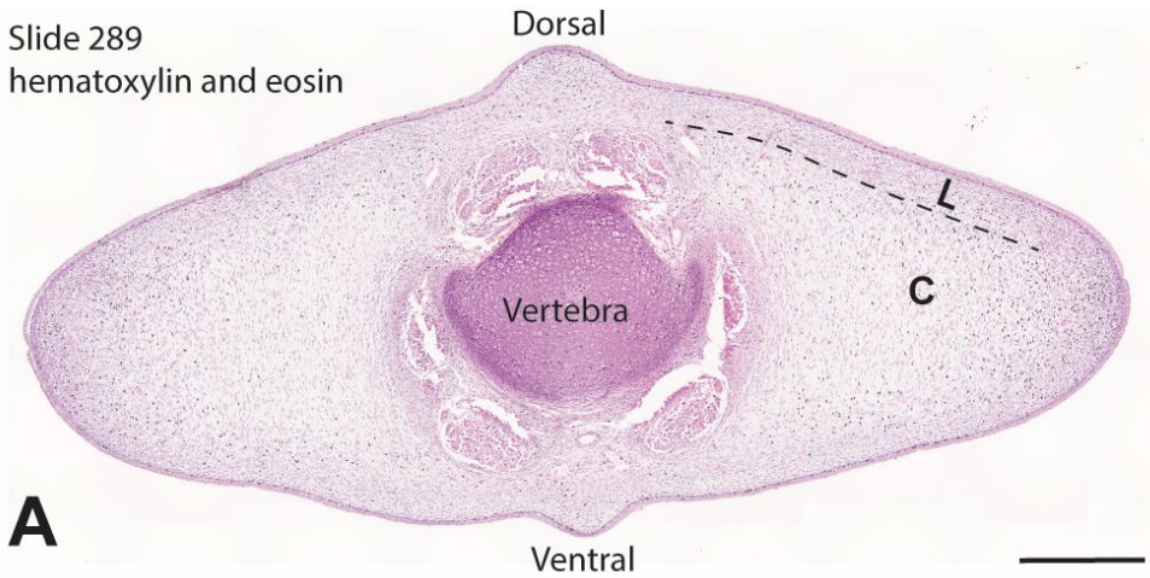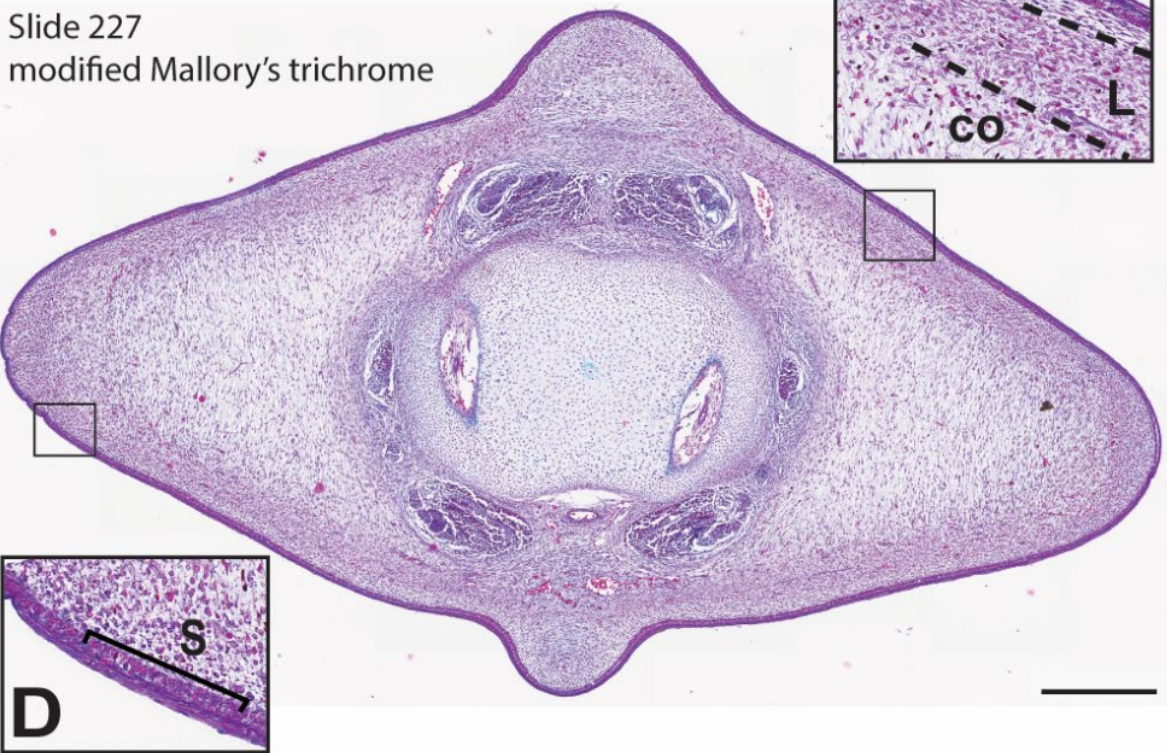
Figure 27: Cross-sections of fluke tissue from NSB-DWM 2009LDL9F. **A**: Hematoxylin and eosin-stained section. **B**: Section stained with a modified Mallory's trichrome. **C**: B – blubber, L – ligamentous layer, Co – core layer. **D**: S – Stratum basale. Scale bar equals 0.5 millimeters.

NSB-DWM 2014LDL7F
CS-20

NSB-DWM 2012LDL10F
Fetus
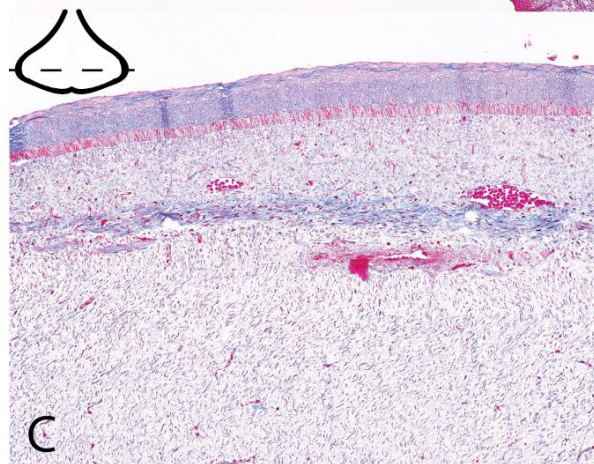
Figure 28: Modified Mallory's trichrome staining of CS-20 NSB-DWM 2014LDL7F (**A**) and fetal specimen NSB-DWM 2012LDL10F (**B, C**). A and B are enlarged images from the lateral edge of left fluke blades. C is an enlarged image of the dorsolateral region of the left fluke blade. Level of section is indicated on the fluke illustrations.

Immunohistochemistry – Of the three flukes sectioned and stained with trichrome, we selected the best-preserved specimen, NSB-DWM 2009LDL9F for further investigation of protein signaling in the flukes. We describe the signaling patterns found for the five proteins tested in this study.

FGF-8 (Figure 29): In the area just caudal to the peduncle there is consistent staining for the FGF-8 antibody (Figure 29A). The protein is found circumferentially in the outermost epithelium, with no stain found deep to the basement membrane. In the distal third of the fluke, caudal to the widest point, the chromogen staining for FGF-8 is comparatively darker (Figure 29B). The staining of the epithelium encapsulates the entirety of the epidermis. The caudalmost section of the fluke has light staining of the outermost layer of the epithelium (Figure 29C). There is no asymmetry to the staining pattern and there is no stain within the mesenchyme or other connective tissues.
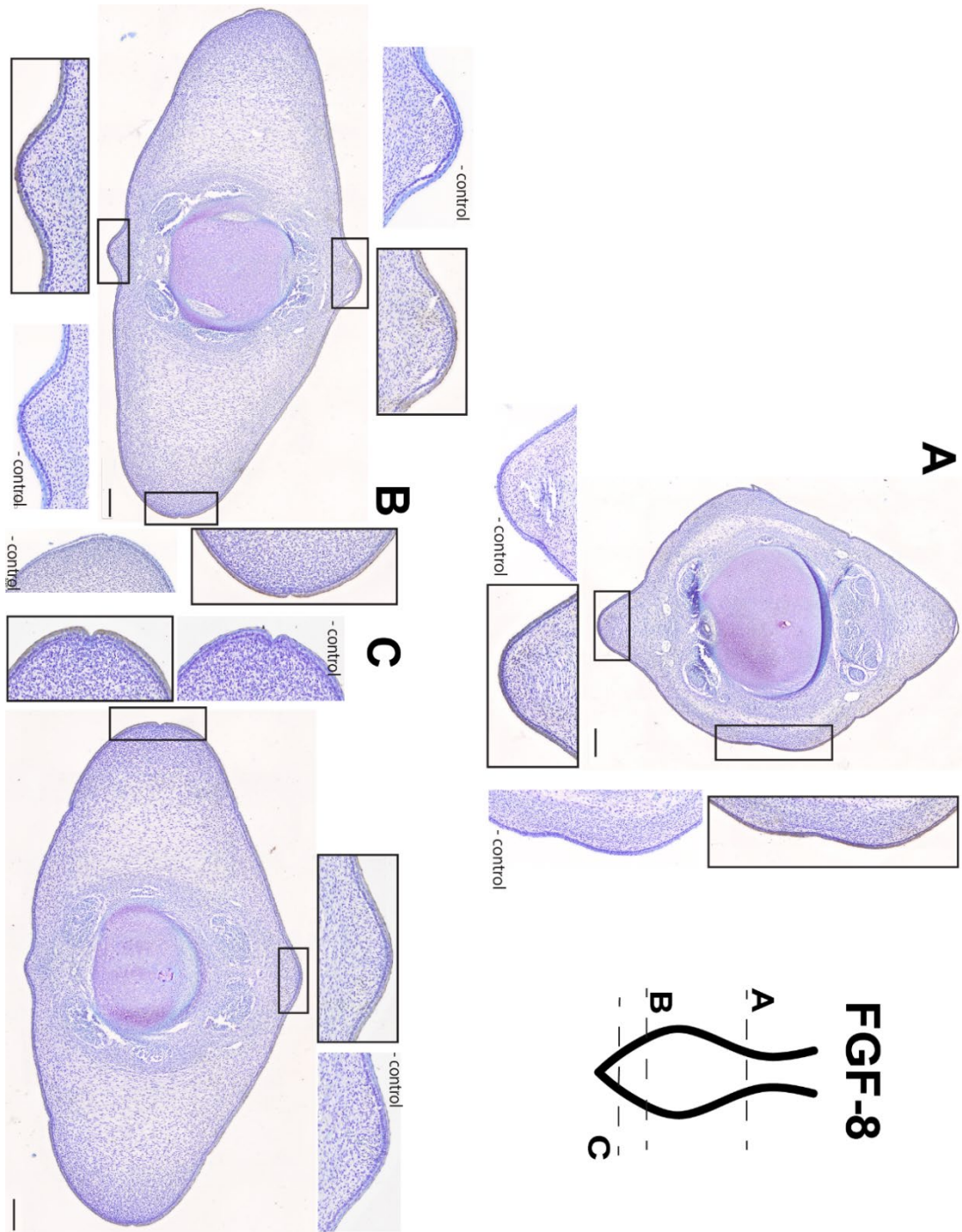
Figure 29: Fluke tissue from NSB-DWM 2009LDL9F stained with FGF-8 antibody and counterstained with 0.01% thionin. Level of section indicated on fluke illustration. Scalebar equals 250 microns.

FGF-10 (Figure 30): The staining pattern for FGF-10 on these tissue sections closely matches the staining pattern seen for FGF-8. In the first section just caudal to the peduncle (Figure 30A) the outermost epithelium demonstrates binding for the FGF-10 antibody except for the right lateral fluke. Along the proximal half of the flukes (Figure 30B), there is dark staining for the FGF-10 antibody within the outermost squamous layer of epithelium. This is consistent circumferentially. At the lateral fluke edges, the staining for FGF-10 comprises the entire squamous layer of the epithelium, though the skin is also much thinner in this region. There is no FGF-10 chromogen found in the stratum basale of the epithelium. At the widest part of the fluke, the staining found in FGF-8 and in the previous FGF-10 section matches (Figure 30C). Intense chromogen staining is found in the outermost epithelium. There is no expression deep to the basement membrane in any portion of the connective tissues. At the tip of the tail (Figure 30D), FGF-10 is highly expressed in the epithelium in a pattern identical to Figures 30B and 30C.
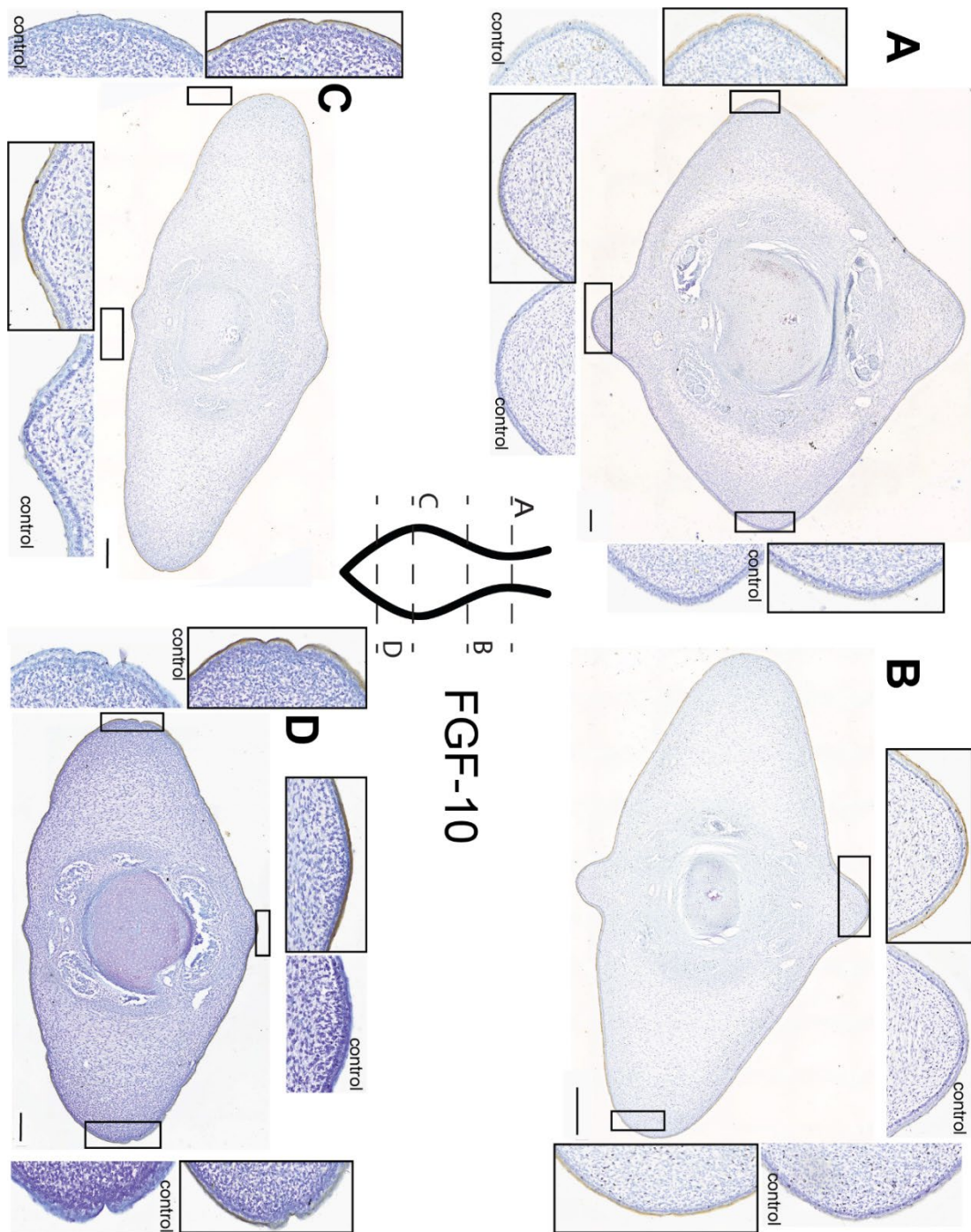
Figure 30: Fluke tissue from NSB-DWM 2009LDL9F stained for FGF-10 antibody and counterstained with 0.01% thionin. Level of section indicated on fluke illustration. Scalebar equals 250 microns.

WNT-7A (Figure 31): At the level of the peduncle (Figure 31A), staining for the WNT-7A antibody can be found in the dorsal, ventral, and lateral epithelium. There does not appear to be any variation in staining pattern between these regions, and the staining appears more concentrated within the squamous and superficial portion of the epithelium. In the cranial half of the diamond-shaped flukes, staining is found circumferentially in the epithelium (Figure 31B). There appears to be a stronger antibody staining in the ventral keel of the fluke section. This is opposite of what is expected for the standard limb WNT-7A signaling pattern, where this protein is found in the dorsal epithelium. In the distal tip of the fluke (Figure 31C) the same pattern is shown but does not demonstrate the dorsoventral asymmetry found in Figure 31B. Here, the epithelium is darkly stained for the WNT-7A antibody in the dorsal and ventral keels as well as the lateral flukes.
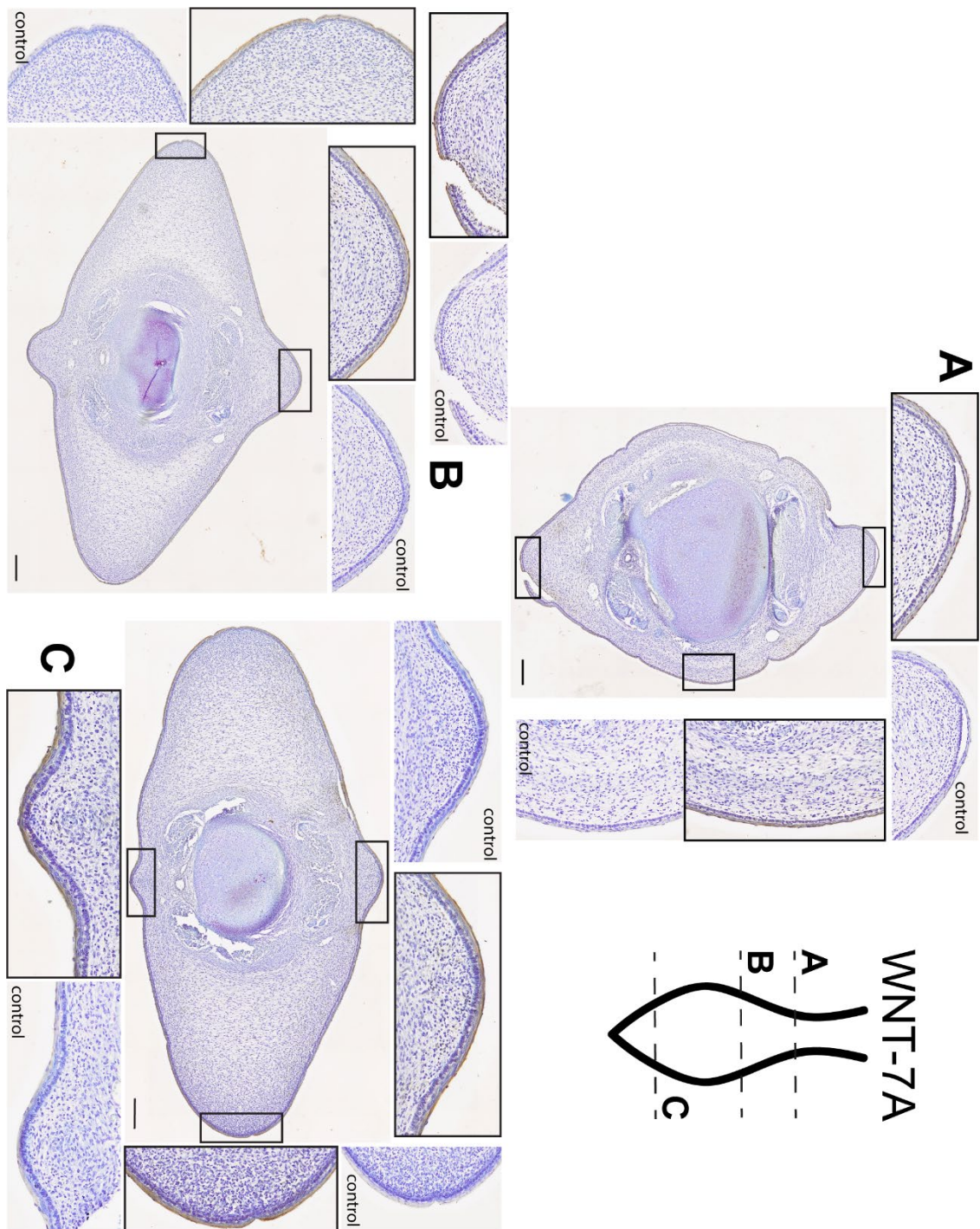
Figure 31: Fluke tissue from 2009LDL9F stained for WNT-7A antibody and counterstained with 0.01% thionin. Level of section indicated on fluke illustration. Scalebar equals 250 microns.

SHH (Figure 32): At the peduncle, SHH signaling is found in the epithelium and in the ligamentous layer of mesenchyme (Figure 32A). The pattern of staining within these two regions is distinct: within the skin the stain is dark and consistent and in the ligamentous layer the SHH antibody binds in a 'speckled' or scattered pattern. Punctate brown binding is clear throughout the superficial mesenchyme and does not appear to show a mediolateral or dorsoventral asymmetry. The region of the flukes just cranial to the widest point also has staining present in the epithelium and within the ligamentous layer of mesenchyme (Figure 32B). Close to the tip of the tail (Figure 32C), there is staining for the SHH antibody in both the epithelium and within the mesenchymal tissue just deep to the epithelium. There is consistent antibody staining within the skin, presence of SHH signaling in the squamous cell layer, and speckled staining within the presumptive ligamentous layer of mesenchymal tissue. As found in other sections, this pattern is circumferential and does not show any major dorsoventral or mediolateral variation. On the right dorsolateral surface are two patches of staining that do not correspond to the common pattern found elsewhere in the tissue; one unusual signaling region is found just deep to the epithelium (1) and the other is deeper still within the densely nucleated mesenchyme of the right lateral fluke (2) within the core layer of the fluke. These 'hotspots' appear to be bilateral; however, the left lateral fluke also has tearing of the epithelium in this region, making precise interpretation of the stain pattern difficult.

In the caudalmost section of the fluke (Figure 32D), epithelial SHH staining is consistent with the other sections. While there is presence of SHH signaling and chromogen staining in the mesenchyme, it appears limited to the ligamentous layer, including the dorsal and ventral keels. This pattern matches the staining described for Figure 32B; however, the intensity of the stain is greatly

reduced compared to that earlier section. Notably, the 'hotspots' found in the previous section are not present in this section.
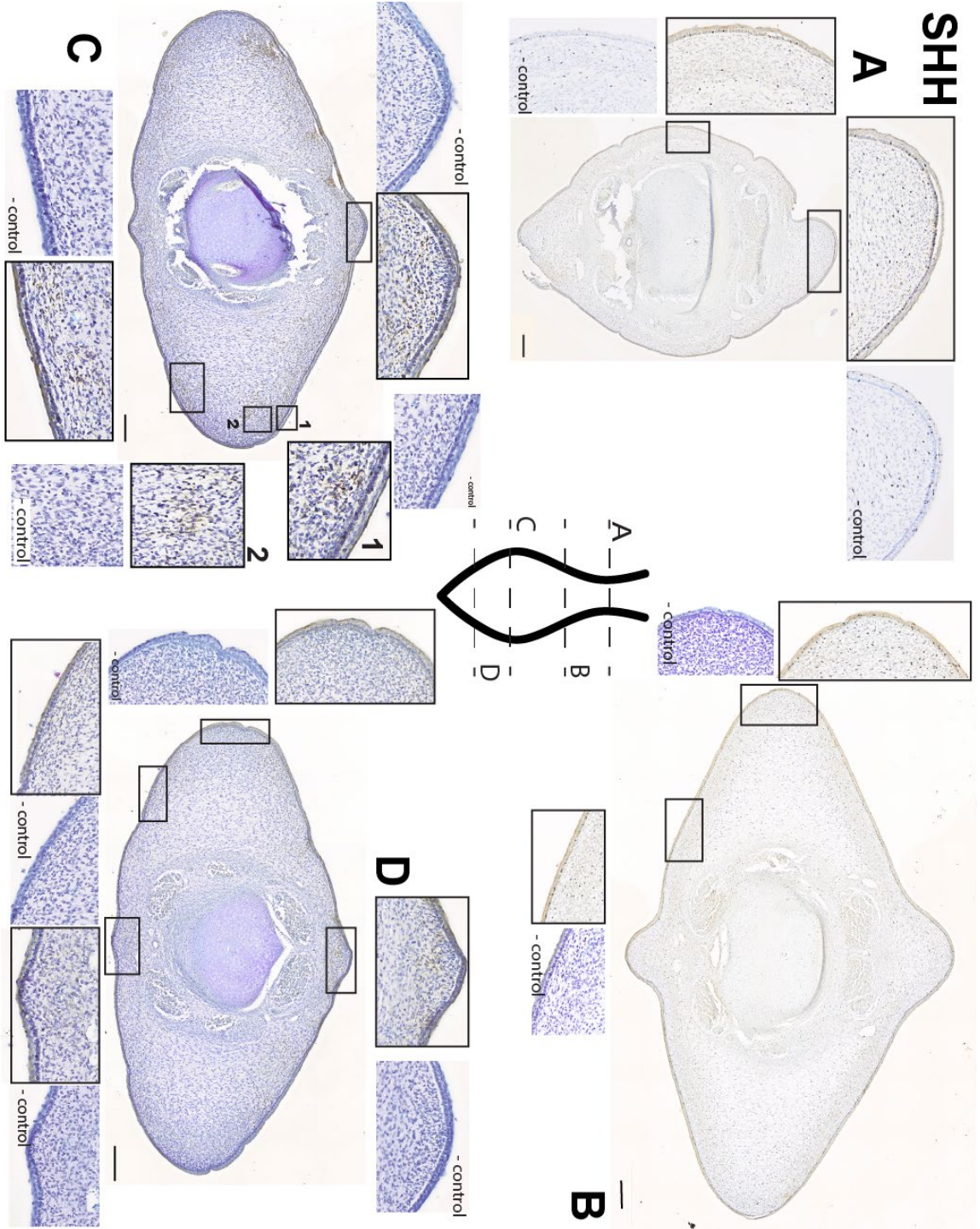
Figure 32: Fluke tissue from NSB-DWM 2009LDL9F stained for SHH antibody and counterstained with 0.01% thionin. 1 and 2 are potential SHH hotspots. Level of section indicated on fluke illustration. Scalebar equals 250 microns.

GREMLIN (Figure 33): Just cranial to the peduncle, there is staining for GREM in the squamous portion of the epithelium (Figure 33A). Like SHH, there is also some punctate staining within the superficial layer of connective tissue just deep to the skin. The speckling of this GREM staining is more diffuse than that seen in SHH. The cranial half of the flukes (Figure 33B) appears to be nearly identical to that of Figure 33A. The only considerable difference between these two sections is the amount of staining within the connective tissue. There is very little staining present in the mesenchyme of Figure 33B, and many of the patches that are present appear in proximity to tears within the tissue. At the widest part of the flukes, staining for the GREM antibody is found in the outermost layer of the epithelium, in a punctate pattern deep to the stratum basale, and in the cartilage of the vertebra (Figure 33C). This protein is the only one found in the deeper layers of the flukes and within the vertebral body. There appears to be some faint staining for GREM in the core layer of the flukes as well, as the tissue exposed to the antibody has a darker hue than the control tissue. Towards the caudal tip of the developing flukes (Figure 33D), the staining is like the previous section, Figure 33C. There is antibody staining in the epithelium and cartilage, with faint grey/brown pigmentation in the core layer. There is little to no GREM staining within the outer layer of connective tissue.
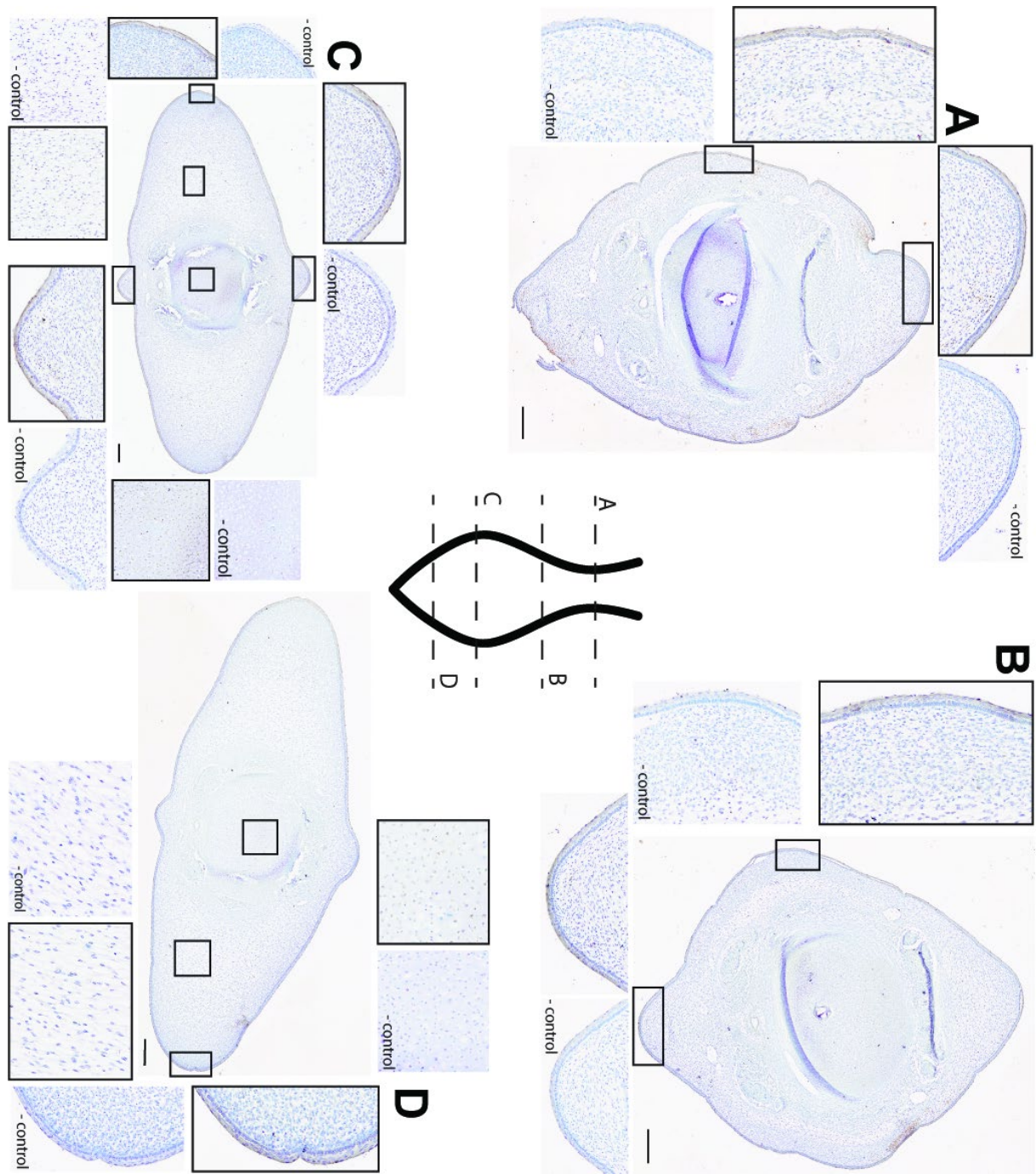
Figure 33: Fluke tissue from NSB-DWM 2009LDL9F stained for GREMLIN antibody and counterstained with 0.01% thionin. Level of section indicated on fluke illustration. Scalebar equals 250 microns.

Our results localized FGF-8, FGF-10, and WNT-7A exclusively to the epidermis of the flukes. Both SHH and GREMLIN showed expression within the epithelium and mesenchymal connective tissue of the flukes. SHH localized to the longitudinal layer of the fluke connective tissue while GREMLIN was found within the deeper core layer of tissue and within the cartilage. In summary, all five proteins investigated in this study showed staining in the epithelium, particularly in the squamous layer of the skin, and only two proteins showed staining within the mesenchymal fluke tissue.

Discussion

Histology Staining – Initial staining of the flukes using hematoxylin and eosin revealed that the flukes are largely comprised of mesenchymal tissue. Though this result is unsurprising, it is worth mentioning that the difference between the core layer and the ligamentous layer can already be discerned in this CS-19 specimen, which is early in fluke outgrowth. This result suggests that these two tissue layers differentiate from each other even earlier in development and warrants further investigation in the future.

The modified Mallory's trichrome provided greater detail to the tissue, showing a secondary layer within the presumed longitudinal layer that may be developing blubber (Figure 27C). Additionally, this particular trichrome protocol is designed to identify highly active cells (Everett and Miller, 1973), which were found in the lateralmost portions of the flukes and also within the stratum basale of the epithelium. The prevalence of highly active cells at the epithelial boundary correlates with our protein findings, where every antibody had some level of binding within that same region.

Additionally, both SHH and GREM were found to express in the tissue just deep to the stratum basale in a punctate pattern, which may be related to their secretory, morphogenic nature.

Both stains elucidate the variation between the major layers of epithelial and connective tissue within the flukes. Prenatal fluke skin is divided into a stratum basale and an overlying stratified squamous epithelium. There is no evidence of epithelial thickening or stratified cuboidal/columnar cell layer in the skin, both of which can be morphological markers of an apical ectodermal ridge. At Carnegie Stage 19, there are already differences in the connective tissue that divide the longitudinal layer from the core layer of the flukes. Differentiation of these two layers occurs at a developmental age younger than our current sample, earlier in fluke patterning and outgrowth. Additionally, there is some evidence for vascularization of the flukes, as small blood vessels can be seen throughout the trichrome stained section, indicated by bright red blood cells. The timing of differentiation of these mesenchymal tissues into fibroblast-like cells and the makeup of their collagen rich extracellular matrix is a topic for future research.

These protein data, when analyzed together, indicate that some of the proteins critical for appendage development have been exapted for the formation of the flukes. First, we assessed the proteins involved in fin and limb proximodistal outgrowth, FGF-8 and FGF-10. In the flukes, FGF-8 is exclusively present within the epithelial tissue. This pattern matches the data found for FGF-8 within the apical ectodermal ridge or fold in other taxa, supporting the appendage hypothesis (Figure 29, 34). In the genital tubercle, FGF-8 has been reported in a small region of the distal urethral epithelium, though this data could not be replicated at the protein level (Haraguchi et al., 2000; Perriton et al., 2002; Seifert et al., 2009).

While there is no epithelial thickening at the lateral margins of the flukes, previous evidence

has shown that AER morphology varies greatly across tetrapods and signaling patterns drive function

of the ectoderm (Cooper et al. 2011). For the protein FGF-10, the stain pattern closely matches FGF-8.

Typically, the developing limb of tetrapods show FGF-10 expression in the mesenchyme underlying

the AER (Ohuchi et al., 1997; Sekine et al., 1999; Ahn et al., 2001; Royle et al., 2021), not concurrently

in the same tissue as seen in this beluga (Figure 34). While there is this distinct heterotopy between a

generalized limb paradigm and the flukes, the presence of FGF-10 in the developing epithelium of the

flukes is still consistent with this protein serving a similar function and acting in concert with FGF-8.

Like the FGF proteins, WNT-7A protein was found circumferentially in the epithelium. While

the tissue layer here is consistent with the appendage hypothesis, the lack of asymmetrical signaling is

not. This pattern seen in the flukes does not lend itself to dorsoventral patterning as seen in the

tetrapod limb, where WNT-7A is only found in the dorsal ectoderm (Parr and McMahon, 1995; Yang

and Niswander, 1995; Logan et al., 1997; Kengaku et al., 1998; Chen and Johnson, 2002; Delgado and

Torres, 2017; Lan et al., 2019) (Figure 31, Figure 9). Given that the flukes are a dorsoventrally

symmetrical organ, this staining pattern may relate to a lack of dorsoventral patterning. If the

cetacean flukes have exapted the vertebrate limb signaling pattern, then the WNT-7A expression

pattern was likely modified to maintain dorsoventral symmetry within the flukes as opposed to the

limb. Experimental knockout of LMX1B within a mouse model expands the ectodermal expression of

WNT-7A to encompass both the dorsal and ventral ectoderm of the modified limb bud (Parr and

McMahon, 1995; Logan et al., 1997; Tzchori et al., 2009). Additionally, reduction of either LMX1B or

EN-1 expression in animal models leads to the development of a limb that is more dorsoventrally

symmetrical than wild-type counterparts (Parr and McMahon, 1995; Loomis et al., 1996; Logan et al., 1997; Chen and Johnson, 2002). Further investigation into LMX1B and EN-1 in the flukes is needed to confirm this working hypothesis about the WNT-7A results.

The epithelial and mesenchymal SHH signaling within the flukes shows variation craniocaudally and between the two tissue types (Figure 32A, 32C). Like the other proteins, SHH signals were present in the epithelium of all sections. However, SHH staining was unusual in that punctate speckling was found throughout the longitudinal layer of mesenchyme in all sections of fluke tissue. The SHH staining consistently showed this pattern. This SHH staining appeared much darker in the distal portion of the fluke compared to the lighter staining near the peduncle, indicating the presence of greater amounts of protein. SHH staining within the mesenchyme is also found in two distinct hotspots within the longitudinal and core layer along the distal aspect of the fluke (Figure 32C) but tearing in the mesenchyme on the left side interrupts this pattern, making interpretation difficult. During the transition from a diamond to a spade-shaped fluke, the caudalmost portion of the tail will experience a greater degree of outgrowth and reshaping, which may explain why the antibody staining for FGF-8, FGF-10, and SHH are all darkest in sections closest to the tip of the tail.

The GREM data for the flukes does not resemble the expected pattern for appendage signaling. In a typical limb, GREM is found between the ZPA and AER. In the beluga flukes, the GREM antibody stained within the longitudinal layer of the mesenchyme and within the epithelium, similar to the SHH staining pattern (Figure 33, 34). Unlike the more discrete regionalization found in developing limbs of other tetrapods including mice, cichlid fish, catfish, and zebrafish (Zúñiga et al., 1999; Michos et al., 2004; Nicoli et al., 2005; Bénazet et al., 2009; Tulenko et al., 2017; Höch et al., 2021), the GREM

staining in the flukes was diffuse throughout the mesenchyme. Within the beluga fluke, it is possible that GREM is promoting and maintaining the feedback loop between FGF-8 and SHH, as has been demonstrated in limb research (Merino et al., 1999; Zúñiga et al., 1999; Bénazet et al., 2009), but direct testing of this hypothesis is needed.

In summary, the protein data from the flukes offers support for the appendage hypothesis. In the strictest sense, only FGF-8 was found in the expected location for an AER; the other four proteins were in different regions or tissue layers than expected for complete homology with fin and limb expression. However, the presence of all five proteins within the flukes provides some evidence that generalized relationships between these proteins are preserved within the flukes. These data highlight the importance of homology and recapitulation in the context of the evolution of a novel appendage.

Novelty and Homology of the flukes

While our dataset precludes any information on causality of the proteins studied, the locality and relationships of the FGFs, SHH, and GREM are all reminiscent of other appendage studies. In this respect, our data are similar to many other protein studies conducted in appendages and highlights the deep homology of the limb patterning paradigm. The flukes resemble a highly modified soft-tissue appendage, akin to cetacean flippers and chiropteran wings.

The non-localized SHH expression pattern found in the flukes is similar to the second wave of signaling reported in the bat wing in Hockman et al. (2008). Both Chiroptera and Cetacea have exceptionally modified bauplans for life in a fluid habitat. Additionally, both bats and dolphins have

independently evolved a similar mechanism for maintaining their interdigital webbing via co-expressed FGF, BMP, and GREM signals in the interdigital tissue (Weatherbee et al., 2006; Cooper et al., 2017). This overlapping pattern has been documented in the highly modified bat wing (Weatherbee et al., 2006; Hockman et al., 2008; Cooper et al., 2012a), and within the Stenella flipper (Cooper et al., 2017). We tested the beluga flukes for BMP4 and found no evidence of protein expression within any of the tissues (data not shown) but do see evidence of overlapping GREM and FGF signaling within the epithelial tissue of the flukes.

Flukes as an appendage

Flukes do not form until completion of somitogenesis within the tail. Caudal somites come from unique paraxial mesoderm which is initially formed from a neuromesodermal bipotential stem cell in the tail bud (Handrigan, 2003; Jurberg et al., 2013; Javali et al., 2017; Mallo, 2020). While there is overlap in the expression patterns of body somites and tail somites, tail somites are a molecularly distinct tissue when compared to the trunk (Takada et al., 1994; Tucker and Slack, 1995; Hall, 2000; Beck, 2015). Initial signaling from trunk somites dictates expression of FGFs and BMPs to permit formation of the limb field, and this pattern may be recapitulated within the tail. However, the flukes are forming entirely from paraxial mesoderm, and not from any form of lateral plate mesoderm or via endodermal signaling. This is similar to median fin development in the catshark (*Scyliorhinus canicula*), where it has been experimentally demonstrated that the dorsal fin arises from paraxial mesoderm and utilizes the same gene cascades as the lateral plate derived pectoral fins (Freitas et al., 2006). Additionally, the olive flounder (*Paralichthys olivaceus*) demonstrated molecular markers for

cells derived from neural crest and paraxial mesoderm in the dorsal fin (Chen et al., 2017). The

flounder dorsal fin expressed SHH, WNT-7A, and FGF-8 in overlapping regions, similar to what is

being observed in the flukes. There is a robust body of evidence suggesting that median and paired

fins are nearly identical in signaling patterns despite developing from different mesodermal

progenitors (Letelier et al., 2018; Stewart et al., 2019; Hawkins et al., 2022)

Overall, our data suggest that cetacean flukes are a novel organ reusing a highly conserved

developmental sequence of protein signaling. The presence of FGF-8, FGF-10, WNT-7A, SHH, and

GREM within the flukes all point to an appendage-like signaling cascade, specifically one similar to a

tetrapod limb bud. This work provides a key insight into the evolution and development of a novel

organ, given that fossil evidence for flukes dates to approximately 40 MYA (Uhen, 2004; Bebej and

Smith, 2018).
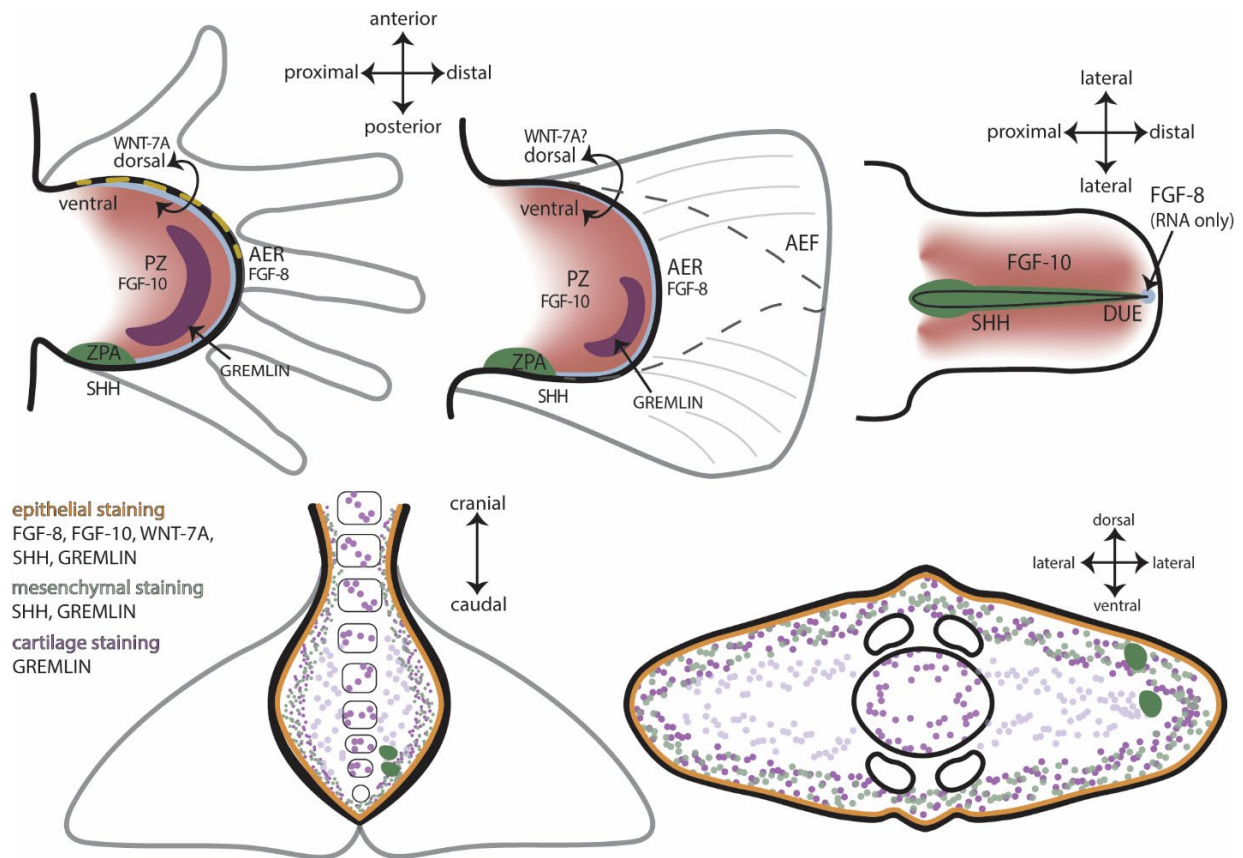
Figure 34: Summary of fluke antibody staining, with illustration of protein signaling during limb (embryonic day 11.5), fin (~20 hours post fertilization), and genital tubercle (embryonic day 13.5) development for comparison. DUE: Distal urethral epithelium. Approximate plane of section indicated by dashed line. Illustrations not to scale.

CHAPTER 7 CONCLUDING REMARKS

The overarching goal of my research is to investigate the morphological and molecular changes in cetacean appendages during the land-to-sea transition, elucidating the evolution and development of the postcranial skeleton and associated soft-tissues. Appendage development in cetaceans is marked by novel soft-tissue modifications to the forelimb, reduction of the hindlimbs, and the *de novo* evolution of the flukes. Through studies involving paleontological and modern cetacean specimens, I have documented key adaptations in the flippers, hindlimbs, and flukes of cetacean from both morphological and molecular perspectives. To address changes in the genome and phenome, I utilized a suite of techniques to identify spatiotemporal changes during the embryonic period of organogenesis (i.e., microscopy, histology, and immunohistochemistry) and evolutionary morphologies (i.e., hard and soft-tissue dissection, 3D imaging, and micro-CT scanning).

Cetacean appendages are dramatically modified for their life in the seas. The evolutionary and developmental pathways taken to achieve these changes to the bauplan are eminently distinct from terrestrial mammals. The forelimbs transform from a weight-bearing structure to a soft-tissue flipper used for steering and control, the hindlimbs and pelvis are dramatically reduced to skeletal remnants encased within the body wall, the post-thoracic spine loses regionalization for a shift to tail-powered locomotion facilitated by evolution of the novel soft-tissue flukes

. Remarkably, all of these appendage modifications appear simultaneously in the basilosaurids during the Eocene epoch, approximately 40 mya (Gingerich and Smith, 1990; Gingerich et al., 1990; Uhen, 2004; Thewissen et al., 2009a) and persist in extant cetaceans.

This dissertation investigates the pectoral and pelvic girdles, and tail flukes in cetaceans. First, assembly and morphological description of the carpus of the early archaeocete *Ambulocetus* allows insight into the first major shifts to the cetacean wrist as Cetacea took its first forays into the Tethys Sea approximately 48 mya (**chapter 3**). Then, using the embryological framework developed from investigation into three cetacean taxa (*Delphinapterus, Balaena, Stenella*) (**chapter 2**), I take an in-depth survey of cetacean hindlimb development and morphology (**chapter 4**). Protein signaling data for hindlimb development is already known for the pan-tropical spotted dolphin (*Stenella attenuata*), and that dataset (Thewissen et al. 2006) can be utilized as a benchmark for hypothesizing the role of candidate proteins in the role of limb development in other cetacean taxa. The flukes of cetaceans are built from two components – the unique vertebrae that support this novel appendage and soft-tissue adnexa. I qualitatively test published hypotheses (Watson and Fordyce, 1993; Buchholtz, 1998) for the identification of the point of insertion of the fluke by dissecting the flukes of one odontocete (*Delphinapterus*) and one mysticete (*Balaena*) (**chapter 5**). Finally, as a novel appendage there is little known about the protein signals that underlie patterning and outgrowth of the flukes. My experimental results show that a suite of proteins critical for outgrowth and patterning of limbs of tetrapods were exapted and play a key role in the outgrowth and patterning of the tail fluke in cetaceans (**chapter 6**), which grants us insight into the fundamental building blocks that are necessary for de-novo evolution of organs, a relatively rare event within the history of vertebrates.

Skeletal phenotypes and locomotion in archaeocetes

Chapters 3 and **5**, which follow carpal and fluke vertebral morphology respectively, offer new information relevant to paleontological research on early cetacean evolution. **Chapter 3** surveys variation in carpal morphologies among archaeocetes and discusses the important functional shifts in wrist shape. This dataset provides some of the first in-depth analyses of hypothesized functional consequences of cetacean carpal evolution. **Chapter 6** discusses potential morphological characteristics than can be applied to the fossil record to identify skeletal correlates of the soft-tissue flukes. Taken together, both chapters contribute to the contexts necessary for recreating archaeocete function, behavior, and locomotion in the forelimb and tail.

Embryonic phenotypes and associated protein signaling

Appendage development in embryonic and fetal cetaceans is addressed in **chapters 2, 4**, and **6**. Access to cetacean embryos is exceedingly rare, and these three chapters capitalize on the incredible resource of bowhead (*Balaena*), beluga *(Delphinapterus),* and pan-tropical spotted dolphin (*Stenella*) embryos housed in the Thewissen lab at NEOMED to compared interspecific heterochrony in appendage development.

Although all cetaceans display tail flukes and studies have shown they act as the main lift-producing propulsor (Fish et al., 2006; Sun et al., 2010, 2011; Ayancik et al., 2020), no studies have yet reported on the patterns of protein signaling shaping the tail flukes in cetaceans. **Chapter 2** of this dissertation was the first to compare ontogenetic development and comparative morphology of the

fluke between a mysticete (*Balaena*) and odontocetes (*Stenella, Delphinapterus*). The fluke research presented in **chapter 6** shows that several common development toolkit genes (FGF-8, FGF-10, WNT7A, SHH, GREM) are present in the developing flukes. Taken together, these three datasets provide a window into the highly modified cetacean appendages (Figure 35).

Although this study documents proteins associated with epithelial and mesenchymal signaling during growth of the tail flukes, corresponding gene expression (mRNA levels) remain unknown. Future molecular research will address the genes associated with outgrowth and patterning of the developing tail flukes. Further research investigating other key appendage genes like Gli, Meis, Engrailed-1, and Sp8 would allow for finer details of fluke patterning and outgrowth to be understood (Loomis et al., 1996; Chen and Johnson, 2002; Kawakami et al., 2004; Zakany et al., 2007; Berenguer and Duester, 2021; Delgado et al., 2021). These transcription factors could be studied via immunohistochemistry or *in-situ* hybridization (ISH). Using a probe for SHH, I was able to successfully tag molecules with the probe, which was visible against a DAPI nuclear stain (figure 36). Refined attempts to optimize a fluorescent ISH protocol will open up the opportunity to test a variety of mRNAs in cetacean tissue, expanding the currently limited toolkit available for the study of field-caught specimens. The effective use of this technology will open up the possibilities for cetacean molecular research.

Development of the Pelvic Girdle

The pelvic girdle of cetaceans is also of evolutionary and locomotor importance. While several studies documented the initial formation of hindlimb buds in embryonic cetaceans, their eventual loss

results in a lack of fully formed limbs in adult cetaceans and loss of all locomotor capabilities. In most mysticetes and the sperm whale, the pelvis and occasionally some reduced hindlimb bones remain embedded within the abdominal wall. Morphological variation in the size of these bony remnants of the pelvic girdle has been the focus of multiple anatomical (Struthers, 1881, 1885, 1893; Omura, 1978, 1980; Watson and Fordyce, 1993; Thewissen et al., 2021b; Cooper et al., 2023) and evolutionary (Gingerich et al., 1990, 2019; Thewissen and Fish, 1997; Uhen, 2004; Gol'din, 2014; Cooper et al., 2023) studies, yet few studies have addressed morphological variation in hindlimb buds during embryonic and fetal development. The hindlimbs of cetaceans are transiently visible in cetacean embryos, and truncation of SHH signaling in the hindlimb is likely a key factor in the cessation and eventual regression of the hindlimb bud (Thewissen et al., 2006). **Chapters 2** and **4** document variation in hindlimb bud morphology, ontogeny, and cartilage formation in a mysticete (*Balaena*) and odontocetes (*Stenella*, *Delphinapterus*). Results showed that *Balaena* retained a hindlimb bud for a greater ontogenetic timespan compared to the odontocetes. Encased within this hindlimb bud were cartilaginous anlagen of the pelvic girdle (e.g., pelvis, femur, possible tibia).
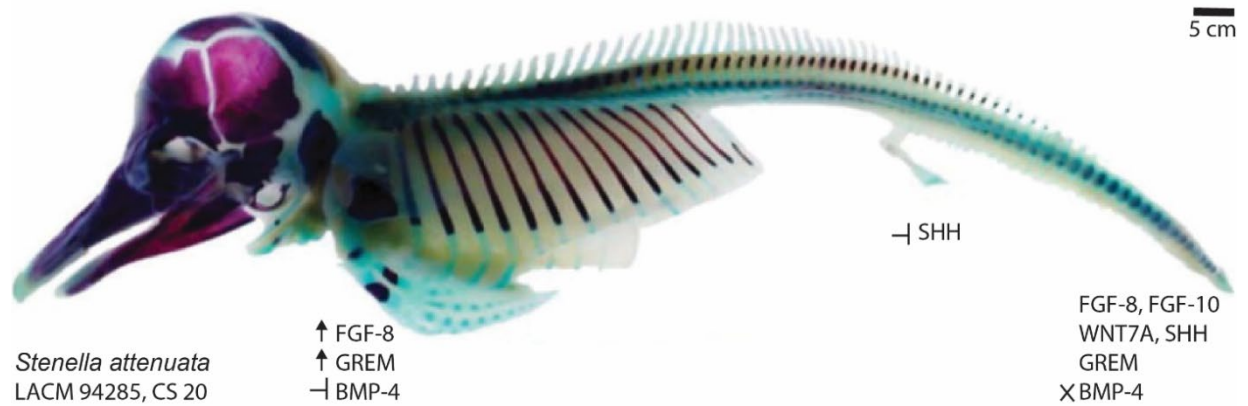
Figure 35: A pan-tropical spotted dolphin (*Stenella attenuata*) embryo stained with alizarin red for bone and alcian blue for cartilage. Changes in appendage gene expression patterns are relative to a common terrestrial mammal such as a mouse.

Contributions to the field of evolutionary developmental biology

This dissertation contributes to the fundamental understanding of cetacean development, particularly in the field of embryology. The creation of the comparative embryonic staging system (**chapter 2**) provides a baseline for future research on both odontocete and mysticete prenatal development. Up to this point, the pan-tropical spotted dolphin has been utilized as the 'model' organism for cetacean embryology – my work here demonstrates that heterochrony between taxa, particularly odontocetes and mysticetes, is profound and must be considered in cetacean embryological research.

Identification of four carpals, two for *Indohyus* and two for the pakicetids, and reconstruction of the wrist of *Ambulocetus*, gives new insight into the earliest changes to the cetacean hand related to the land-to-sea transition.

155

The research presented here on fluke identity, embryology, and development provides essential knowledge on this unusual soft-tissue appendage. The vertebral morphology dataset clarifies the traits necessary to recognize the identity of caudal skeletal elements and their relationship to the overlying soft tissue. Developmental regulation was completely unknown before the presentation of the immunohistochemical data in this dissertation. My work not only provides the first steps for understanding the formation of flukes, but also has wider implications for the genetic patterns and signaling necessary to evolve a novel appendage. This protein signaling research can potentially inform our understanding of limb development and appendage evolution in other tetrapods, such as development of manatee paddles, the uropatagium in bats, or the presence/absence of the adipose fin in some catfish and salmonids.
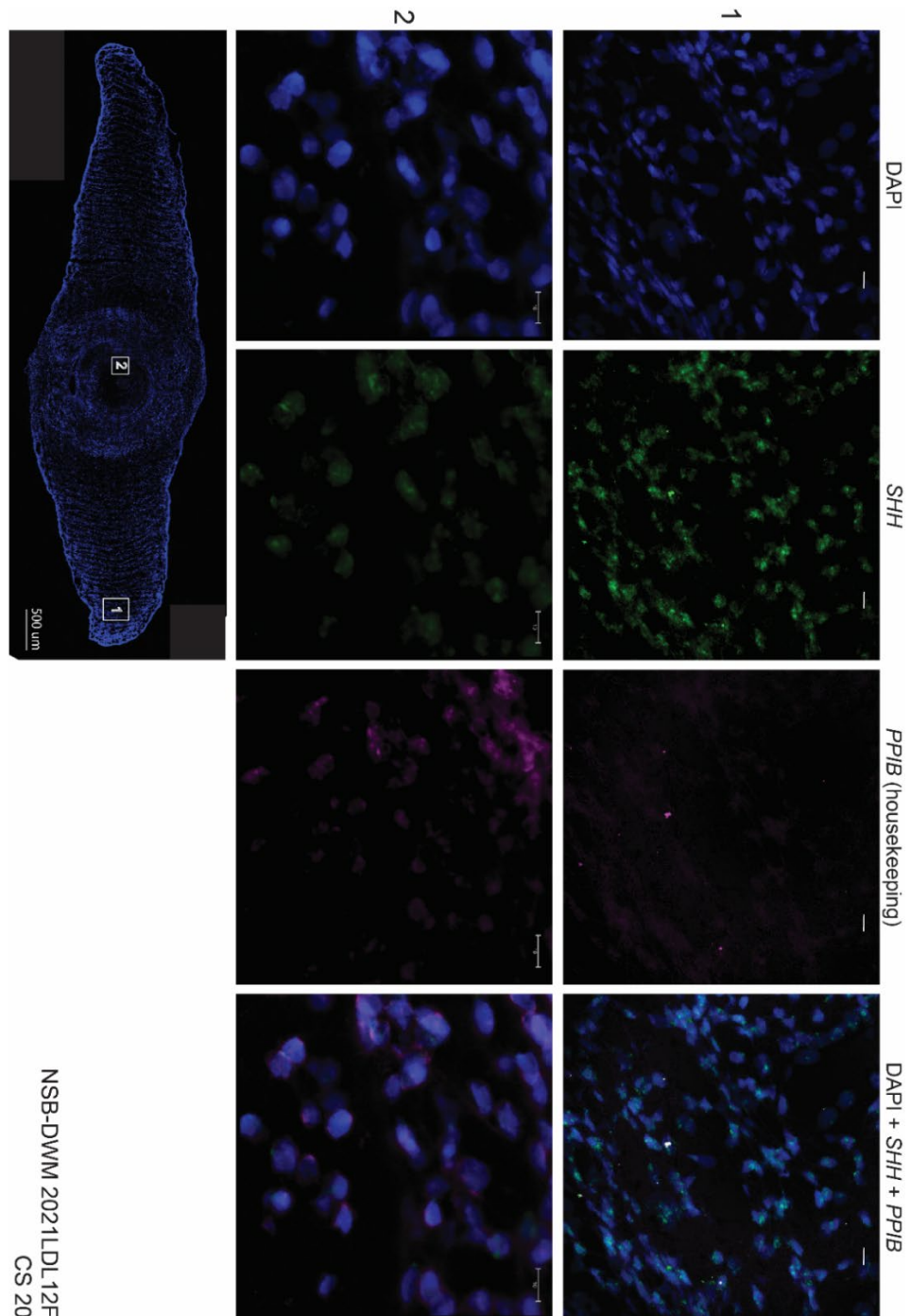
Figure 36: Confocal images of embryonic beluga fluke tissue. Images are shown for DAPI staining as well as for two probes: SHH (green) and PPIB (purple), a housekeeping gene. Tissue was prepared and stained us3ing a modified RNAscope (biotechne) multiplex fluorescent assay protocol. 1: Mesenchymal tissue in lateral fluke, corresponding to known region of SHH protein detection via IHC. 2: Cartilage of vertebral body, no evidence of SHH protein signaling from IHC dataset. The scalebar is 10 microns on insets, 500 microns on whole section of fluke.

REFERENCES

Abbasi, A. A. 2011. Evolution of vertebrate appendicular structures: Insight from genetic and

palaeontological data. Developmental Dynamics 240:1005–1016.

Adamska, M., B. T. MacDonald, Z. H. Sarmast, E. R. Oliver, and M. H. Meisler. 2004. En1 and

Wnt7a interact with Dkk1 during limb development in the mouse. Developmental Biology

272:134–144.

Agarwal, P., J. N. Wylie, J. Galceran, O. Arkhitko, C. Li, C. Deng, R. Grosschedl, and B. G. Bruneau.

2003. Tbx5 is essential for forelimb bud initiation following patterning of the limb field in

the mouse embryo. Development 130:623–633.

Ahn, K., Y. Mishina, M. C. Hanks, R. R. Behringer, and E. Bryan Crenshaw. 2001. BMPR-IA

signaling is required for the formation of the apical ectodermal ridge and dorsal-ventral

patterning of the limb. Development 128:4449–4461.

Altabef, M., J. D. W. Clarke, and C. Tickle. 1997. Dorso-ventral ectodermal compartments and

origin of apical ectodermal ridge in developing chick limb. Development 124:4547–4556.

Amano, T., T. Sagai, H. Tanabe, Y. Mizushina, H. Nakazawa, and T. Shiroishi. 2009.

Chromosomal dynamics at the Shh locus: Limb bud-specific differential regulation of

competence and active transcription. Developmental Cell 16:47–57.

Amasaki, H., H. Ishikawa, and M. Daigo. 1989. Developmental changes of the fore- and hind-

limbs in the fetuses of the southern minke whale, *Balaenoptera acutorostrata*. Anat. Anz.m

Jena 169:145–148.

Anderssen, M. S. 1918. Studier over mammarorganernes utvikling hos *Phocaena communis*. Bergens Museums Aarbok 3:1–49.

Andrews, R. C. 1921. A remarkable case of external hind limbs in a humpback whale. American Museum Novitates 9:1–6.

Armfield, B. A., J. C. George, C. J. Vinyard, and J. G. M. Thewissen. 2011. Allometric patterns of fetal head growth in mysticetes and odontocetes: Comparison of *Balaena mysticetus* and *Stenella attenuata*. Marine Mammal Science 27:819–827.

Armfield, B. A., Z. Zheng, S. Bajpai, C. J. Vinyard, and J. G. M. Thewissen. 2013. Development and evolution of the unique cetacean dentition. PeerJ 1:e24.

Armfield, B. A., A. W. Seifert, Z. Zheng, E. M. Merton, J. R. Rock, M. C. Lopez, H. V Baker, and M. J. Cohn. 2016. Molecular characterization of the genital organizer: Gene expression profile of the mouse urethral plate epithelium. Journal of Urology 196:1295–1302.

Ayancik, F., F. E. Fish, and K. W. Moored. 2020. Three-dimensional scaling laws of cetacean propulsion characterize the hydrodynamic interplay of flukes' shape and kinematics. Journal of the Royal Society Interface 17.

Bandyopadhyay, A., K. Tsuji, K. Cox, B. D. Harfe, V. Rosen, and C. J. Tabin. 2006. Genetic Analysis of the roles of BMP2, BMP4, and BMP7 in limb patterning and skeletogenesis. PLoS Genetics 2:e216.

Bastida, M. F., R. Sheth, and M. A. Ros. 2009. A BMP-Shh negative-feedback loop restricts Shh expression during limb development. Development 136:3779–3789.

Bebej, R. M., and K. M. Smith. 2018. Lumbar mobility in archaeocetes (Mammalia: Cetacea) and

the evolution of aquatic locomotion in the earliest whales. Zoological Journal of the Linnean

Society 182:695–721.

Bebej, R. M., M. Ul-Haq, I. S. Zalmout, and P. D. Gingerich. 2012. Morphology and function of the

vertebral column in *Remingtonocetus domandaensis* (Mammalia, Cetacea) from the Middle

Eocene Domanda Formation of Pakistan. Journal of Mammalian Evolution 19:77–104.

Beck, C. W. 2015. Development of the vertebrate tailbud. Wiley Interdisciplinary Reviews:

Developmental Biology 4:33–44.

Bejder, L., and B. K. Hall. 2002. Limbs in whales and limblessness in other vertebrates:

Mechanisms of evolutionary and developmental transformation and loss. Evolution and

Development 4:445–458.

Bénazet, J. D., M. Bischofberger, E. Tiecke, A. Gonçalves, J. F. Martin, A. Zuniga, F. Naef, and R.

Zeller. 2009. A self-regulatory system of interlinked signaling feedback loops controls

mouse limb patterning. Science 323:1050–1053.

Berenguer, M., and G. Duester. 2021. Role of retinoic acid signaling, FGF signaling and meis

genes in control of limb development. Biomolecules 11:1–11.

Berta, A., and C. E. Ray. 1990. Skeletal morphology and locomotor capabilities of the archaic

pinniped *Enaliarctos mealsi*. Journal of Vertebrate Paleontology 10:141–157.

Berta, A., S. Kienle, G. Bianucci, and S. Sorbi. 2015a. A reevaluation of *Pliophoca etrusca* (Pinnipedia, Phocidae) from the pliocene of Italy: Phylogenetic and biogeographic implications. Journal of Vertebrate Paleontology 35:1.

Berta, A., E. G. Ekdale, N. T. Zellmer, T. A. Deméré, S. S. Kienle, and M. Smallcomb. 2015b. Eye, nose, hair, and throat: External anatomy of the head of a neonate gray whale (Cetacea, Mysticeti, Eschrichtiidae). Anatomical Record 298:648–659.

Böhmer, C., E. Amson, P. Arnold, A. H. Van Heteren, and J. A. Nyakatura. 2018. Homeotic transformations reflect departure from the mammalian "rule of seven" cervical vertebrae in sloths: Inferences on the Hox code and morphological modularity of the mammalian neck. BMC Evolutionary Biology 18.

Boulet, A. M., A. M. Moon, B. R. Arenkiel, and M. R. Capecchi. 2004. The roles of Fgf4 and Fgf8 in limb bud initiation and outgrowth. Developmental Biology 273:361–372.

Brown, R. E., and J. P. Butler. 2000. The absolute necessity of chest-wall collapse during diving in breath-hold diving cetaceans. Aquatic Mammals 26:26–32.

Buchholtz, E. A. 1998. Implications of vertebral morphology for locomotor evolution in early Cetacea; pp. 325–351 in J. G. M. Thewissen (ed.), The Emergence of Whales, 1st ed. Springer US, Boston, Massechusetts.

Buchholtz, E. A. 2007. Modular evolution of the cetacean vertebral column. Evolution and Development 9:278–289.

Buchholtz, E. A., and J. K. Gee. 2017. Finding sacral: Developmental evolution of the axial skeleton
of odontocetes (Cetacea). Evolution & Development 19:190–204.

Buchholtz, E. A., A. C. Booth, and K. E. Webbink. 2007. Vertebral anatomy in the Florida
manatee, *Trichechus manatus latirostris*: A developmental and evolutionary analysis.
Anatomical Record 290:624–637.

Cáceres-Saez, I., N. A. Dellabianca, L. E. Pimper, F. Pereyra-Bonnet, G. H. Cassini, and R. N. P.
Goodall. 2015. Sexual dimorphism and morphometric relationships in pelvic bones of
Commerson's dolphins (Cephalorhynchus c. commersonii) from tierra del fuego, Argentina.
Marine Mammal Science 31:734–747.

Chan, Y. F., M. E. Marks, F. C. Jones, G. Villarreal, M. D. Shapiro, S. D. Brady, A. M. Southwick, D.
M. Absher, J. Grimwood, J. Schmutz, R. M. Myers, D. Petrov, B. Jónsson, D. Schluter, M. A.
Bell, and D. M. Kingsley. 2010. Adaptive evolution of pelvic reduction in sticklebacks by
recurrent deletion of a pitxl enhancer. Science 327:302–305.

Chen, H., and R. L. Johnson. 2002. Interactions between dorsal-ventral patterning genes lmx1b,
engrailed-1 and wnt-7a in the vertebrate limb. International Journal of Developmental
Biology 46:937–941.

Chen, J., X. Liu, X. Yao, F. Gao, and B. Bao. 2017. Dorsal fin development in flounder, *Paralichthys
olivaceus*: Bud formation and its cellular origin. Gene Expression Patterns 25–26:22–28.

Christiansen, F., M. M. Uhart, L. Bejder, P. Clapham, Y. Ivashchenko, D. Tormosov, N. Lewin, and M. Sironi. 2022. Fetal growth, birth size and energetic cost of gestation in southern right whales. Journal of Physiology 600:2245–2266.

Clack, J. A. 2009. The fin to limb transition: New data, interpretations, and hypotheses from paleontology and developmental biology. Annual Review of Earth and Planetary Sciences 37:163–179.

Clifford, A. B. 2010. The evolution of the unguligrade manus in artiodactyls. Journal of Vertebrate Paleontology 30:1827–1839.

Cloutier, R., A. M. Clement, M. S. Y. Lee, R. Noël, I. Béchard, V. Roy, and J. A. Long. 2020. *Elpistostege* and the origin of the vertebrate hand. Nature 579:549–554.

Cohn, M. J. 2011. Development of the external genitalia: Conserved and divergent mechanisms of appendage patterning. Developmental Dynamics 240:1108–1115.

Cohn, M. J., and C. Tickle. 1999. Developmental basis of limblessness and axial patterning in snakes. Nature 399:474-479.

Cooper, K. L., K. E. Sears, A. Uygur, J. Maier, K. S. Baczkowski, M. Brosnahan, D. Antczak, J. A. Skidmore, and C. J. Tabin. 2014a. Patterning and post-patterning modes of evolutionary digit loss in mammals. Nature 511:41–45.

Cooper, L. N., B. A. Armfield, and J. G. M. Thewissen. 2011. Evolution of the apical ectoderm in the developing vertebrate limb; pp. 472 in Epigenetics: linking genotype and phenotype in development and evolution. University of California Press, Berkeley.

Cooper, L. N., C. J. Cretekos, and K. E. Sears. 2012a. The evolution and development of

mammalian flight. Wiley Interdisciplinary Reviews: Developmental Biology 1:773–779.

Cooper, L. N., R. Suydam, and J. G. M. Thewissen. 2023. Cetacean evolution: Copulation and

birthing consequences of pelvic and hindlimb reduction; in B. Würsig and D. Orbach (eds.),

Sex in cetaceans: Morphology, behavior, and evolution of sexual strategies.

Cooper, L. N., A. Berta, S. D. Dawson, and J. S. Reidenberg. 2007a. Evolution of hyperphalangy

and digit reduction in the cetacean manus. Anatomical Record 290:654–672.

Cooper, L. N., S. D. Dawson, J. S. Reidenberg, and A. Berta. 2007b. Neuromuscular anatomy and

evolution of the cetacean forelimb. The Anatomical Record 290:1121–1137.

Cooper, L. N., J. G. M. Thewissen, S. Bajpai, and B. N. Tiwari. 2012b. Postcranial morphology and

locomotion of the Eocene raoellid *Indohyus* (Artiodactyla: Mammalia). Historical Biology

24:279–310.

Cooper, L. N., K. E. Sears, B. A. Armfield, B. Kala, M. Hubler, and J. G. M. Thewissen. 2017.

Review and experimental evaluation of the embryonic development and evolutionary

history of flipper development and hyperphalangy in dolphins (Cetacea: Mammalia).

Genesis 56:1–14.

Cooper, L. N., E. R. Seiffert, M. Clementz, S. I. Madar, S. Bajpai, S. T. Hussain, and J. G. M.

Thewissen. 2014b. Anthracobunids from the middle Eocene of India and Pakistan are stem

perissodactyls. PLoS ONE 9.

Cooper, L. N., N. Sedano, S. Johansson, B. May, J. D. Brown, C. M. Holliday, B. W. Kot, and F. E. Fish. 2008. Hydrodynamic performance of the minke whale (*Balaenoptera acutorostrata*) flipper. Journal of Experimental Biology 211:1859–1867.

Daeschler, E. B., N. H. Shubin, and F. A. Jenkins. 2006. A Devonian tetrapod-like fish and the evolution of the tetrapod body plan. Nature 440:757–763.

Delgado, I., and M. Torres. 2017. Coordination of limb development by crosstalk among axial patterning pathways. Developmental Biology 429:382–386.

Delgado, I., G. Giovinazzo, S. Temiño, Y. Gauthier, A. Balsalobre, J. Drouin, and M. Torres. 2021. Control of mouse limb initiation and antero-posterior patterning by Meis transcription factors. Nature Communications 12.

Dines, J. P., E. Otárola-Castillo, P. Ralph, J. Alas, T. Daley, A. D. Smith, and M. D. Dean. 2014. Sexual selection targets cetacean pelvic bones. Evolution 68:3296–3306.

Domning, D. P. 2018. Sirenian Evolution; pp. 856–859 in B. Würsig, J. G. M. Thewissen, and K. M. Kovacs (eds.), The Encyclopedia of Marine Mammals, Third. Academic Press.

Duboc, V., and M. P. O. Logan. 2011. Pitx1 is necessary for normal initiation of hindlimb outgrowth through regulation of Tbx4 expression and shapes hindlimb morphologies via targeted growth control. Development 138:5301–5309.

Eschricht, D. F., J. Reinhardt, and W. Lilljeborg. 1866. Recent Memoirs on the Cetacea (R. Hardwicke (ed.)). Ray Society, London, 50–150 pp.

Everett, M. M., and W. A. Miller. 1973. Adaptation of Mallory's trichrome stain to embryonic and

    fetal material. Biotechnic and Histochemistry 48:5–8.

Farnkopf, I. C., J. C. George, T. Kishida, D. J. Hillmann, R. S. Suydam, and J. G. M. Thewissen.

    2021. Olfactory epithelium and ontogeny of the nasal chambers in the bowhead whale

    (*Balaena mysticetus*). Anatomical Record 305:643–667.

Fedak, T. J., and B. K. Hall. 2004. Perspectives on hyperphalangy: patterns and processes. Journal

    of Anatomy 204:151–163.

Felts, W. J. L. 1966. Some functional and structural characteristics of cetacean flippers and flukes;

    pp. 255–276 in K. S. Norris (ed.), Whales, Dolphins, and Porpoises, 1st ed. University of

    California Press, Berkeley.

Fish, F. E. 1984. Kinematics of undulatory swimming in the American alligator. 839–843.

Fish, F. E. 1994. Association of propulsive swimming mode with behavior in river otters (*Lutra

    canadensis*). Journal of Mammalogy 75:989–997.

Fish, F. E. 1998. Biomechanical perspective on the origin of cetacean flukes; pp. 303–324 in J. G.

    M. Thewissen (ed.), The Emergence of Whales, 1st ed. Springer US, Boston, Massachusetts.

Fish, F. E., and J. J. Rohr. 1999. Review of Dolphin Hydrodynamics and Review of Dolphin

    Hydrodynamics and. Spawar.

Fish, F. E., and G. V. Lauder. 2006. Passive and active flow control by swimming fishes and

    mammals. Annual Review of Fluid Mechanics 38:193–224.

Fish, F. E., M. K. Nusbaum, J. T. Beneski, and D. R. Ketten. 2006. Passive cambering and flexible propulsors: Cetacean flukes. Bioinspiration and Biomimetics 1.

Fordyce, R. E., J. L. Goedert, L. G. Barnes, and B. J. Crowley. 2000. Pelvic girdle elements of Oligocene and Miocene Mysticeti: whale hind legs in transition. Journal of Vertebrate Paleontology 3.

Franzen, J. 1983. Fossilfundstelle Messel, Nr. 35: Ein zweites Skelett von *Messelobunodon* (Mammalia, Artiodactyla, Dichobunidae) aus der «Grube Messel» bei Darmstadt (Deutschland, S-Hessen). Senckenbergiana Lethaea 64:403–445.

Freitas, R., G. J. Zhang, and M. J. Cohn. 2006. Evidence that mechanisms of fin development evolved in the midline of early vertebrates. Nature 442:1033–1037.

Frost, K. J., T. Gray, W. Goodwin, R. Schaeffer, R. Suydam, C. J. Kathryn Frost, and A. Beluga Whale. 2021. Alaska Beluga Whale Committee—a unique model of co-management. Polar Research 40:5611.

Garten, J. L., and F. E. Fish. 2020. Comparative histological examination of the integument of odontocete flukes. Aquatic Mammals 46:367–381.

Gatesy, J. 1998. Molecular evidence for the phylogenetic affinities of Cetacea; pp. 63–111 in J. G. M. Thewissen (ed.), The Emergence of Whales, 1st ed. Springer US, Boston, Massachusetts.

Gavazzi, L., L. N. Cooper, S. Usip, R. Suydam, R. Stimmelmayr, J. C. George, G. O'Corry-Crowe, C. W. Hsu, and J. Thewissen. 2023. Comparative embryology of *Delphinapterus leucas*

(beluga whale), *Balaena mysticetus* (bowhead whale), and *Stenella attenuata* (pan-tropical spotted dolphin) (Cetacea: Mammalia). Journal of Morphology 284.

Gavazzi, L. M., L. N. Cooper, F. E. Fish, S. T. Hussain, and J. G. M. Thewissen. 2020. Carpal morphology and function in the earliest cetaceans. Journal of Vertebrate Paleontology 40:1–10.

Gehrke, A. R., I. Schneider, E. De La Calle-Mustienes, J. J. Tena, C. Gomez-Marin, M. Chandran, T. Nakamura, I. Braasch, J. H. Postlethwait, J. L. Gómez-Skarmeta, and N. H. Shubin. 2015. Deep conservation of wrist and digit enhancers in fish. Proceedings of the National Academy of Sciences of the United States of America 112:803–808.

Geisler, J. H. 2019. Whale Evolution: Dispersal by Paddle or Fluke. Current Biology 29:R294–R296.

Geisler, J. H., and J. M. Theodor. 2009. Hippopotamus and whale phylogeny. Nature 458:E1–E4.

George, J. C., J. Bada, J. Zeh, L. Scott, S. E. Brown, T. O'Hara, and R. Suydam. 1999. Age and growth estimates of bowhead whales (*Balaena mysticetus*) via aspartic acid racemization. Canadian Journal of Zoology 77:571–580.

George, J. C., R. Stimmelmayr, R. Suydam, S. Usip, G. Givens, T. Sformo, and J. G. M. Thewissen. 2016. Severe bone loss as part of the life history strategy of bowhead whales. PLOS ONE 11:e0156753.

Gingerich, P. D. 2003. Land-to-sea transition in early whales: evolution of Eocene Archaeoceti (Cetacea) in relation to skeletal proportions and locomotion of living semiaquatic mammals. Paleobiology 29:429–454.

Gingerich, P. D., and B. H. Smith. 1990. Forelimb and hand of *Basilosaurus isis* (Mammalia, Cetacea) from the middle Eocene of Egypt. Journal of Vertebrate Paleontology 10:237–251.

Gingerich, P. D., B. H. Smith, and E. L. Simons. 1990. Hind limbs of Eocene *Basilosaurus*: Evidence of feet in whales. Science 249:154–157.

Gingerich, P. D., M. S. M. Antar, and I. S. Zalmout. 2019. *Aegicetus gehennae*, a new late Eocene protocetid (Cetacea, Archaeoceti) from Wadi Al Hitan, Egypt, and the transition to tail-powered swimming in whales. PLoS ONE 14.

Gingerich, P. D., H. Ul Haq, I. S. Zalmout, I. H. Khan, and M. S. Malkani. 2001. Origin of whales from early artiodactyls: hands and feet of Eocene Protocetidae from Pakistan. Science 293:2239–2242.

Gingerich, P. D., M. Ul-Haq, W. Von Koenigswald, W. J. Sanders, B. H. Smith, and I. S. Zalmout. 2009. New protocetid whale from the middle Eocene of Pakistan: birth on land, precocial development, and sexual dimorphism. PLoS ONE 4:1–20.

Goldbogen, J. A., D. E. Cade, J. Calambokidis, A. S. Friedlaender, J. Potvin, P. S. Segre, and A. J. Werth. 2017. How baleen whales feed: The biomechanics of engulfment and filtration. Annual Review of Marine Science 9:367–386.

Goldbogen, J. A., J. Calambokidis, D. A. Croll, M. F. Mckenna, E. Oleson, J. Potvin, N. D. Pyenson, G. Schorr, R. E. Shadwick, and B. R. Tershy. 2012. Scaling of lunge-feeding performance in rorqual whales: mass-specific energy expenditure increases with body size and progressively limits diving capacity. Functional Ecology 26:216–226.

Gol'din, P. 2014. Naming an innominate: Pelvis and hindlimbs of Miocene whales give an insight into evolution and homology of cetacean pelvic girdle. Evolutionary Biology 41:473–479.

Gorivodsky, M., and P. Lonai. 2003. Novel roles of Fgfr2 in AER differentiation and positioning of the dorsoventral limb interface. Development 130:5471–5479.

Gough, W. T., F. E. Fish, D. K. Wainwright, and H. Bart-Smith. 2018. Morphology of the core fibrous layer of the cetacean tail fluke. Journal of Morphology 1–9.

Gray, N. M., K. Kainec, S. Madar, L. Tomko, and S. Wolfe. 2007. Sink or swim? Bone density as a mechanism for buoyancy control in early cetaceans. The Anatomical Record 290:638–653.

Gredler, M. L. 2016. Developmental and evolutionary origins of the amniote phallus. Integrative and Comparative Biology 56:694–704.

Guldberg, G., and F. Nansen. 1894. On the development and structure of the whale. John Grieg, 1–70 pp.

Haddad, D., S. Huggenberger, M. Haas-Rioth, L. S. Kossatz, H. H. A. Oelschläger, and A. Haase. 2012. Magnetic resonance microscopy of prenatal dolphins (Mammalia, Odontoceti, Delphinidae) - Ontogenetic and phylogenetic implications. Zoologischer Anzeiger 251:115–130.

Hall, B. K. 2000. A role for epithelial-mesenchymal interactions in tail growth/morphogenesis and chondrogenesis in embryonic mice. Cells Tissues Organs 166:6–14.

Hampe, O., H. Franke, C. A. Hipsley, N. Kardjilov, and J. Müller. 2015. Prenatal cranial ossification of the humpback whale (*Megaptera novaeangliae*). Journal of Morphology 276:564–582.

Haraguchi, R., R. Mo, C. C. Hui, J. Motoyama, S. Makino, T. Shiroishi, W. Gaffield, and G. Yamada. 2001. Unique functions of sonic hedgehog signaling during external genitalia development. Development 128:4241–4250.

Haraguchi, R., K. Suzuki, R. Murakami, M. Sakai, M. Kamikawa, M. Kengaku, K. Sekine, H. Kawano, S. Kato, N. Ueno, and G. Yamada. 2000. Molecular analysis of external genitalia formation: The role of fibroblast growth factor (fgf) genes during genital tubercle formation. Development 127:2471–2479.

Harfe, B. D., P. J. Scherz, S. Nissim, H. Tian, A. P. McMahon, and C. J. Tabin. 2004. Evidence for an expansion-based temporal Shh gradient in specifying vertebrate digit identities. Cell 118:517–528.

Hawkins, M. B., K. Henke, M. P. H. Correspondence, and M. P. Harris. 2021. Latent developmental potential to form limb-like skeletal structures in zebrafish. Cell 184:1–13.

Hawkins, M. B., D. Jandzik, F. J. Tulenko, A. N. Cass, T. Nakamura, N. H. Shubin, M. C. Davis, and D. W. Stock. 2022. An Fgf-Shh positive feedback loop drives growth in developing unpaired fins. Proceedings of the National Academy of Sciences of the United States of America 119:10–12.

Heide-Jørgensen, M. P., and E. Garde. 2011. Fetal growth of narwhals (*Monodon monoceros*). Marine Mammal Science 27:659–664.

Heide-Jørgensen, M. P., E. S. Nordøy, N. Øien, L. P. Folkow, L. Kleivane, A. S. Blix, M. V Jensen, and K. L. Laidre. 2001. Satellite tracking of minke whales (*Balaenoptera acutorostrata*) off the coast of northern Norway. Journal of Cetacean Resource Management 3:175–178.

Hickman, G. 1979. The mammalian tail: a review of functions. Mammal Review 9:143–157.

Höch, R., R. F. Schneider, A. Kickuth, A. Meyer, and J. M. Woltering. 2021. Spiny and soft-rayed fin domains in acanthomorph fish are established through a BMP-gremlin-shh signaling network. Proceedings of the National Academy of Sciences of the United States of America 118.

Hockman, D., C. J. Cretekos, M. K. Mason, R. R. Behringer, D. S. Jacobs, and N. Illing. 2008. A second wave of Sonic hedgehog expression during the development of the bat limb. Proceedings of the National Academy of Sciences of the United States of America 105:16982–16987.

Houssaye, A., P. Tafforeau, C. De Muizon, and P. D. Gingerich. 2015. Transition of Eocene whales from land to sea: evidence from bone microstructure. PLoS ONE 10:1–28.

Hsu, C. W., S. Kalaga, U. Akoma, T. L. Rasmussen, A. E. Christiansen, and M. E. Dickinson. 2019. High resolution imaging of mouse embryos and neonates with x-ray micro-computed tomography. Current Protocols in Mouse Biology 9:e63.

Hsu, C. W., L. Wong, T. L. Rasmussen, S. Kalaga, M. L. McElwee, L. C. Keith, R. Bohat, J. R. Seavitt, A. L. Beaudet, and M. E. Dickinson. 2016. Three-dimensional microCT imaging of mouse development from early post-implantation to early postnatal stages. Developmental Biology 419:229–236.

Hulbert, R. C. 1998. Postcranial osteology of the North American middle Eocene protocetid *Georgiacetus*; pp. 235–267 in J. G. M. Thewissen (ed.), The Emergence of Whales, 1st ed. Plenum Press, New York.

Infante, C. R., A. M. Rasys, and D. B. Menke. 2018. Appendages and gene regulatory networks: Lessons from the limbless. Genesis 56:1–8.

Kato, H. 1988. Ossification pattern of the vertebral epiphyses in the southern minke whale. Sci. Rep. Whales Res. Inst. 39:11–19.

Kawakami, Y., C. Rodríguez-Esteban, T. Matsui, J. Rodríguez-León, S. Kato, and J. C. Izpisúa Belmonte. 2004. Sp8 and Sp9, two closely related buttonhead-like transcription factors, regulate Fgf8 expression and limb outgrowth in vertebrate embryos. Development 131:4763–4774.

Keane, M., J. Semeiks, A. E. Webb, Y. I. Li, V. Quesada, T. Craig, L. B. Madsen, S. van Dam, D. Brawand, P. I. Marques, P. Michalak, L. Kang, J. Bhak, H. S. Yim, N. V. Grishin, N. H. Nielsen, M. P. Heide-Jørgensen, E. M. Oziolor, C. W. Matson, G. M. Church, G. W. Stuart, J. C. Patton, J. C. George, R. Suydam, K. Larsen, C. López-Otín, M. J. O'Connell, J. W. Bickham,

B. Thomsen, and J. P. deMagalhães. 2015. Insights into the evolution of longevity from the bowhead whale genome. Cell Reports 10:112–122.

Kellogg, R. 1928. The history of whales - their adaptations to life in the water. The Quarterly Review of Biology 3.

Kellogg, R. 1936. A review of the Archaeoceti. Carnegie Institute of Washingon Publication 482:1–366.

Kengaku, M., J. Capdevila, C. Rodriguez-Esteban, J. De La Peña, R. L. Johnson, J. C. I. Belmonte, and C. J. Tabin. 1998. Distinct WNT pathways regulating AER formation and dorsoventral polarity in the chick limb bud. Science 280:1274–1277.

Kleinenberg, S. E. 1969. Beluga (*Delphinapterus Leucas*): Investigation of the Species. pp.

Klima, M. 1999. Development of the Cetacean Nasal Skull, 149th ed. Springer, 1–152 pp.

Kojeszewski, T., and F. E. Fish. 2007. Swimming kinematics of the Florida manatee (*Trichechus manatus latirostris*): hydrodynamic analysis of an undulatory mammalian swimmer. Journal of Experimental Biology 210:2411–2418.

Kozhemyakina, E., A. Ionescu, and A. B. Lassar. 2014. GATA6 Is a Crucial Regulator of Shh in the Limb Bud. PLoS Genet 10:1004072.

Kükenthal, W. 1889. Die Hand der Cetaceen; pp. 23–69 in Vergleichend-anatomische und entwickelungsgeschichtliche untersuchungen an Walthieren. Gustav Fischer, Jena.

Kükenthal, W. 1893. Verggleichend-anatomische und entwicklunggeschichliche Untersuchungen

    an Walthieren: Bau und Entwicklung der Cetaceennase. Denkschr Med Naturw Ges Jena

    3:322–349.

Kükenthal, W. 1914. Untersuchungen an Walen. Zeitschrift Fur Naturwissenschaften 51:1–122.

Kumar, K. 1992. *Paratritemnodon indicus* (Creodonta: Mammalia) from the early middle Eocene

    Subathu Formation, NW Himalaya, India, and the Kalakot mammalian community

    structure. Paläontologisches Zeitschrift 66:387–403.

Kumar, K. 1998. Tertiary vertebrates from the pre-Siwalik himalayan foreland basin, Northwest

    India. Workshop on Himalayan Foreland Basin with Special Reference to Pre-Siwalik

    Tertiaries 33–36.

Kumar, K., and A. Sahni. 1985. Eocene mammals from the upper Subathu group, Kashmir

    Himalaya, India. Journal of Vertebrate Paleontology 5:153–168.

Lambert, O., G. Bianucci, R. Salas-Gismondi, C. Di Celma, E. Steurbaut, M. Urbina, and C. de

    Muizon. 2019. An amphibious whale from the middle Eocene of Peru reveals early South

    Pacific dispersal of quadrupedal cetaceans. Current Biology 29:1352-1359.e3.

Lan, L., W. Wang, Y. Huang, X. Bu, and C. Zhao. 2019. Roles of Wnt7a in embryo development,

    tissue homeostasis, and human diseases. Journal of Cellular Biochemistry 120:18588–18598.

Lanzetti, A., A. Berta, and E. G. Ekdale. 2020. Prenatal development of the humpback whale:

    Growth rate, tooth loss and skull shape changes in an evolutionary framework. Anatomical

    Record 303:180–204.

Leal, F., and M. J. Cohn. 2015. Development of hemipenes in the ball python snake python regius. Sexual Development 9:6–20.

Letelier, J., E. De La Calle-Mustienes, J. Pieretti, S. Naranjo, I. Maeso, T. Nakamura, J. Pascual-Anaya, N. H. Shubin, I. Schneider, J. R. Martinez-Morales, and J. L. Gómez-Skarmeta. 2018. A conserved Shh cis-regulatory module highlights a common developmental origin of unpaired and paired fins. Nature Genetics 50:504–509.

Lewandoski, M., X. Sun, and G. R. Martin. 2000. Fgf8 signaling from the AER is essential for normal limb development. Nature Genetics 26:460–463.

Lewis, O. J., R. J. Hamshere, and T. M. Bucknill. 1970. The anatomy of the wrist joint. Journal of Anatomy 106:539–52.

Liang, N., L. Deme, Q. Kong, L. Sun, Y. Cao, T. Wu, X. Huang, S. Xu, and G. Yang. 2022. Divergence of Tbx4 hindlimb enhancer HLEA underlies the hindlimb loss during cetacean evolution. Genomics 114:110292.

Lillie, M. A., A. W. Vogl, S. Raverty, M. Haulena, W. A. McLellan, G. B. Stenson, and R. E. Shadwick. 2017. Controlling thoracic pressures in cetaceans during a breath-hold dive: Importance of the diaphragm. Journal of Experimental Biology 220:3464–3477.

Logan, C., A. Hornbruch, I. Campbell, and A. Lumsden. 1997. The role of Engrailed in establishing the dorsoventral axis of the chick limb. Development 124:2317–2324.

Logan, M., and C. J. Tabin. 1999. Role of Pitx1 Upstream of Tbx4 in Specification of Hindlimb Identity. Science 283:1736–1739.

Loomis, C. A., E. Harris, J. Michaud, W. Wurst, M. Hanks, and A. L. Joyner. 1996. The mouse
Engrailed-1 gene and ventral limb patterning. Nature 382:360–363.

Lopez-Rios, J. 2016. The many lives of SHH in limb development and evolution. Seminars in Cell
and Developmental Biology 49:116–124.

Maas, M. C., S. T. Hussain, J. J. M. Leinders, and J. G. M. Thewissen. 2001. A new isectolophid
tapiromorph (Perissodactyla, Mammalia) from the early Eocene of Pakistan. Journal of
Paleontology 75:407–417.

Madar, S. I. 2007. The postcranial adaptations of early Eocene pakicetid cetaceans. Journal of
Paleontology 81:176–200.

Madar, S. I., J. G. M. Thewissen, and S. T. Hussain. 2002a. Additional holotype remains of
Ambulocetus natans (Cetacea, Ambulocetidae), and their implications for locomotion in
early whales. Journal of Vertebrate Paleontology 22:405–422.

Madar, S. I., J. G. M. Thewissen, and S. T. Hussain. 2002b. Additional holotype remains of
Ambulocetus natans (Cetacea, ambulocetidae), and their implications for locomotion in
early whales. Journal of Vertebrate Paleontology 22:405–422.

Mahmood, R., J. Bresnick, A. Hornbruch, C. Mahony, N. Morton, K. Colquhoun, P. Martin, A.
Lumsden, C. Dickson, and I. Mason. 1995. A role for FGF-8 in the initiation and
maintenance of vertebrate limb bud outgrowth. Current Biology 5:797–806.

Martínez-Cáceres, M., O. Lambert, and C. de Muizon. 2017. The anatomy and phylogenetic

affinities of *Cynthiacetus peruvianus*, a large Dorudon-like basilosaurid (Cetacea,

Mammalia) from the late Eocene of Peru. Geodiversitas 39:7–163.

Marx, F. G., A. Collareta, A. Gioncada, K. Post, O. Lambert, E. Bonaccorsi, M. Urbina, and G.

Bianucci. 2017. How whales used to filter: exceptionally preserved baleen in a Miocene

cetotheriid. Journal of Anatomy 231:212–220.

McGlinn, E., and C. J. Tabin. 2006. Mechanistic insight into how Shh patterns the vertebrate

limb. Current Opinion in Genetics & Development 16:426–432.

Mercader, N. 2007. Early steps of paired fin development in zebrafish compared with tetrapod

limb development. Development Growth and Differentiation 49:421–437.

Merino, R., J. Rodriguez-Leon, D. Macias, Y. Gañan, A. N. Economides, and J. M. Hurle. 1999. The

BMP antagonist Gremlin regulates outgrowth, chondrogenesis and programmed cell death

in the developing limb. Development 126:5515–5522.

Michos, O., L. Panman, K. Vintersten, K. Beier, R. Zeller, and A. Zuniga. 2004. Gremlin-mediated

BMP antagonism induces the epithelial-mesenchymal feedback signaling controlling

metanephric kidney and limb organogenesis. Development 131:3401–3410.

Miyakawa, N., T. Kishiro, Y. Fujise, G. Nakamura, H. Kato, N. Miyakawa, T. Kishiro, Y. Fujise, G.

Nakamura, and H. Kato. 2016. Sexual dimorphism in pelvic bone shape of the North Pacific

common minke whales (*Balaenoptera acutorostrata*). Open Journal of Animal Sciences

6:131–136.

Moon, A. M., and M. R. Capecchi. 2000. Fgf8 is required for outgrowth and patterning of the limbs. Nature Genetics 26:455.

Moon, A. M., A. M. Boulet, and M. R. Capecchi. 2000. Normal limb development in conditional mutants of Fgf4. Development (Cambridge, England) 127:989–96.

Moran, M. M., S. Nummela, and J. G. M. Thewissen. 2011. Development of the skull of the pantropical spotted dolphin (*Stenella attenuata*). Anatomical Record 294:1743–1756.

Moran, M. M., S. Bajpai, J. C. George, R. Suydam, S. Usip, and J. G. M. Thewissen. 2015. Intervertebral and epiphyseal fusion in the postnatal ontogeny of cetaceans and terrestrial mammals. Journal of Mammalian Evolution 22:93–109.

Morris, S. C., and J. B. Caron. 2014. A primitive fish from the Cambrian of North America. Nature 2014 512:7515 512:419–422.

Newton, A. H., and C. A. Smith. 2021. Regulation of vertebrate forelimb development and wing reduction in the flightless emu. Developmental Dynamics 250:1248–1263.

Nganvongpanit, K., P. Cherdsukjai, B. Boonsri, K. Buddhachat, P. Kaewmong, and K. Kittiwattanawong. 2020. Pelvic bone morphometric analysis in the dugong (*Dugong dugon*). Scientific Reports 2020 10:1 10:1–12.

Nicoli, S., C. N. Gilardelli, O. Pozzoli, M. Presta, and F. Cotelli. 2005. Regulated expression pattern of gremlin during zebrafish development. Gene Expression Patterns 5:539–544.

Norton, W. H. J., J. Ledin, H. Grandel, and C. J. Neumann. 2005. HSPG synthesis by zebrafish Ext2 and Extl3 is required for Fgf10 signaling during limb development. Development 132:4963–4973.

O'Connor, S. M., T. J. Dawson, R. Kram, and J. Maxwell Donelan. 2014. The kangaroo's tail propels and powers pentapedal locomotion. Biology Letters 10:1–4.

Oelschläger, H. A. 1989. Early development of the olfactory and terminalis systems in baleen whales. Brain, Behavior and Evolution 34:171–183.

Oelschläger, H. H. A. 2000. Morphological and functional adaptations of the toothed whale head to aquatic life. Historical Biology 14:33–39.

Ogawa, T. 1953. On the presence and disappearance of the hind limb in the cetacean embryos. Sci. Rpts. Whales Research Inst. 8:127–132.

Ogawa, T., and T. Kamiya. 1957. A case of the Cachalot with protruded rudimentary hind limbs. Sci. Rep. Whale Res. Inst. 12:197–208.

Ohuchi, H., T. Nakagawa, A. Yamamoto, A. Araga, T. Ohata, Y. Ishimaru, H. Yoshioka, T. Kuwana, T. Nohno, M. Yamasaki, N. Itoh, and S. Noji. 1997. The mesenchymal factor, FGF10, initiates and maintains the outgrowth of the chick limb bud through interaction with FGF8, an apical ectodermal factor. Development 124:2235–2244.

O'Leary, M. A., and K. D. Rose. 1995. Postcranial skeleton of the early Eocene mesonychid *Pachyaena* (Mammalia: Mesonychia). Journal of Vertebrate Paleontology 15:401–430.

Omura, H. 1978. Preliminary report on the morphological study of pelvic bones of the minke whale from the Antarctic. Sci. Rpts. of the Whales Res. Inst. 271–279.

Omura, H. 1980. Morphological study of pelvic bones of the minke whale from the Antarctic. Sci. Rpts. of the Whales Res. Inst. 32:25–37.

Onimaru, K., and L. Marcon. 2021. Systems biology approach to the origin of the tetrapod limb; pp. 89–113 in Evolutionary Systems Biology. Springer International Publishing, Cham.

O'Rahilly, R., and F. Müller. 2001. Human Embryology and Teratology, 3rd ed. Wiley-Liss Inc., 1–520 pp.

Osterwalder, M., D. Speziale, M. Shoukry, R. Mohan, R. Ivanek, M. Kohler, C. Beisel, X. Wen, S. J. Scales, V. M. Christoffels, A. Visel, J. Lopez-Rios, and R. Zeller. 2014. HAND2 targets define a network of transcriptional regulators that compartmentalize the early limb bud mesenchyme. Developmental Cell 31:345–357.

Parr, B. A., and A. P. McMahon. 1995. Dorsalizing signal Wnt-7a required for normal polarity of D-V and A-P axes of mouse limb. Nature 374:350–353.

Patten, B. M. 1931. Embryology of the pig, 2nd ed. P. Blakiston's Son & Co., Inc., 327 pp.

Perriton, C. L., N. Powles, C. Chiang, M. K. Maconochie, and M. J. Cohn. 2002. Sonic hedgehog signaling from the urethral epithelium controls external genital development. Developmental Biology 247:26–46.

Pilleri, G. 1990. Paratypus von *Balaenoptera siberi* (Cetacea: Mysticeti) aus der Pisco Formation

Perus; pp. 205–215 in G. Pilleri (ed.), Beitra¨ge zur pala¨ ontologe der cetaceen und

pinnipedier der Pisco Formation Perus II. Hirnanatomisches Istitut der Universitat Bern

Ostermundigen, Waldau-Berne, Switzerland.

Pivorunas, A. 1979. The feeding mechanisms of baleen whales. American Scientist 67:432–440.

Pizette, S., C. Abate-Shen, and L. Niswander. 2001. BMP controls proximodistal outgrowth, via

induction of the apical ectodermal ridge, and dorsoventral patterning in the vertebrate limb.

Development 128:4463–4474.

Ranga Rao, A. 1972. Further students on the vertebrate fauna of Kalakot, India. New mammalian

genera and species from the Kalakot Zone of Himalayan foot hills near Kalakot, Jammu &

Kashmir State, India. Directorate of Geology, Oil & Natural Gas Commission, Dehra Dun,

India. Special Paper 1:1–22.

Ranga Rao, A. 1973. Notices of two mammals from the upper Eocene Kalakot beds, India.

Directorate of Geology, Oil & Natural Gas Commission, Dehra Dun, India. Special Paper 2:1–

6.

Reese, C. S., J. A. Calvin, J. C. George, and R. J. Tarpley. 2001. Estimation of fetal growth and

gestation in bowhead whales. Journal of the American Statistical Association 96:915–923.

Richardson, M. K., and H. H. A. Oelschläger. 2002. Time, pattern, and heterochrony: A study of

hyperphalangy in the dolphin embryo flipper. Evolution and Development 4:435–444.

Richardson, M. K., and A. D. Chipman. 2003. Developmental constraints in a comparative

framework: A test case using variations in phalanx number during amniote evolution.

Journal of Experimental Zoology Part B: Molecular and Developmental Evolution 296:8–22.

Richardson, M. K., J. E. Jeffery, and C. J. Tabin. 2004. Proximodistal patterning of the limb:

Insights from evolutionary morphology. Evolution and Development 6:1–5.

Richardson, M. K., S. M. H. Gobes, A. C. van Leeuwen, J. A. E. Polman, C. Pieau, and M. R.

Sánchez-villagra. 2009. Heterochrony in limb evolution: Developmental mechanisms and

natural selection. Journal of Experimental Zoology Part B: Molecular and Developmental

Evolution 312:639–664.

Rodriguez-Esteban, C., J. W. R. Schwabe, J. De La Peña, B. Foys, B. Eshelman, and J. C. Izpisúa

Belmonte. 1997. Radical fringe positions the apical ectodermal ridge at the dorsoventral

boundary of the vertebrate limb. Nature 386:360–366.

Rommel, S. 1990. Osteology of the bottlenose dolphin; pp. 29–49 in The bottlenose dolphin.

Rose, K. D. 1982. Skeleton of *Diacodexis*, oldest known artiodactyl. Science 216:621–623.

Rose, K. D., and M. A. O'Leary. 1995. The manus of *Pachyaena gigantea* (Mammalia:

Mesonychia). Journal of Vertebrate Paleontology 15:855–859.

Roston, R. A., and V. L. Roth. 2019. Cetacean skull telescoping brings evolution of cranial sutures

into focus. Anatomical Record 302:1055–1073.

Roston, R. A., and V. L. Roth. 2021. Different transformations underlie blowhole and nasal passage development in a toothed whale (Odontoceti: *Stenella attenuata*) and a baleen whale (Mysticeti: *Balaenoptera physalus*). Journal of Anatomy 1–16.

Roston, R. A., D. Lickorish, and E. A. Buchholtz. 2013. Anatomy and age estimation of an early blue whale (*Balaenoptera musculus*) Fetus. The Anatomical Record 296:709–722.

Roux, W. 1883. Beiträge zur Morphologie der functionellen Anpassung. Archiv Fur Anatomie, Physiologie Und Wissenschaftliche Medicin 4:76–162.

Royle, S. R., C. J. Tabin, and J. J. Young. 2021. Limb positioning and initiation: An evolutionary context of pattern and formation. Developmental Dynamics dvdy.308.

Ryder, J. A. 1885. On the development of the Cetacea, together with consideration of the probable homologies of the flukes of cetaceans and sirenians. Bulletin of U.S. Fishing Commission 427–485.

Sahni, A., and S. K. Khare. 1971. Three new Eocene mammals from Rajauri District, Jammu and Kashmir. Journal of the Palaeontological Society of India 16:41–53.

Sahni, A., and S. K. Khare. 1972. Additional Eocene mammals from the Subathu Formation of Jammu and Kashmir. Journal of the Palaeontological Society of India 17:31–49.

Scherz, P. J., E. McGlinn, S. Nissim, and C. J. Tabin. 2007. Extended exposure to Sonic hedgehog is required for patterning the posterior digits of the vertebrate limb. Developmental Biology 308:343–354.

Scott, W. 1888. On some new and little known creodonts. Academy of the Natural Sciences of Philadelphia.

Sears, K. E., J. A. Maier, A. Sadier, D. Sorensen, and D. J. Urban. 2018. Timing the developmental origins of mammalian limb diversity. Genesis 56.

Sedmera, D., I. Misek, and M. Klima. 1997a. On the development of cetacean extremities: I. Hindlimb rudimentation in the spotted dolphin (*Stenella attenuata*). European Journal of Morphology 35:25–30.

Sedmera, D., I. Misek, and M. Klima. 1997b. On the development of the cetacean extremities: II. Morphogenesis and histogenesis of the flippers in the spotted dolphin (*Stenella attenuata*). European Journal of Morphology 35:117–123.

Sedmera, D., I. Misek, M. Klima, and R. P. Thompson. 2003. Heart development in the spotted dolphin (*Stenella attenuata*). Anatomical Record - Part A Discoveries in Molecular, Cellular, and Evolutionary Biology 273:687–699.

Seifert, A. W., T. Yamaguchi, and M. J. Cohn. 2009. Functional and phylogenetic analysis shows that Fgf8 is a marker of genital induction in mammals but is not required for external genital development. Development 136:2643–2651.

Sekine, K., H. Ohuchi, M. Fujiwara, M. Yamasaki, T. Yoshizawa, T. Sato, N. Yagishita, D. Matsui, Y. Koga, N. Itoh, and S. Kato. 1999. Fgf10 is essential for limb and lung formation. Nature Genetics 21:138–141.

Selever, J., W. Liu, M.-F. Lu, R. R. Behringer, and J. F. Martin. 2004. Bmp4 in limb bud mesoderm regulates digit pattern by controlling AER development. Developmental Biology 276:268–279.

Shapiro, M. D., M. A. Bell, and D. M. Kingsley. 2006. Parallel genetic origins of pelvic reduction in vertebrates. Proceedings of the National Academy of Sciences of the United States of America 103:13753–13758.

Shu, D. G., H. L. Luo, S. Conway Morris, X. L. Zhang, S. X. Hu, L. Chen, J. Han, M. Zhu, Y. Li, and L. Z. Chen. 1999. Lower Cambrian vertebrates from South China. Nature 402:42–46.

Simões-Lopes, P. C., and C. S. Gutstein. 2004. Notes on the anatomy, positioning and homology of the pelvic bones in small cetaceans (Cetacea, Delphinidae, Pontoporiidae). Latin American Journal of Aquatic Mammals 3:157–162.

Simon, M., M. Johnson, P. Tyack, and P. T. Madsen. 2009. Behaviour and kinematics of continuous ram filtration in bowhead whales (Balaena mysticetus). Proceedings of the Royal Society B: Biological Sciences 276:3819–3828.

Slijper, E. J. 1961. Locomotion and locomotory organs in whales and dolphins (Cetacea). Symposium of the Zoological Society 5:77–94.

Slijper, E. J. 1966. Functional morphology of the reproductive system in Cetacea; pp. 277–319 in K. S. Norris (ed.), Whales, dolphins, and porpoises. University of California Press.

De Smet, W. M. A. 1977. The regions of the cetacean vertebral column; pp. 59–80 in R. J. Harrison (ed.), Functional Anatomy of Marine Mammals. vol. 3. Academic Press.

Steinman, K. J., J. K. O'Brien, S. L. Monfort, and T. R. Robeck. 2012. Characterization of the estrous cycle in female beluga (*Delphinapterus leucas*) using urinary endocrine monitoring and transabdominal ultrasound: Evidence of facultative induced ovulation. General and Comparative Endocrinology 175:389–397.

Štěrba, O., M. Klima, and B. Schildger. 2000. Embryology of Dolphins: staging and ageing of embryos and fetuses of some cetaceans; pp. 1–133 in Advances in anatomy, embryology, and cell biology. Springer Verlag, Berlin.

Stewart, T. A., M. M. Bonilla, R. K. Ho, and M. E. Hale. 2019. Adipose fin development and its relation to the evolutionary origins of median fins. Scientific Reports 9.

Struthers, J. 1881. On the bones, articulations, and muscles of the rudimentary hind-limb of the Greenland right-whale (*Balaena mysticetus*). Journal of Anatomy and Physiology 15:141–321.

Struthers, J. 1885. On the rudimentary hindlimb of *Megaptera longimana*. American Naturalist 124–127.

Struthers, J. 1893. On the rudimentary hind-limb of a great fin whale (*Balaenoptera musculus*) in comparison with those of the humpback whale and the Greenland right-whale. Journal of Anatomy and Physiology 27:291–335.

Stump, C. W., J. P. Robins, and M. L. Carde. 1960. The development of the embryo and membranes of the humpback whale, *Megaptera jodosa* (Bonnaterre). Marine and Freshwater Research 11:365–386.

Sun, L., X. Rong, X. Liu, Z. Yu, Q. Zhang, W. Ren, G. Yang, and S. Xu. 2022. Evolutionary genetics of flipper forelimb and hindlimb loss from limb development-related genes in cetaceans. BMC Genomics 23:1–10.

Sun, Q., H. Morikawa, K. Ueda, H. Miyahara, and M. Nakashima. 2011. Bending properties of tail flukes of dolphin. Journal of Biomechanical Science and Engineering 6:15–25.

Sun, Q., H. Morikawa, S. Kobayashi, K. Ueda, H. Miyahara, and M. Nakashima. 2010. Structure and mechanical properties on tail flukes of dolphin. Journal of Aero Aqua Bio-Mechanisms 1:45–50.

Sun, X., F. V. Mariani, and G. R. Martin. 2002. Functions of FGF signaling from the apical ectodermal ridge in limb development. Nature 418:501–508.

Suydam, R. S. 2009. Age, growth, reproduction, and movements of beluga whales (*Delphinapterus leucas*) from the eastern Chukchi Sea. University of Washington, 1–169 pp.

Suydam, R. S., and J. C. George. 2021. Current indigenous whaling; pp. 519–536 in J. C. George and J. G. M. Thewissen (eds.), The Bowhead Whale, 1st ed. Elsevier.

Suzuki, K., D. Bachiller, Y. P. P. Chen, M. Kamikawa, H. Ogi, R. Haraguchi, Y. Ogino, Y. Minami, Y. Mishina, K. Ahn, E. B. Crenshaw, and G. Yamada. 2003. Regulation of outgrowth and apoptosis for the terminal appendage: External genitalia: Development by concerted actions of BMP signaling. Development 130.

Swartz, S. M., M. S. Groves, H. D. Kim, and W. R. Walsh. 1996. Mechanical properties of bat wing membrane skin. Journal of Zoology 239:357–378.

Tabin, C., and L. Wolpert. 2007. Rethinking the proximodistal axis of the vertebrate limb in the molecular era. Genes and Development 21:1433–1442.

Takada, S., K. L. Stark, M. J. Shea, G. Vassileva, J. A. McMahon, and A. P. McMahon. 1994. Wnt-3a regulates somite and tailbud formation in the mouse embryo. Genes and Development 8:174–189.

Tanaka, H., G. Li, Y. Uchida, M. Nakamura, T. Ikeda, and H. Liu. 2019. Measurement of time-varying kinematics of a dolphin in burst accelerating swimming. PLoS ONE 14:1–25.

Tarpley, R. J., D. J. Hillmann, J. C. George, and J. G. M. Thewissen. 2021. Female and male reproduction; pp. 185–211 in J. C. George and J. G. M. Thewissen (eds.), The Bowhead Whale, 1st ed. Elsevier.

Thewissen, J. G. M. 2018. Highlights of cetacean embryology. Aquatic Mammals 44:591–602.

Thewissen, J. G. M., and S. T. Hussain. 1990. Postcranial Osteology of the most Primitive Artiodactyl: *Diacodexis pakistanenesis*. Anat. Histol. Embryol. 19:37–48.

Thewissen, J. G. M., and F. E. Fish. 1997. Locomotor evolution in the earliest cetaceans: Functional model, modern analogues, and paleontological evidence. Paleobiology 23:482–490.

Thewissen, J. G. M., and J. Heyning. 2007. Embryogenesis and development in *Stenella attenuata* and other cetaceans; pp. 307–329 in Reproductive Biology and Phylogeny of Cetacea, 1st ed.

Thewissen, J. G. M., S. T. Hussain, and M. Arif. 1994. Fossil evidence for the origin of aquatic locomotion in archaeocete whales. Science 263:210–212.

Thewissen, J. G. M., S. I. Madar, and S. T. Hussain. 1996. *Ambulocetus natans*, an Eocene cetacean (Mammalia) from Pakistan. CFS Courier Forschungsinstitut Senckenberg 190:1–86.

Thewissen, J. G. M., E. M. Williams, and S. T. Hussain. 2001a. Eocene mammal faunas from Northern Indo-Pakistan. Journal of Vertebrate Paleontology 21:347–366.

Thewissen, J. G. M., L. N. Cooper, and R. R. Behringer. 2012. Developmental biology enriches paleontology. Journal of Vertebrate Paleontology 32:1223–1234.

Thewissen, J. G. M., A. C. Nanda, and S. Bajpai. Indohyus, endemic radiation of raoellid artiodactyls in the Eocene of India and Pakistan; pp. in G. V. R. Prasad and R. Patnaik (eds.), Biological Consequences of Plate Tectonics: New Perspectives on Post-Gondwanaland Break-up. Springer.

Thewissen, J. G. M., E. M. Williams, L. J. Roe, and S. T. Hussain. 2001b. Skeletons of terrestrial cetaceans and the relationship of whales to artiodactyls. Nature 413:277–281.

Thewissen, J. G. M., L. N. Cooper, J. C. George, and S. Bajpai. 2009a. From Land to Water: The origin of whales, dolphins, and porpoises. Evolution: Education and Outreach 2:272–288.

Thewissen, J. G. M., L. N. Cooper, M. T. Clementz, S. Bajpai, and B. N. Tiwari. 2007. Whales originated from aquatic artiodactyls in the Eocene epoch of India. Nature 450:1190–1194.

Thewissen, J. G. M., L. N. Cooper, M. T. Clementz, S. Bajpai, and B. N. Tiwari. 2009b. Thewissen et al. reply. Nature 458.

Thewissen, J. G. M., M. J. Cohn, L. S. Stevens, S. Bajpai, J. Heyning, and W. E. Horton. 2006. Developmental basis for hind-limb loss in dolphins and origin of the cetacean bodyplan. Proceedings of the National Academy of Sciences of the United States of America 103:8414–8418.

Thewissen, J. G. M., T. L. Hieronymus, J. C. George, R. Suydam, R. Stimmelmayr, and D. McBurney. 2017. Evolutionary aspects of the development of teeth and baleen in the bowhead whale. Journal of Anatomy 230:549–566.

Thewissen, J. G. M., D. J. Hillmann, J. C. George, R. J. Tarpley, G. Sheffield, R. Stimmelmayr, and R. Suydam. 2021a. Postcranial skeleton and musculature; pp. 137–150 in J. G. M. Thewissen and J. C. George (eds.), The Bowhead Whale, 1st ed. Elsevier.

Thewissen, J. G. M., D. J. Hillmann, J. C. George, R. Stimmelmayr, R. J. Tarpley, G. Sheffield, and R. Suydam. 2021b. Prenatal Development; pp. 117–126 in J. G. M. Thewissen and J. C. George (eds.), The Bowhead Whale, 1st ed. Elsevier.

Thompson, A. C., T. D. Capellini, C. A. Guenther, Y. F. Chan, C. R. Infante, D. B. Menke, and D. M. Kingsley. 2018. A novel enhancer near the pitx1 gene influences development and evolution of pelvic appendages in vertebrates. ELife 7.

Tissières, V., F. Geier, B. Kessler, E. Wolf, R. Zeller, and J. Lopez-Rios. 2020. Gene regulatory and expression differences between mouse and pig limb buds provide insights into the evolutionary emergence of artiodactyl traits. Cell Reports.

Tschopp, P., B. Tarchini, F. Spitz, J. Zakany, and D. Duboule. 2009. Uncoupling time and space in the collinear regulation of Hox genes. PLoS Genetics 5:1000398.

Tucker, A. S., and J. M. W. Slack. 1995. Tail bud determination in the vertebrate embryo. Current Biology 5:807–813.

Tulenko, F. J., J. L. Massey, E. Holmquist, G. Kigundu, S. Thomas, S. M. E. Smith, S. Mazan, and M. C. Davis. 2017. Fin-fold development in paddlefish and catshark and implications for the evolution of the autopod. Proceedings of the Royal Society B: Biological Sciences 284.

Tzchori, I., T. F. Day, P. J. Carolan, Y. Zhao, C. A. Wassif, L. Q. Li, M. Lewandoski, M. Gorivodsky, P. E. Love, F. D. Porter, H. Westphal, and Y. Yang. 2009. LIM homeobox transcription factors integrate signaling events that control three-dimensional limb patterning and growth. Development 136:1375–1385.

Uhen, M. D. 1998. New protocetid (Mammalia, Cetacea) from the late middle Eocene cook mountain formation of Louisiana. Journal of Vertebrate Paleontology 18:664–668.

Uhen, M. D. 2004. Form, function, and anatomy of *Dorudon atrox* (Mammalia, Cetacea): an archaeocete from the Middle to Late Eocene of Egypt. Papers on Paleontology 34:1–238.

Uhen, M. D. 2008. New protocetid whales from Alabama and Mississippi, and a new cetacean clade, Pelagiceti. Journal of Vertebrate Paleontology 28:589–593.

Uhen, M. D. 2014. New material of *Natchitochia jonesi* and a comparison of the innominata and locomotor capabilities of Protocetidae. Marine Mammal Science 30:1029–1066.

Varga, Z., and M. Varga. 2022. Gene expression changes during the evolution of the tetrapod limb. Biologia Futura 2022 73:4 73:411–426.

Vautrin, Q., F. Lihoreau, B. Sambou, M. Thiam, J. E. Martin, R. Tabuce, S. Adnet, R. Lebrun, A. Charruault, R. Sarr, and L. Hautier. 2019. From limb to fin: an Eocene protocetid forelimb from Senegal sheds new light on the early locomotor evolution of cetaceans. Palaeontology 63:51–66.

Vogel, A., C. Rodriguez, and J. C. Izpisúa-Belmonte. 1996. Involvement of FGF-8 in initiation, outgrowth and patterning of the vertebrate limb. Development 122:1737–1750.

Wada, N., H. Hori, and M. Tokuriki. 1993. Electromyographic and kinematic studies of tail movements during falling in cats. Journal of Morphology 217:105–113.

Wagner, G. P., and C. H. Chiu. 2001. The tetrapod limb: A hypothesis on its origin. Journal of Experimental Zoology.

Watson, a G., and R. E. Fordyce. 1993. Skeleton of two minke whales, *Balaenoptera acutorostrata*, stranded on the south-east coast of New Zealand. New Zealand Natural Sciences 20:1–14.

Weatherbee, S. D., R. R. Behringer, J. J. Rasweiler IV, and L. A. Niswander. 2006. Interdigital webbing retention in bat wings illustrates genetic changes underlying amniote limb diversification. Proceedings of the National Academy of Sciences of the United States of America 103:15103–15107.

Weber, P. W., L. E. Howie, M. M. Murray, and F. E. Fish. 2009. Lift and drag performance of odontocete cetacean flippers. Journal of Experimental Biology 212:2149–2158.

Yalden, D. W. 1971. The functional morphology of the carpus in ungulate mammals. Acta Anatomica 78:461–487.

Yamada, G., K. Suzuki, R. Haraguchi, S. Miyagawa, Y. Satoh, M. Kamimura, N. Nakagata, H. Kataoka, A. Kuroiwa, and Y. Chen. 2006. Molecular genetic cascades for external genitalia formation: An emerging organogenesis program. Developmental Dynamics 235:1738–1752.

Yang, Y., and L. Niswander. 1995. Interaction between the signaling molecules WNT7a and SHH during vertebrate limb development: Dorsal signals regulate anteroposterior patterning. Cell 80:939–947.

Yano, T., and K. Tamura. 2013. The making of differences between fins and limbs. Journal of Anatomy 222:100–113.

Young, J. W., G. A. Russo, C. D. Fellmann, M. A. Thatikunta, and B. A. Chadwell. 2015. Tail function during arboreal quadrupedalism in squirrel monkeys (*Saimiri boliviensis*) and tamarins (*Saguinus oedipus*). Journal of Experimental Zoology Part A: Ecological Genetics and Physiology 323:556–566.

Yu, K., and D. M. Ornitz. 2008. FGF signaling regulates mesenchymal differentiation and skeletal patterning along the limb bud proximodistal axis. Development 135:483–491.

Zakany, J., G. Zacchetti, and D. Duboule. 2007. Interactions between HOXD and Gli3 genes control the limb apical ectodermal ridge via Fgf10. Developmental Biology 306:883–893.

Zhang, X. G., and X. G. Hou. 2004. Evidence for a single median fin-fold and tail in the Lower

    Cambrian vertebrate, *Haikouichthys ercaicunensis*. J. Evol. Biol. 17:1162–1166.

Zúñiga, A., A. P. G. Haramis, A. P. McMahon, and R. Zeller. 1999. Signal relay by BMP antagonism

    controls the SHH/FGF4 feedback loop in vertebrate limb buds. Nature 401:598–602.